UNIVERSITY OF CALIFORNIA

SANTA CRUZ

VULNERABILITY OF A SUBARCTIC BARRIER SPIT TO GLOBAL WARMING INDUCED CHANGES IN STORM SURGE AND WAVE RUNUP: SHAKTOOLIK, ALASKA

A thesis submitted in partial satisfaction
of the requirements for the degree of

MASTER OF SCIENCE

in

EARTH SCIENCES

by

Karin Ohman

December 2012

The thesis of Karin Ohman
is approved:

_____
Professor Gary Griggs

_____
Dr. Li Erikson

_____
Professor Andrew Moore

_____
Tyrus Miller
Vice Provost and Dean of Graduate Studies

Table of Contents

List of Figures

List of Tables

Abstract

Karin Ohman

Vulnerability of a subarctic barrier spit to global warming induced changes in storm surge and wave runup: Shaktoolik, Alaska

The native Inupiaq community of Shaktoolik, in northwestern Alaska, is located on a low-lying barrier spit in Norton Sound. The inhabited portion of the spit is 7.1 m above MLLW at its highest and only ~200 m across. The community is vulnerable to marine flooding on both the open ocean and lagoon sides of the spit during large storms. Storm events in this region typically occur during the fall and winter months, often when the coastline is protected from flooding and erosion by shorefast ice. High latitudes are experiencing the greatest increases in temperature due to global warming and the reduced duration and extent of sea ice is affecting Alaskan coastal communities. Continued reduction of sea ice, which typically protects the coastline from exposure during large storm events in late fall and winter, may result in the need to relocate many Native Alaskan coastal settlements.

The goal of this study was to quantify changes in storm surge and wave runup during ice-free months for the mid- to late-21st century. A combination of field data, including beach profiles, offshore bathymetry, debris line position, and sediment grain size, as well as modeled meteorological data were used to address the research goals. An analytical approach was developed to quantify storm surge in Alaskan coastal communities with historical meteorological data from the North American Regional Reanalysis. This analytical model was used to calculate projected storm surge flooding levels in Shaktoolik for the mid- and late-21st century for both a

moderate and high greenhouse gas emissions scenario (RCP 4.5 and RCP 8.5 respectively), with meteorological output from the MIROC5 global climate model. Additionally, projected wave runup heights during storm events were determined numerically using WAVEWATCH III to calculate wave height and period from the projected MIROC5 meteorological data and SBEACH to model the maximum runup heights along the Shaktoolik shoreline.

Total storm water levels (storm surge plus wave runup height) were calculated for 236 projected storm events in the Bering Sea and used to find the return periods of flooding for each emissions scenario. When compared to modeled historic storm surge, the results show that the moderate emissions scenario is similar to the historical. The 100-yr surge level is +6.3 m above MLLW for the moderate emissions scenario and +6.1 m historically. The high emissions scenario produces lower storm frequency than the moderate emissions scenario and the return periods of flooding for storm surge are lower than the historical values, the 100-yr surge level is +5.0 m. When wave setup and runup are included in the total flood levels the 100-yr flood level is +10.2 m above MLLW for the moderate emissions scenario and +8.7 m for the high emissions scenario, compared to +10.4 m historically. All three of these flooding levels overtop the highest ground elevation in the community.

Acknowledgements

I would like to thank my co-authors Li Erikson and Nicole Kinsman for their expertise and guidance throughout the research process, my adviser Gary Griggs for his advice and support, and my parents for their continued support of my academic pursuits.

Chapter 1

Introduction

The Native Alaskan community of Shaktoolik, located on Norton Sound along the western coast of Alaska, is home to approximately 220 people who thrive primarily on a fishing and subsistence lifestyle. The location of the village is shown in Figure 1.1. The village is one of many Native Alaskan communities along the coasts of Alaska. Shaktoolik has been occupied since 1839 and was originally located 6 miles inland, up the Tagoomenik River, from the current location on the coast (Native Village of Shaktoolik IRA Council, 2012). In 1933 the village relocated to a new site on Norton Sound on a barrier spit, now known as the Shaktoolik Spit. This location, the Old Village Site, was subject to high winds and erosion of the coastline during storm events so the community moved once more to its present location in 1967. The New Village Site is further north along the spit near the mouth of the Tagoomenik River (Figure 1.2). At its present location, Shaktoolik is still exposed to high winds and devastating effects from storm surge and wave runup. During storm events, flooding occurs on both the open water and lagoon sides of the spit.

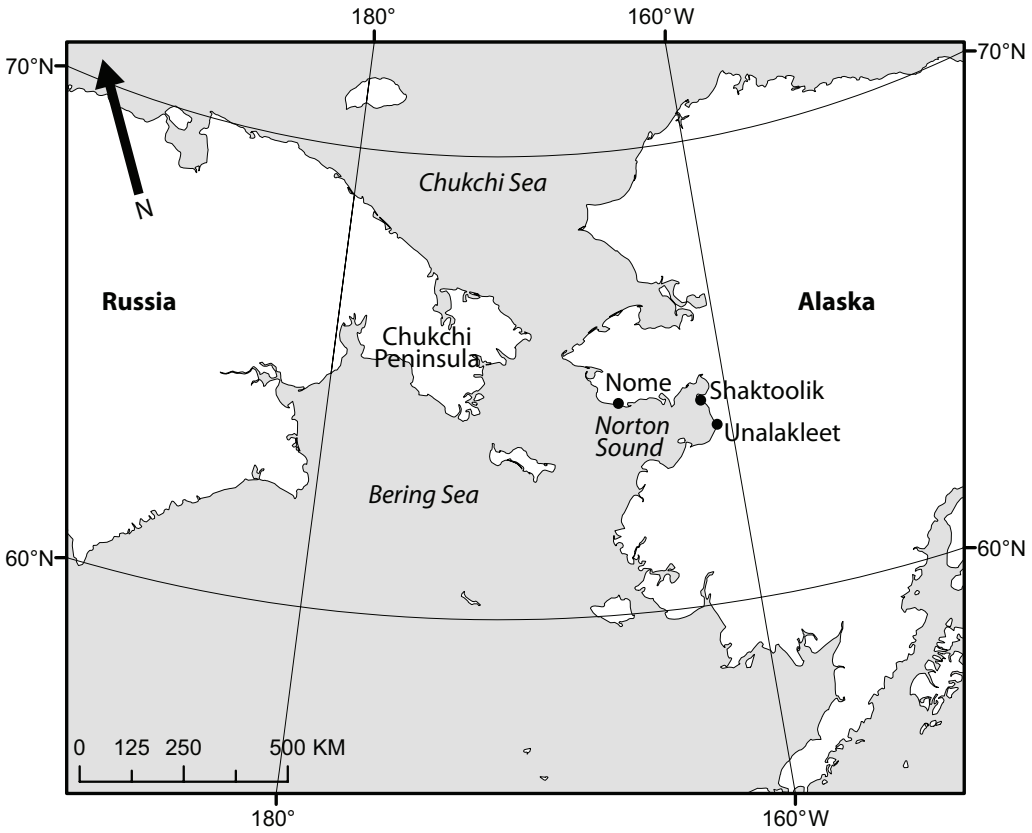

Figure 1.1. Map of region and location of Shaktoolik.

Figure 1.2. Satellite image of Shaktoolik spit (imagery from Terrametrics, 2012).

Historically, one of the largest storms recorded in the region was from November 11-13, 1974. The event was a series of three storms, a quasistationary storm over the Chukchi Peninsula in Russia and two frontal waves in the area. This storm caused an estimated $90,000 worth of damage (in 2012 dollars) in Shaktoolik (Wise et al., 1981). On November 8-10, 2011, another large storm event occurred in the region. This large low-pressure system moved through the Bering Sea and into Norton Sound. The minimum pressure reached at the center of the cyclone was 945 mb, making it the strongest storm to hit northwestern Alaska since 1974 (NASA Earth Observatory, 2011). Events such as these cause significant flooding in the community of Shaktoolik. While previous work focuses on historic events, this study aims to quantify both historical flood events and potential changes in the frequency and intensity of storm events under the influence of climate change.

1.1 Geologic and Climate Setting

Shaktoolik is located at 64° 21' N and 161° 11' W. It is approximately 200 km east of Nome and 53 km north of Unalakleet. The village sits near the end of a low-lying sand and gravel spit that built up from the southeast, separating the Tagoomenik River from Norton Sound. The highest elevation at the current village site is 7.1 m above MLLW and the maximum width of the barrier spit is ~200 m. The topography of the surrounding area is also very low-lying, with predominantly tundra vegetation cover and no trees. The climate in Shaktoolik is subarctic with maritime

influences characterized by long, usually very cold winters and short, cool summers. The average precipitation at Nome is 42.2 cm of rainfall and 145.3 cm of snowfall per year (NCDC, 2011). The average high temperature is -10.3°C in January and 14.8°C in July.

Norton Sound, the body of water adjacent to the community, averages 20 meters in depth and is susceptible to high storm surge levels because of the relatively shallow waters. Shaktoolik sits on the northeast corner of Norton Sound. The fetch is about 800 km across the sound to the middle of the Bering Sea, where storms initiate surges that eventually reach Shaktoolik.

Typical storm paths that reach the Bering Sea originate and intensify in the western North Pacific, east of Japan, over the warm western boundary current called the Kuroshio Current. These storms travel northeastward and develop into mature cyclones near the dateline, also the center of the Aleutian Low. Most of these storms continue eastward into the Gulf of Alaska or eastern North Pacific, but some travel northwards along the Siberian coast and into the Bering Sea. The Bering Sea tends to be anomalously warm during winters in which this storm track is active (Rodionov, 2007). These storms can be intensified further during the fall due to the temperature gradient between the cold Siberian continental air mass and relatively warm ocean air over the Bering Sea. Statistical analyses of storm records in Nome suggest that Bering Sea storms are linked to a 3-7 year period cycle of storms associated with the El Niño Southern Oscillation (ENSO), and a 10-11 year period cycle of larger storms

associated with the Western Pacific Oscillation (WPO) or Pacific Decadal Oscillation (PDO) (Mason et al., 1997) (Stabeno et al., 1999).

The storm climatology for Shaktoolik was developed to identify when most storms occur and what trends in storm frequency over the past few decades have occurred. Weather data for Shaktoolik, from airport records, are only available from November 2010 to the present. In order to quantify storm events, atmospheric pressure data from the city of Unalakleet (55 km to the south) were used to examine storm frequency and strength from 1973 to present day (NCDC, 2011). Storm events were identified as atmospheric pressure levels below 1000 mb and individual storms were defined as the low pressures occurring greater than 3 days apart. On average, 13 storms occurred each year based on the 1973-2011 record from Unalakleet, Alaska. Figure 1.3 shows a graph of storm frequency per year and minimum yearly surface pressure observed (NCDC, 2011). The lowest pressure observed in Unalakleet was 958.18 mb in November 1979 in which flooding occurred along the Yukon-Kuskokwim delta at the southern extent of Norton Sound (Mason et al., 1997). There are no observable trends in storm frequency or intensity over time for this record.

Storm frequency and maximum fetch distance, grouped by month from 1973 to 2011, is displayed in Figure 1.4 (NCDC, 2011). The majority of storms occur during the late fall months from October through December when shorefast ice has formed and the coastline is protected from storm surge and erosion. But as global climate warms and sea ice extent and duration decrease, these storms may have a greater impact on flooding and coastal erosion in this region.

Data collected at the Shaktoolik weather station over the past year, since the station was set up, show that 15 storm events have occurred since November 2010 and the minimum pressure reached was 977.77 mb in January and April of 2011 (NCDC, 2011). The November 2011 storm had a minimum atmospheric pressure of 982.44 mb recorded in Shaktoolik. In Unalakleet, the minimum pressure reached during the November 2011 storm was 983.89 mb, very similar to the Shaktoolik station located 53 km north.

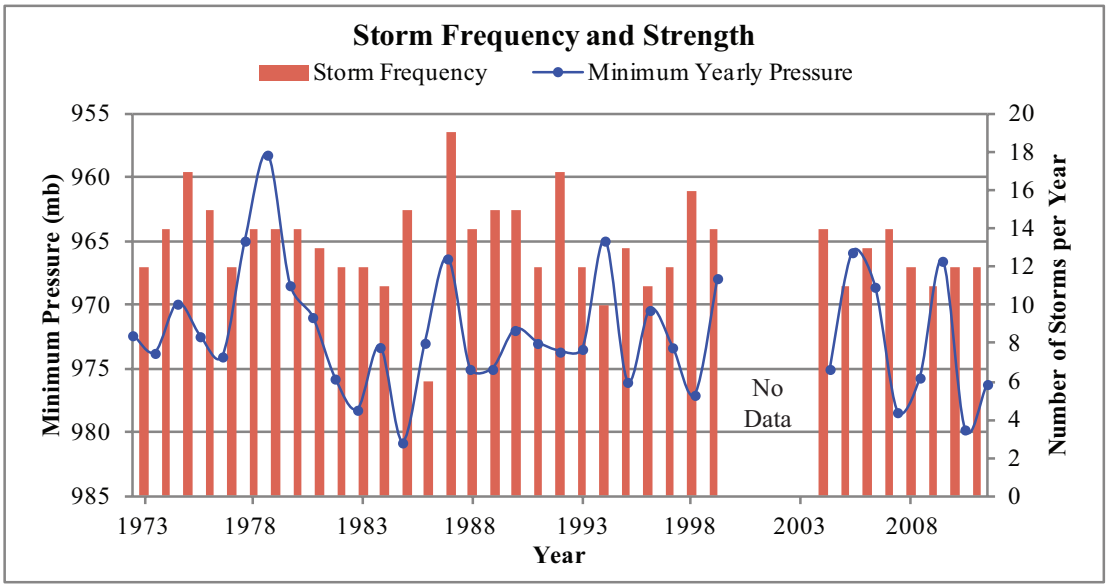

Figure 1.3. Graph of storm frequency and strength from Unalakleet weather station (NOAA atmospheric pressure data). Individual storms identified as pressures below 1000 mb and at least 3 days apart. Red bars indicate the number of storms in a given year. Blue dots show the minimum pressure reached that year during a storm event.

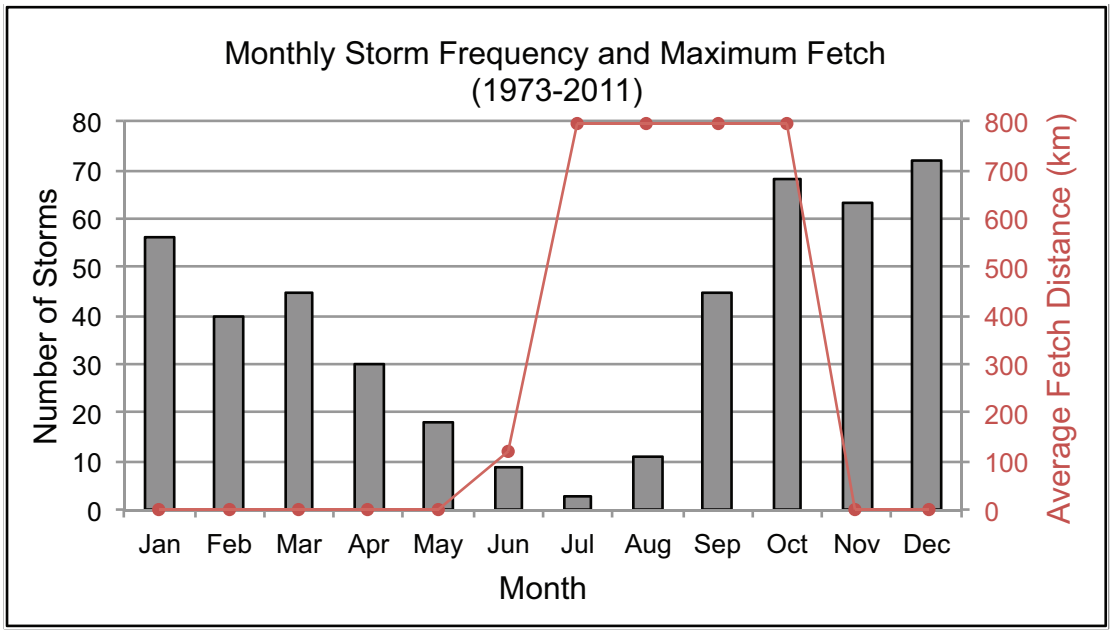

Figure 1.4. Storm frequency and maximum fetch per month from 1973-2011, based on Unalakleet NOAA weather data. Blue bars indicate number of storms per month for the period of record where individual storms were identified as pressures below 1000 mb and greater than 3 days apart. Red dots show the maximum fetch distance at Shaktoolik based on median monthly sea ice extent from the National Snow & Ice Data Center (NSIDC, 2012).

1.2 Components of Total Water Level

Storm Surge is driven by wind forcing and, generally to a lesser extent, atmospheric pressure. Figure 1.5 shows the physical components of storm surge, with wind being the most important factor in producing storm surge. As more rapidly moving and less viscous air travels over the surface of a body of water it transfers momentum to the water. This creates a surface stress that drags the surface water parallel to the wind direction, which produces wave activity and entrains the surface mass of water. The distance over which wind exerts stress on the body of water is known as the fetch. Longer wind duration and larger fetch allows for more water to be entrained and results in a greater storm surge and larger waves at the coastline.

Kamphuis (2000) describes wind driven storm surge analytically using the following equation:

$$\frac{dS}{dx} = \frac{\zeta (U \cos\phi)^2}{gD} \tag{1.1}$$

where

$\frac{dS}{dx}$ is the change in storm surge height with cross-shore distance as it approaches the shoreline (dimensionless)

ζ is a constant (= 3.2 x 10^{-6})

U is the wind speed in units of ms^{-1}

ϕ is the angle in degrees between the wind direction and the cross-shore direction (x-axis)

g is the acceleration due to gravity (= 9.81 ms^{-2})

D is the new depth of the water with the surge, and is equal to the initial water depth plus surge height (d+S), in units of m

Equation 1.1 shows that storm surge is larger in shallow water, where D is smaller. In areas where the continental shelf is wide, the effects of storm surge are heightened as the water is piled up over a large area like a wedge. In Norton Sound, where the average depth is only 20 m, and at Shaktoolik where the fetch can be as large as 800 km, storm surge at the coastline can be devastating to the low-lying area where the village is situated.

The second component of storm surge is pressure driven. This effect is smaller than that of the wind forcing, but should not be overlooked. Known as the inverse barometer effect, low atmospheric pressures physically draw up the water level. This process adds to the wind driven surge to create a total storm surge height. The equation for pressure driven storm surge is also described in Kamphuis (2000):

$$\Delta h = \frac{0.1 \text{ x } \Delta p}{\rho g} \tag{1.2}$$

where

Δh is the change in water height in units of m

Δp is the difference in barometric pressure between offshore (upwind, at the distance of maximum fetch) and the coast (downwind), in units of mb

ρ is the water density in units of kgm^{-3}

Equation 1.2 shows that a decrease in pressure of 10 mb corresponds to about a 0.1 m sea level rise. Very strong storms come through this region of Alaska and atmospheric pressures can drop to 940 mb, so the input of pressure driven storm surge potentially has a significant impact on the overall storm surge height.

Wave runup is the conversion of wave energy to potential energy that causes waves to travel up the foreshore (Figure 1.5). Most wave energy is dissipated at the surf zone due to breaking waves but a portion of the energy results in runup (Stockdon et al., 2006). The runup process at the foreshore is shown in Figure 1.6. Wave runup is responsible for the majority of beach erosion and extreme runup can have devastating effects on infrastructure at the coastline. Wave runup height

depends on deep-water wave height, the interdependent deep-water wavelength and period, and beach slope. The equation used for extreme wave runup was developed by Stockdon et al. (2006) and states that:

$$R_2 = 1.1\left(0.35\beta_f(H_0L_0)^{1/2} + \frac{[H_0L_0(0.563\beta_f^2 + 0.004)]^{1/2}}{2}\right) \quad (1.3)$$

where

R_2 is the 2% runup height, the height that only the highest 2% of wave runup values observed will reach or exceed, in units of m

H_o is the deep-water wave height in units of m

L_o is the deep-water wavelength in units of m

β_f is the foreshore slope

Equation 1.3 shows that a steeper beach slope, greater wave height, and longer wavelength result in larger runup heights on the foreshore. Since the extreme wave runup events will cause the most significant damage at the shoreline, the R_2 wave runup height defined as the value exceeded by 2% of wave runup events and is used for short-term statistics, such as the duration of a single storm event (FEMA, 2007). When the effects of extreme wave runup during storm events are combined with the elevated sea levels due to storm surge, the total water level during a storm event can be calculated:

$$TWL = R_2 + dS + \Delta h \quad (1.4)$$

where

TWL is total storm water level in units of m

R_2 is the 2% wave runup height in units of m

dS is storm surge height due to wind forcing in units of m

Δh is change in water level due to changes in atmospheric pressure in units of m

The total water level during a storm event is the combined effect of storm surge and wave runup. The impact of wave activity on top of the elevated sea level during extreme events can result in increased beach erosion, damage to infrastructure, and in low-lying areas such as Shaktoolik, overtopping of the sand spit and flooding of the village. The overall total water level is also influenced by factors not associated with the storm event, such as global sea-level rise, isostatic rebound, and changes in ocean circulation in response to cyclical events such as El-Niño Southern Oscillation (ENSO). Swash, the rush of seawater up the beach after the breaking of a wave, is a minimal factor in overall total water level during a storm event, so it was ignored for the purposes of this study. There is no tide gage in Shaktoolik, the closest one is in Nome, Alaska, but a short-term station was set up by the USACE from July 14 to August 23, 2010 (USACE, 2011)(Chapman et al., 2011). The data from this station show a mean tidal range of 0.74 m and a diurnal range of 1.15 m. Relative sea level rise in the region, calculated from the nearest tide gage in Nome, Alaska, is estimated at +0.06 mm/yr using the monthly averaged water level data (Figure 1.7). Seasonal fluctuations in water level have not been removed from the record and the time-series is not long enough for any conclusive evidence about relative sea level in Nome. The monthly averaged data do imply minimal long-term relative sea level rise, however.

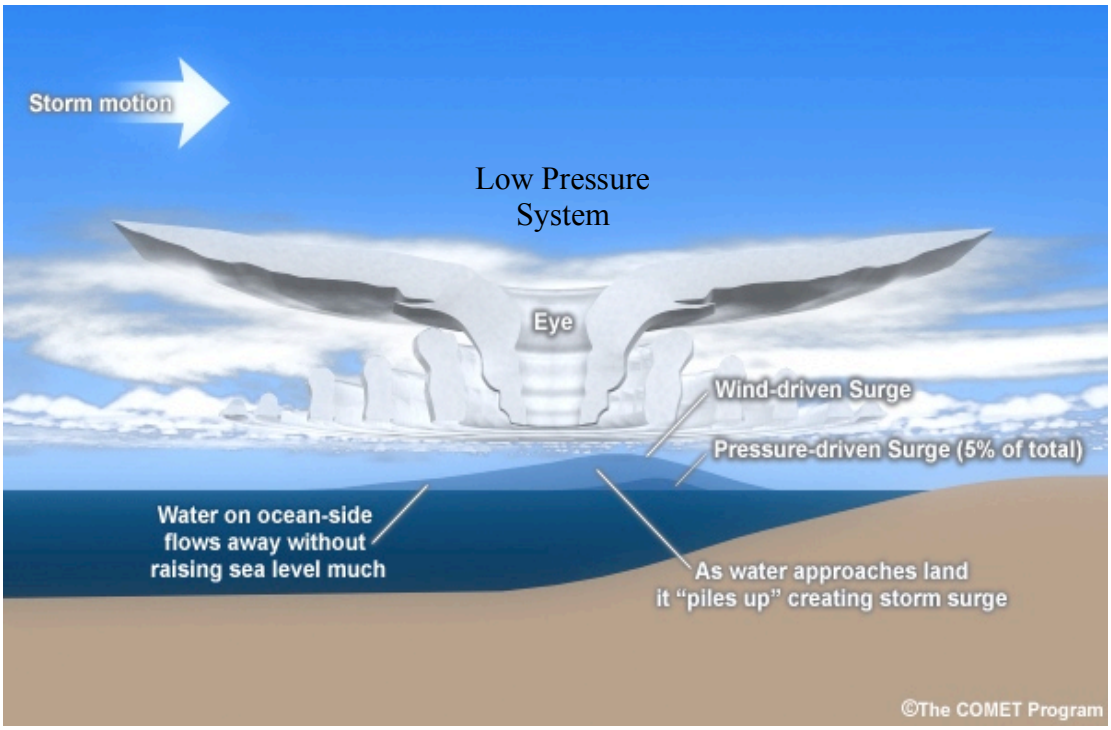

Figure 1.5. The components of storm surge as a storm moves onshore: wind driven surge plus the pressure driven surge equal total storm surge (modified from The University Corporation for Atmospheric Scientists: The COMET Program, 2012).

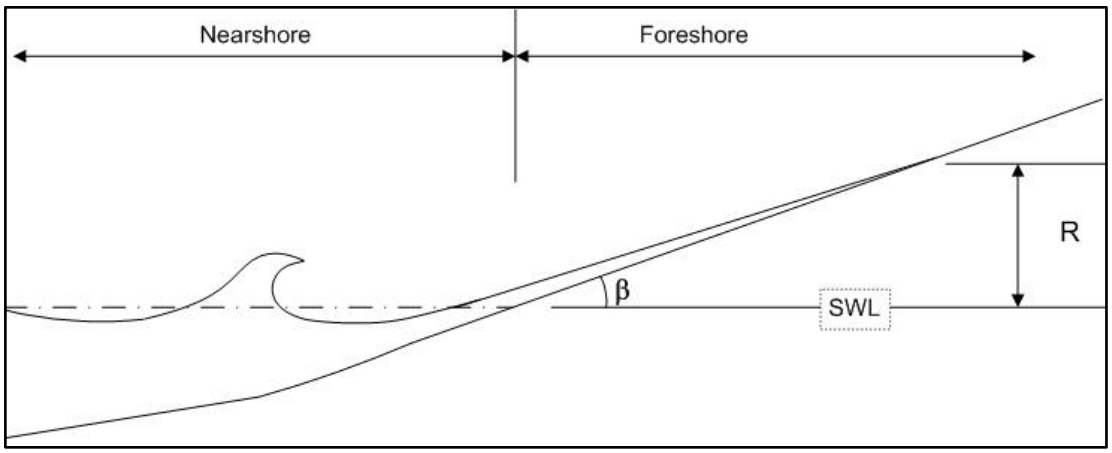

Figure 1.6. The components of wave runup as the wave approaches the shoreline. Where β is the foreshore slope, SWL is still water level, and R is runup height (Sorensen, 1997).

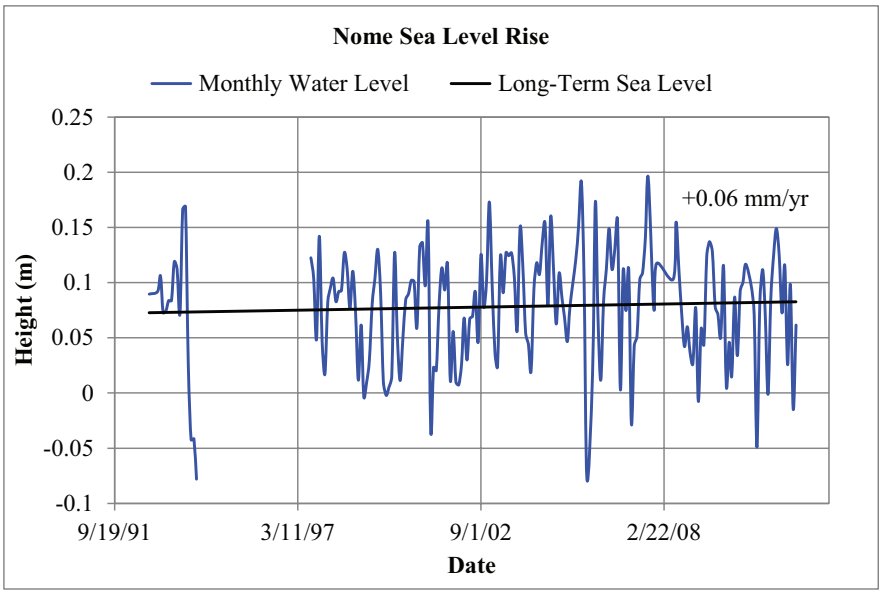

Figure 1.7. Long-term sea level record for Nome, Alaska. Trends of monthly averaged water level heights show a sea level rise of +0.06 mm/yr. Seasonal water level variations have not been removed and the times-series is not long enough for conclusive evidence about relative sea level rise. Data from NOAA Tides & Currents (2012).

1.3 Previous Work

Studies of storm surge and wave runup analysis in Shaktoolik are limited due to the lack of physical measurements of flooding levels. Former studies in Norton Sound have relied on surface pressure charts or satellite data to compute winds for modeling storm surge and wave heights in the region.

Wise et al. (1981) developed the storm surge climatology for Alaska of 90 separate surge occurrences along the Bering Sea coast, including Norton Sound. These storm surge cases were compiled from a number of sources including technical papers, government agency records, newspaper articles and personal accounts. Of the 90 occurrences, Norton Sound had the greatest number of reported storms, 26 total with 23 of those storms occurring during the fall season. A statistical model for

calculating the recurrence interval of storm surge events was also established by Wise et al. (1981). For the eastern Norton Sound coast, surge height of 2.4 m was estimated for the 10-yr flood, 3.2 m for the 50-yr flood, and 3.4 m for the 100-yr flood.

Following the large storm in November 1974, Sallenger (1983) collected debris line positions and beach profile surveys around Norton Sound to measure the extent of storm surge and wave runup along the coast. The inland extent of the debris lines provides a combined measurement of wind induced storm surge, inverse barometric effect surge, wave setup, and wave runup. Debris line measurements were taken at 2 locations along the Shaktoolik Spit, one south of the community at the base of the spit and the other along the open water side beach in of the community. At the base of the spit, debris lines following the November 1974 storm reached as far inland as 40 m and as high as 4.1 m relative to local mean sea level. In front of the community, debris lines reached as far inland as 69 m and up to 4.9 m height relative to local mean sea level. The eastern Norton Sound region, including Shaktoolik, experienced the highest water levels of the entire Norton Sound region based on debris line data.

Johnson and Kowalik (1986) numerically modeled the November 1974 storm and incorporated both pack ice and shorefast ice into the model. They found that including the damping effects of shorefast ice results in measurable differences in storm surge height results. For the eastern Norton Sound region they calculated that

surge heights reached 4.6 m, which is comparable to the 4.9 m measured by Sallenger (1983).

In fall of 1992, a tide gage was installed at Nome. Blier et al. (1997) were able to use the newly installed tide gage records to validate numerical model results from the National Oceanic and Atmospheric Administration (NOAA) extra-tropical storm surge (E-T surge) model. The E-T surge is a dynamic surge forecast model modified from the Sea, Lake, and Overland Surges from Hurricanes (SLOSH) developed by the National Weather Service (NWS) for forecasting tropical cyclones. The model performed well for longer duration storm events but did not simulate short-term storm events very well.

Currently, the E-T surge model is used by the NWS to forecast storm surge in Norton Sound from approaching extra-tropical cyclones. This began in 2008 when the operational E-T surge model was extended to cover the Alaskan coastline. The model has been upgraded since the early 1990s to a higher resolution of 1.00° latitude by 1.00° longitude data at 3-hour intervals, to better capture short-term storm events (Glahn et al., 2009).

The U.S. Army Corps of Engineers (USACE), Alaska District and the Coastal and Hydraulics Laboratory carried out the most recent and extensive study of storm surge and wave runup in Shaktoolik during the summer of 2010 (USACE, 2011)(Chapman et al., 2011). In the report, the USACE identified 56 storm events to hit the community between years 1954-2009. For each of these events they calculated water levels due to storm surge using the Advanced Circulation Model

(ADCIRC) and wave runup heights using the Numerical Model for Simulating Storm-Induced Beach Change (SBEACH). Historical wind field values were developed from satellite data for the region. Their results showed that the October 1, 1960 storm produced the highest runup, at 5.68 m relative to mean lower low water level (MLLW), and water elevation from storm surge and predicted tides at 5.52 m, for a peak total water level of 11.2 m during the storm event. The November 1974 storm had the second highest estimated total water level, 4.27 m MLLW wave runup plus 4.98 m water elevation for a total of 9.25 m peak total water level. Both of these storms would have overtopped the spit at both the new and old village sites; the highest elevation of the spit in the present day community is only 7.1 m.

In this study the USACE also estimated the recurrence interval for flooding events. They found that the largest storms on record in October 1960 and November 1974, which resulted in water overtopping the spit, had a flood recurrence interval of 58.2 and 48.1 years, respectively. Furthermore the 25-year flood level will significantly inundate the community, reaching the elevation of the road, and cause damage to homes and other infrastructure.

The first storm surge measurements ever recorded in Shaktoolik were taken a few days after the November 2011 storm passed through by the Alaska Division of Geological and Geophysical Surveys. Maximum storm surge height was 4.4 m relative to local mean sea level on the Tagoomenik River side of the community (Kinsman and DeRaps, 2012). The measurements were taken along the river as opposed to the open-water side of the spit because of the reduced impact of tides,

wave setup and runup on the river. Therefore it assumes that the value for flooding better represents isolated storm surge height. On the open-water side of the spit, maximum wave runup in the community was measured at 2.3 m and extreme wave runup along the spit was measured at 4.4 m near the old community site. The combined effect of wave runup and storm surge on the open-water side was 6.7 m at the community and 8.8 m further down the spit near the old community. The values for wave runup and storm surge are averages of 5 to 6 measurements collected in the field.

Storm surge measurements were taken in Nome using the same technique and compared to the tide gauge there for validation. In Nome, the estimated error between the onshore measurements was +0.4 m higher than the tide gage. Therefore the storm surge measurements for Shaktoolik have at most a +0.4 m error, but the error is probably lower since measurements could be taken in the more controlled riverbank environment. The measurements of storm surge in Shaktoolik are also similar to predicted storm surge levels modeled by the National Weather Service (Lingaas, 2011).

1.4 Motivation

Previous work in the area has modeled past storm surge and wave runup levels using a statistical approach (USACE, 2011)(Chapman et al., 2011). This study differs in that global climate model (GCM) data are used to calculate storm surge and wave runup analytically instead of estimating these parameters from historic events,

which inherently assumes that the climate is stationary (non-changing). GCM weather forcing data account for projected climate change over the 21st century and therefore are advantageous for forecasting future storm surge and wave runup because they do not assume that the past climate reflects the future climate. The development of an analytical equation for storm surge is also useful for the coastal communities in the area because they can quickly calculate anticipated high water levels associated with an approaching storm.

The overall goal of this study is to provide the community of Shaktoolik, and other coastal Alaskan communities, with estimates of historical storm surge and wave runup levels as well as projected high water levels for the mid- to late-21st century. There are three main objectives for this study.

1. Develop and calibrate an analytical approach for calculating storm surge using historic data.

2. Calculate projected total water levels, both storm surge and wave runup, for the mid- to late-21st century using projected climate data.

3. Calculate projected flood return periods and compare these to historical flood return periods.

The community of Shaktoolik was chosen for this study because of the vulnerability to high winds and storm surge based on its location on Norton Sound. The village also has little to no previous data collected for flood levels and weather patterns. Shaktoolik is one of many Native Alaskan communities at risk for flooding and erosion, especially in consideration of climate change. The more information on

trends in storm intensity and flooding that can be provided, the more prepared these communities will be for the future.

Chapter 2

Fieldwork

Fieldwork conducted in July 2011 with the Alaska Division of Geological and Geophysical Surveys (Alaska DGGS) focused on mapping the on land and nearshore coastal morphology of the barrier system. This study is in support of a larger geohazard mapping project with the Alaska DGGS. Prior to this, limited baseline data about the Shaktoolik coastal zone were available. In the nearshore, bathymetric data were obtained seaward of the spit, in the inlet, and within the lagoon. Nearshore measurements characterize the offshore depths, which are important for calculating storm surge height, and the inlet channel morphology. Onshore, beach profiles and wrackline positions were surveyed, and grain size samples were collected along the spit. These data provide insight into the past flood levels, and the extent of possible wave runup and flooding in the future.

2.1 Bathymetry

Bathymetric summer profiles were collected along transects using a Humminbird 898c SI depth finder. Transects were positioned offshore, across the inlet, and across the lagoon (Figure 2.1). Four offshore profiles were collected normal to the shoreline: north of the inlet, at the inlet, at the community, and at the old community site. These profiles extended about 2 kilometers offshore into Norton Sound. Two other profiles were collected, one a cross-section of the inlet and the other a cross-section of the widest part of the lagoon.

The Global Positioning System (GPS) associated with the Humminbird did not function correctly so a handheld GPS, Garmin 76 CSX was used to collect GPS points associated with the bathymetric depths and logged points every 10 to 30 seconds depending on the transect. For transects in which the GPS logged every 30 seconds, post-processing of the bathymetric data assumed a constant speed between GPS points in order to use more of the depth points, which were collected every second (1 Hz) by the Humminbird.

Other post-processing of the data showed that in shallow water, less than 4 meters depth, the Humminbird did not always record the correct depths. When compared with the depth imaging created by the Humminbird, the depth readouts did not always match up. To correct for this, the depth images were digitized using Didger 2.0 software and known GPS control points, then accurate depths were collected from the digitized images. Again, constant speeds were inferred between known GPS point. Figure 2.2 shows an example of one of these depth images used for digitizing the depths. The final depth data were then corrected for tides, based on the Mean Lower Low Water (MLLW) level at the closest NOAA tide gauge in Nome, and for the depth of the transducer below water level.

Finalized bathymetric profiles are shown in Figures 2.3 and 2.4. In the offshore the profiles generally are very shallow, the maximum depth at 2.2 km offshore is 7.3 meters. At the old community site, there is a steeper offshore slope compared to the new community site, which may contribute to the foreshore erosion at the old site that is not seen at the new site. Error estimates for the data points are

+/-1 m in the horizontal direction and +/-0.1 m in the vertical direction. These error estimates exist in the horizontal and vertical directions due to accuracy associated with the digitizing method. Error in the horizontal is larger because of the additional error associated with the accuracy of the handheld GPS device.

Further offshore, bathymetry was obtained from Smith and Sandwell (1997). Offshore bathymetry, extending from the nearshore out to the Bering Sea at a distance of 797 km away, was recorded along a single transect and represents the maximum fetch over which storm surge can build up before it reaches Shaktoolik. For both the storm surge and wave runup calculations in Shaktoolik, the offshore bathymetry provided by Smith and Sandwell was merged with the nearshore bathymetry collected in the field, to create profiles extending from the surf zone to further offshore. Figure 2.5 shows the bathymetric profile used in the analytical storm surge model.

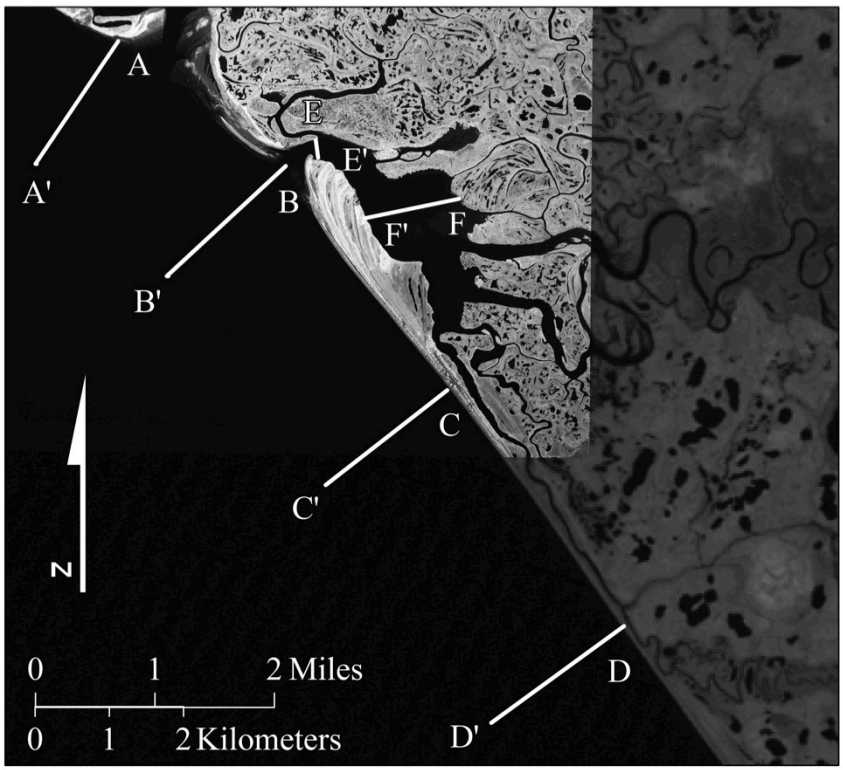

Figure 2.1. Map of bathymetric transect locations: four profiles were conducted offshore, one across the inlet, and one across the widest part of the lagoon. Satellite imagery from Landsat USGS (2007).

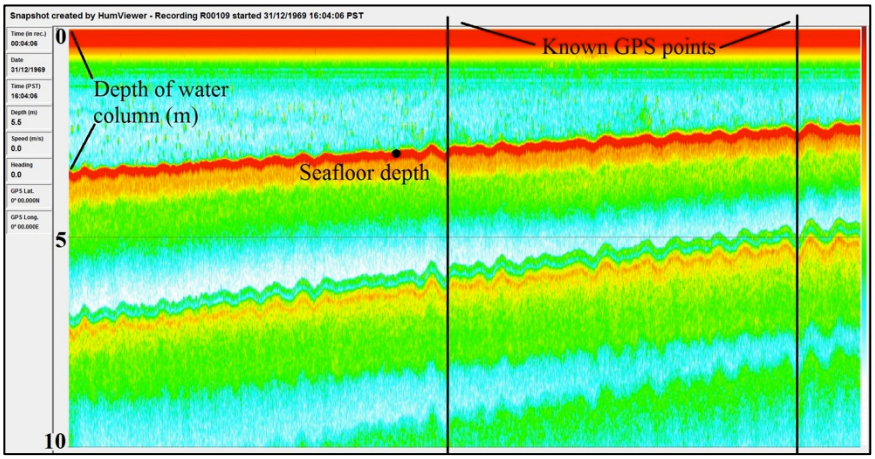

Figure 2.2. Picture of the depth readout provided by the Humminbird depth finder. These images were digitized between known GPS points to provide accurate depth readings for the bathymetric survey. A constant boat speed was assumed between known GPS points.

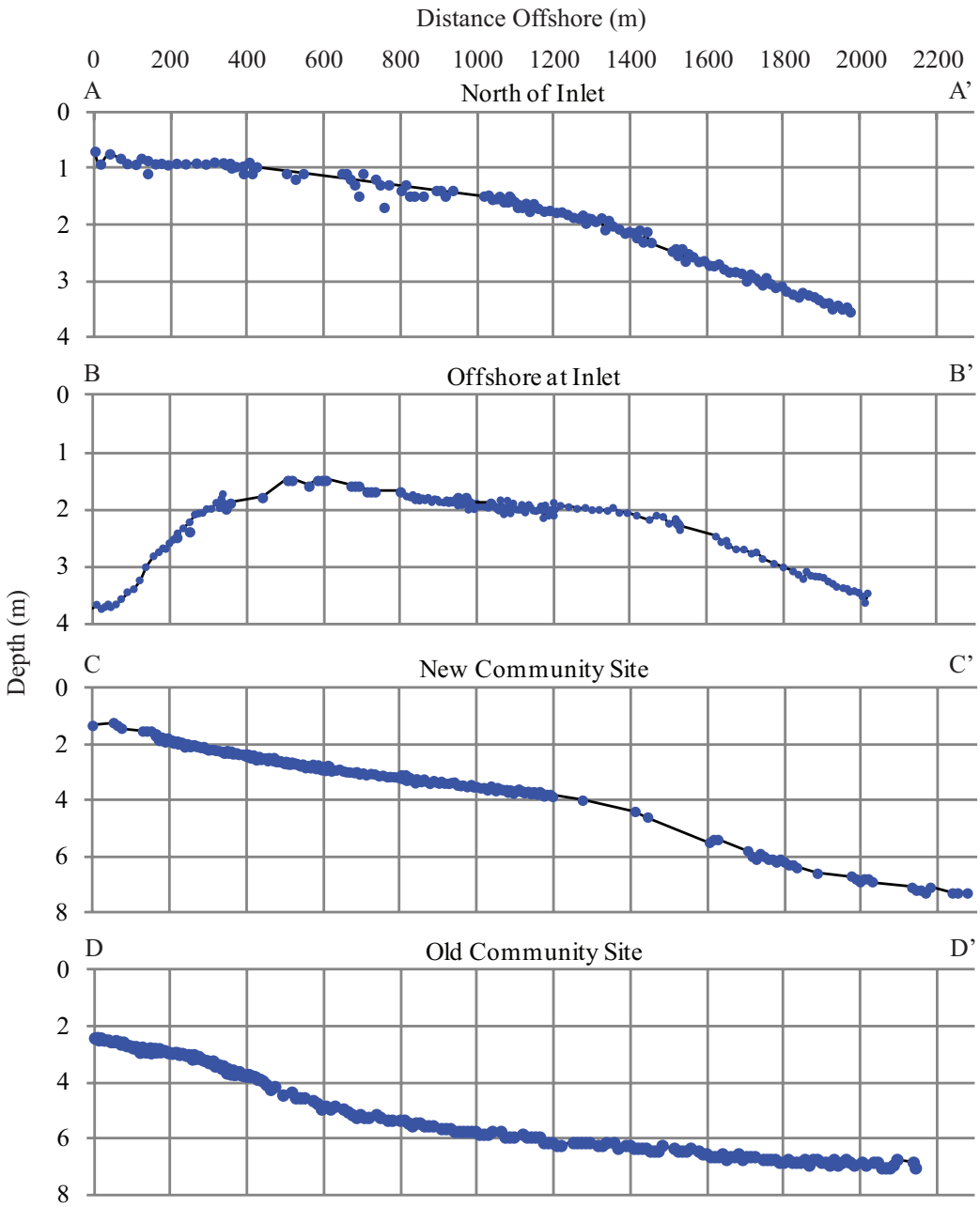

Figure 2.3. Depth profiles for each offshore transect. Letters correspond to locations on the map in Figure 2.1, for example Figure 3A is the profile north of the inlet from A to A' in Figure 2.1.

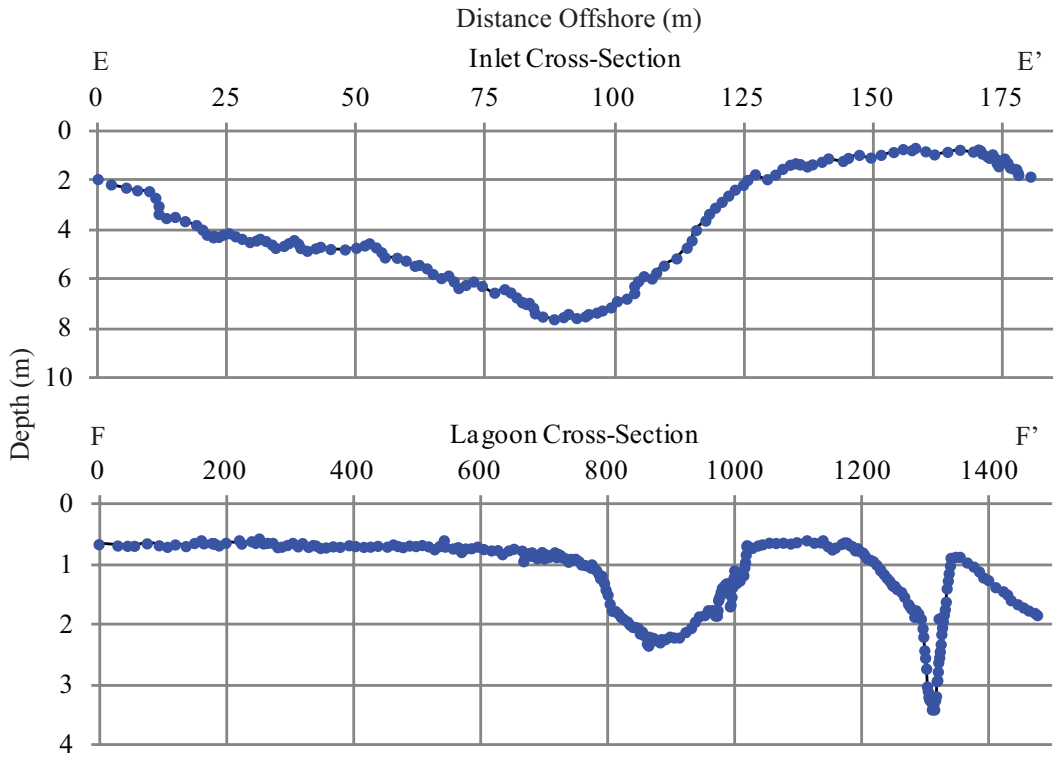

Figure 2.4. Depth profiles for the inlet and lagoon cross-sections. Letters correspond to locations on the map in Figure 2.1, for example Figure 3E is the profile north of the inlet from E to E' in Figure 2.1.

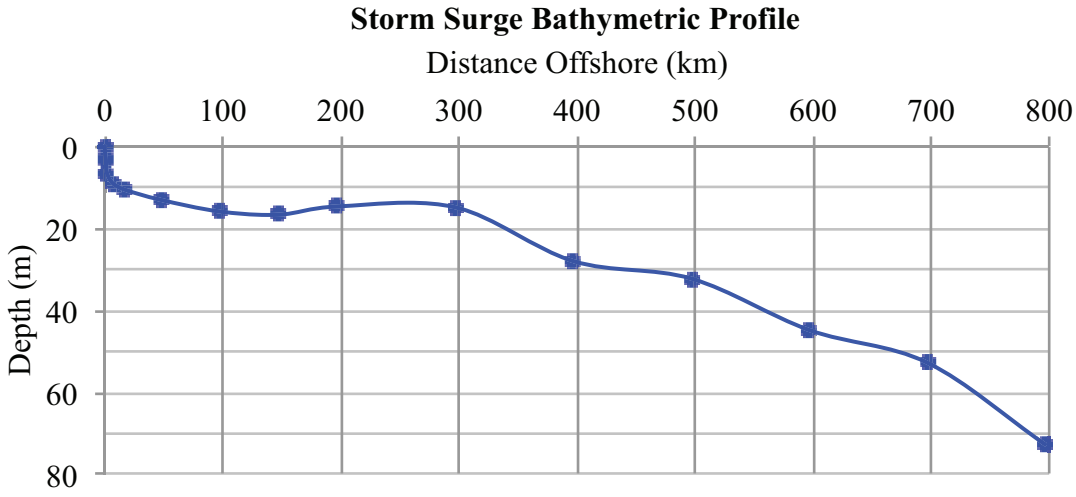

Figure 2.5. Storm surge depth profile extending from nearshore waters at Shaktoolik to maximum fetch 797 km away in the Bering Sea.

2.2 Debris Lines

Debris lines along the Shaktoolik Spit primarily consist of large woody debris piled up on the foreshore. The woody debris is deposited on the beach during storm events and associated flooding. The seaward positions of the large debris lines were documented alongshore using a Garmin 76 CSX handheld GPS. Two distinct debris lines were identified and GPS coordinates were collected alongshore at the lower (seaward) extent of the debris. Figure 2.6 shows a photo of these two debris lines in front of the current community. GPS points were collected on the island north of the inlet, along the lagoon near the inlet, and along the open water beach from the inlet down past the old community site.

The presence of large debris lines as far inland as 30 m and as high as 5.4 m above MLLW in front of the community indicates high historic flood levels from storm events. Furthermore, these large debris lines could potentially serve as a barrier for the community from storm surge and wave runup, or as a destructive force as high flood levels inundate the community and carry the debris further inland. The storm magnitude and time of deposition is investigated later in this study.

Figure 2.6. Photo of the upper and lower debris lines on the open ocean beach in front of the community.

2.3 Beach Profiles

Cross-shore beach profiles were conducted along the Shaktoolik spit and north of the inlet using high-precision Global Positioning System (GPS) equipment. GPS points were collected for 46 transects; 43 from the open-water side of the spit and three on the lagoon side next to the community. Figure 2.7 shows a map of the transect locations. Profiles were taken starting at the landward swash limit and moving inland. Along each transect, boundary points were identified at the swash limit, wet-dry line (if different from the swash at the time of survey), grain size transitions, manmade features, vegetation lines, seaward and inland extent of debris lines, ridges or runnels, and noticeable slope breaks such as a berm crest or scarp. GPS locations and notes were documented at each of the boundary points present along each transect. In addition, many photographs of sediment were taken and a few sediment samples were collected for grain size analysis.

Two of the profiles were chosen as locations for the wave runup analysis: transect numbers 18 and 29 because they correspond to offshore bathymetric surveys at the new and old community sites (see Figure 2.7). The cross-sections of these profiles are shown in Figure 2.8.

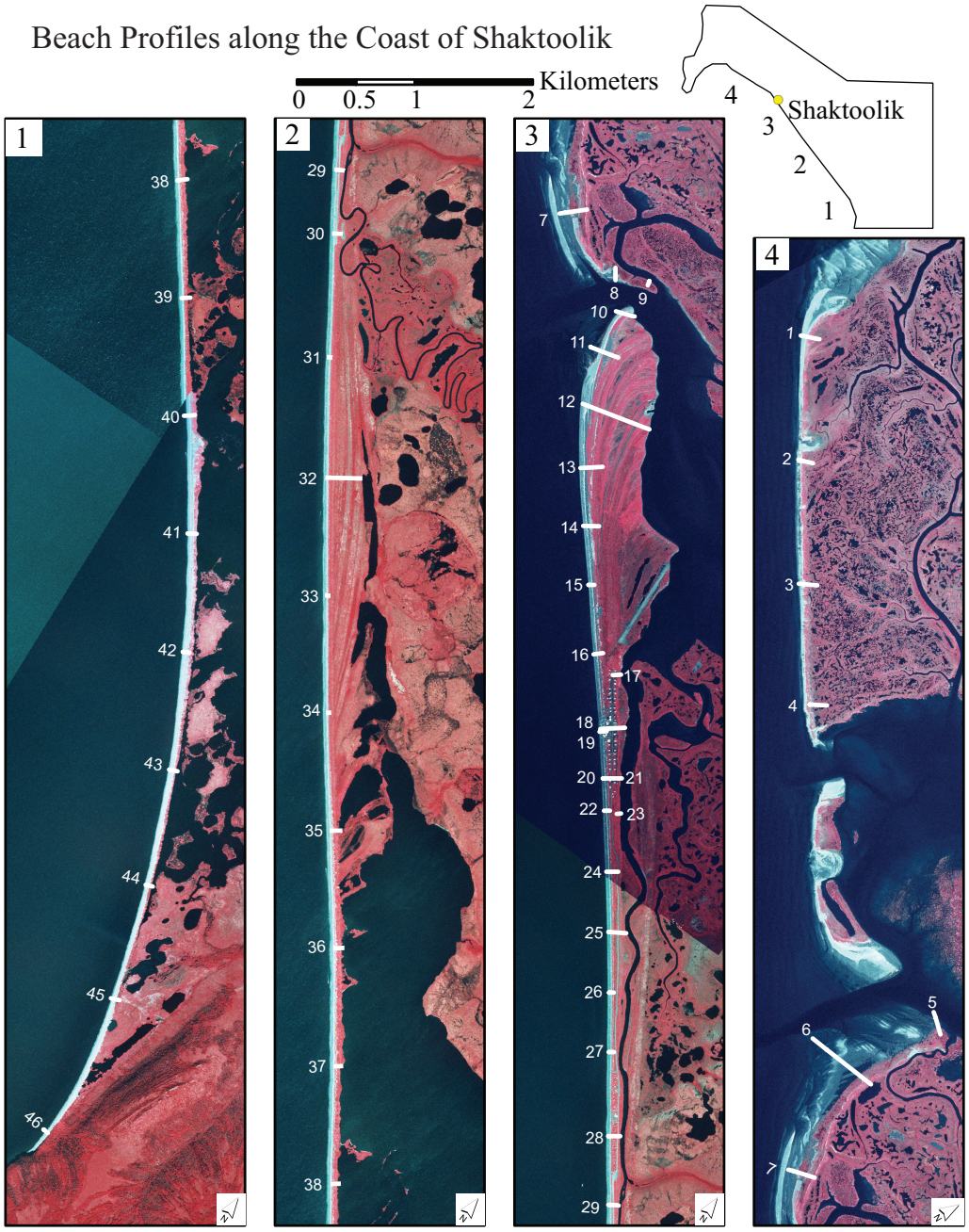

Figure 2.7. Map of beach profile locations along the Shaktoolik spit. Modified from an unpublished figure by N. Kinsman and J. Smith, DGGS, 2012. Adapted with permission.

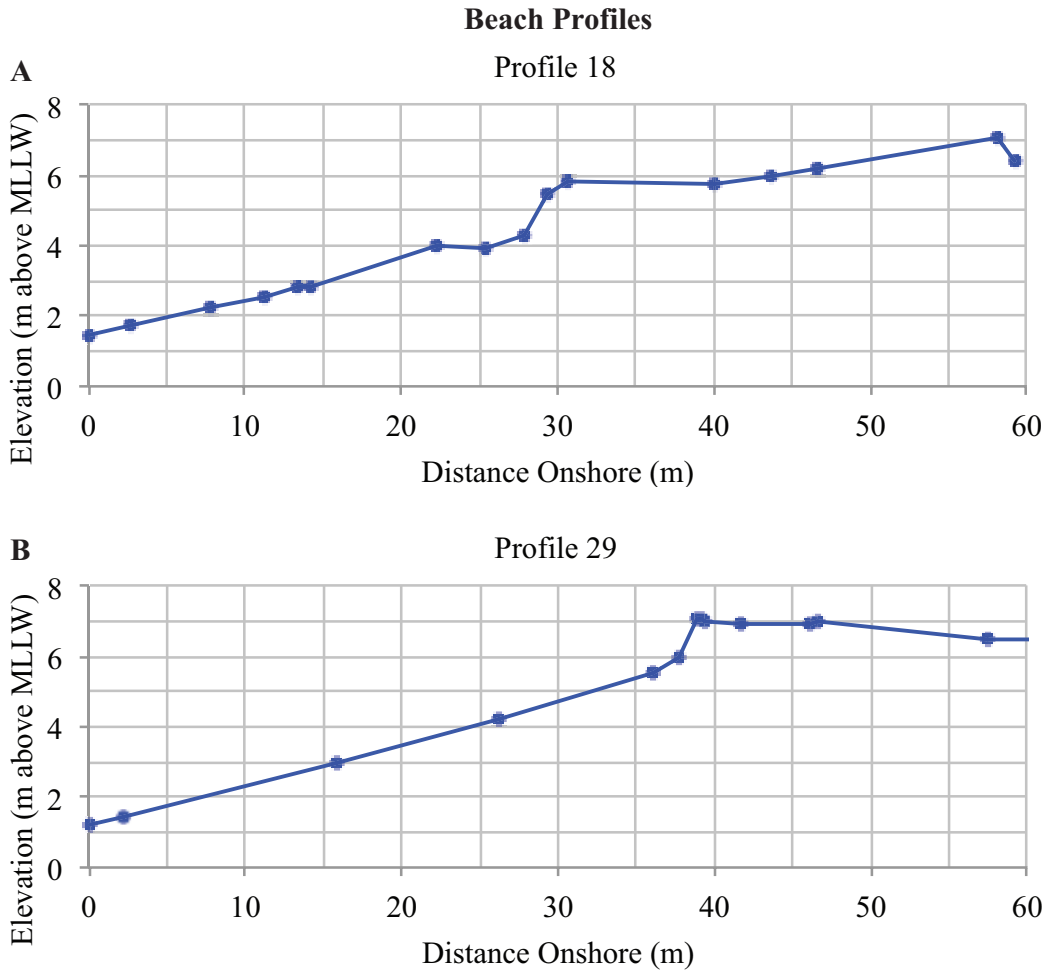

Figure 2.8. Cross-sections of beach profiles used in the wave runup analysis. Graph A shows the elevations in the New Community in front of the school. Graph B shows the elevations at the Old Community site.

2.4 Grain Size Analysis

Grain size analysis of the foreshore was conducted using samples collected along the beach profile transects. A total of 269 samples were collected, 43 physical sediment samples and 226 in situ digital images of sediment. The majority of the samples consisted of coarse sands to gravels and poorly sorted (had a wide range of

grain sizes). To analyze this wide array of grain sizes, an autocorrelation grain size analysis technique was used.

From a digital photo of sediment, the autocorrelation method estimates mean grain size based on the similarity between pixels to determine different grains in the sample. This technique was developed at the U.S. Geological Survey Pacific Coastal and Marine Science Center and has proven to accurately estimate mean grain size and sorting for mixed grain size beaches (Warrick et al., 2009). An extension of the original technique calculates grain size based on a two-dimensional form in the frequency domain rather than the one-dimensional form in the spatial domain. This method only requires information about the spatial resolution of the image and eliminates the need for calibration using sediment samples (Buscombe et al., 2010). Error estimates using this method are comparable to the one-dimensional autocorrelation technique. The two-dimensional technique is best for this project since many of the grain size samples are digital images of sediment collected in the field so they cannot be used for calibration in the lab.

The 43 sediment samples that were brought back from the field were photographed in the lab three times, mixing the sediment each time, using a digital camera. Once all 269 samples were in digital form, each sample was documented and notes on the grain size and sorting of the sample were recorded. The images were copied and cropped so that only clearly resolved sediments were visible; debris, vegetation, and scale were excluded from the cropped photos and any photos that appeared blurry were eliminated. Since many of the photos taken in the field were

not exactly orthogonal to the ground surface, the images were cropped to an area next to the scale bar so that the scale is accurate. Cropped images also captured representative samples of the entire image; Figure 2.8 shows photos of some of the sediment samples collected.

The original photos were run through a MATLAB script to estimate the scale, in millimeters per pixel, using scale bars in the images. Each photo collected in the field had a slightly different scale. Cropped images were run through the autocorrelation MATLAB script to determine the mean grain size and sorting of each sample in pixels. Sorting results included normally distributed percentile grain sizes: 5^{th} (d05), 10^{th} (d10), 16^{th} (d16), 25^{th} (d25), 50^{th} (d50), 75^{th} (d75), 86^{th} (d84), 90^{th} (d90), and 95^{th} (d95). The mean grain size and sorting sizes, in pixels, was then multiplied by the scale, in millimeters per pixel, to get the mean grain size in millimeters. Results were compared to notes taken on each sample to ensure that the mean grain size calculations were accurate. In some cases the photos had to be cropped differently and run through the autocorrelation script a second time. For the samples brought back from the field, in which three photos of each sample were taken, an average of the three mean grain sizes and sorting sizes were used.

The results of the autocorrelation technique were validated using a point count method to compare mean grain size values. The point count method is the best validation of the autocorrelation technique because it uses the same digital image and is based on surface area, like the autocorrelation method, and not volume which sieving methods rely on (Buscombe et al, 2010). Point counts were conducted on 10

of the digital image samples picked with varying mean grain size estimates and sorting. The samples were divided into a 10 x 10 grid so that there were 100 intersections on each image. For the very coarse-grained samples, a 5 x 5 grid (25 intersections) was used because there were fewer grains to measure. Grains located at each intersection were measured and the average was taken of all 100 grains, or 25 grains for the 5 x 5 grid. This average represents the mean grain size of the sample and was compared directly to the mean grain size estimated by the autocorrelation method. Results of the validation analysis are shown in Figure 2.10.

A total of 226 sediment samples were used in the final results. Some samples had to be eliminated because the pixel resolution was too low, the photo was blurry, or the sample was not from the shoreface. The results of the grain size analysis show that average mean grain size from all the samples collected is 12.04 mm, and the median is very similar at 12.15 mm diameter. Gravels and pebbles dominate Shaktoolik's beaches and most of the samples were poorly sorted. There is also an increase in average grain size laterally from the end of the spit near the present day community to the base of the spit where it meets land. Figure 2.11 displays the change in grain size laterally along the spit.

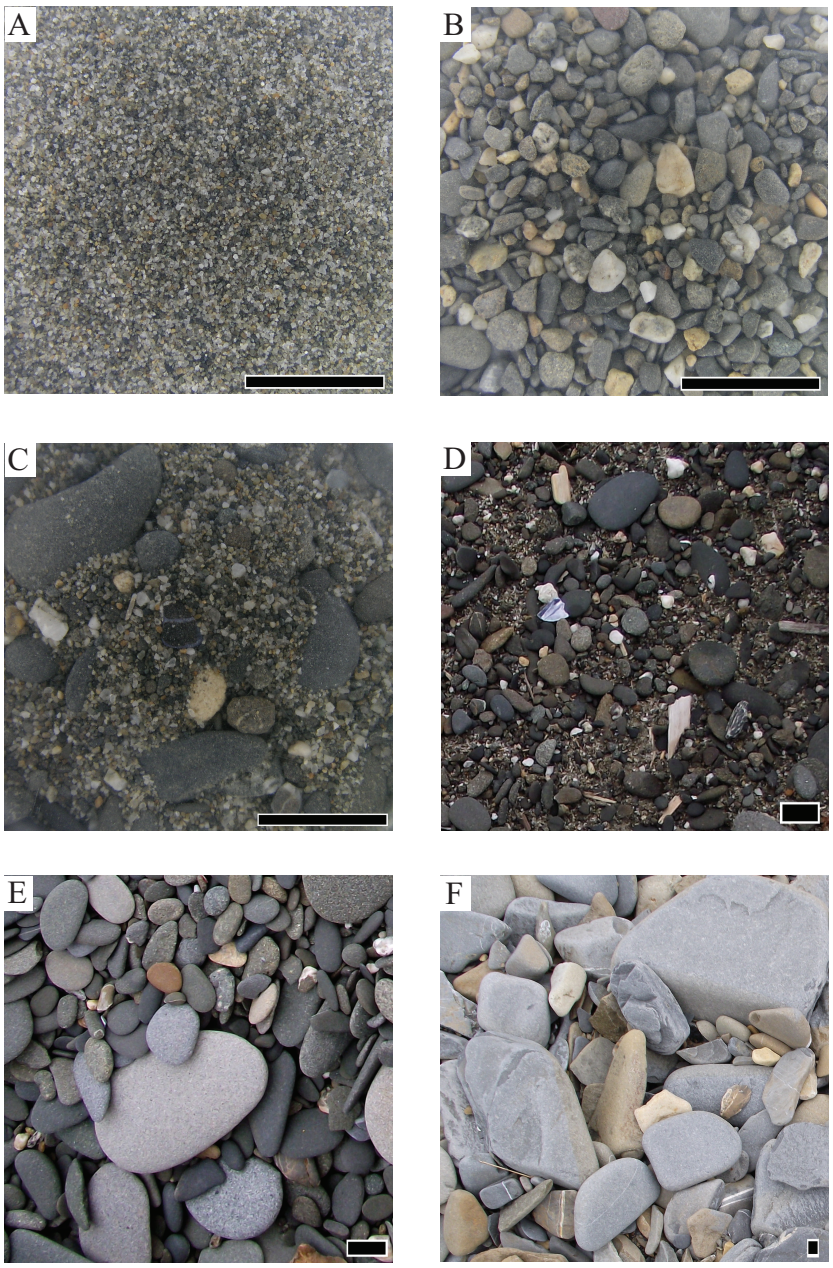

Figure 2.9. Sediment samples from Shaktoolik's beaches. The black bar represents 1 cm. These images display the wide variations in grain size and sorting along the beaches. Mean grain sizes calculated: (a) 0.61 mm, (b) 2.48 mm, (c) 2.25 mm, (d) 4.02 mm, (e) 15.92 mm, and (f) 64.64 mm.

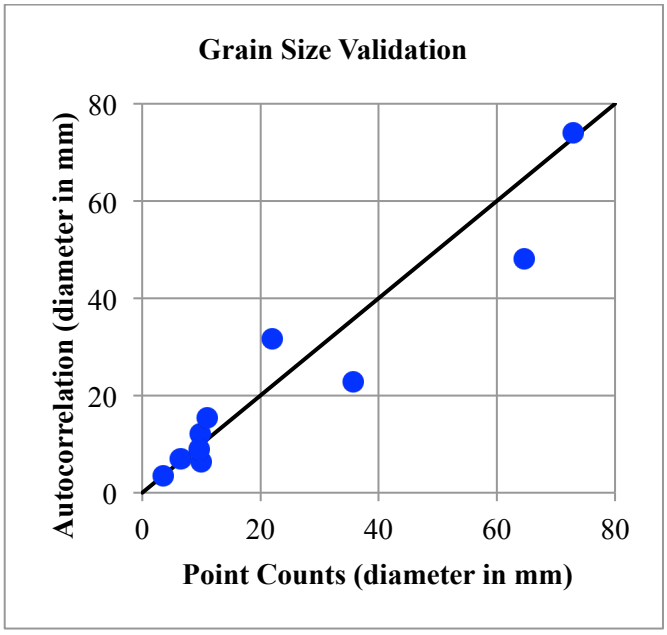

Figure 2.10. Validation of grain size analysis using the autocorrelation method. Results from the point counts are plotted on the x-axis versus the results from the autocorrelation on the y-axis. $R^2 = 0.91$ for these dataset.

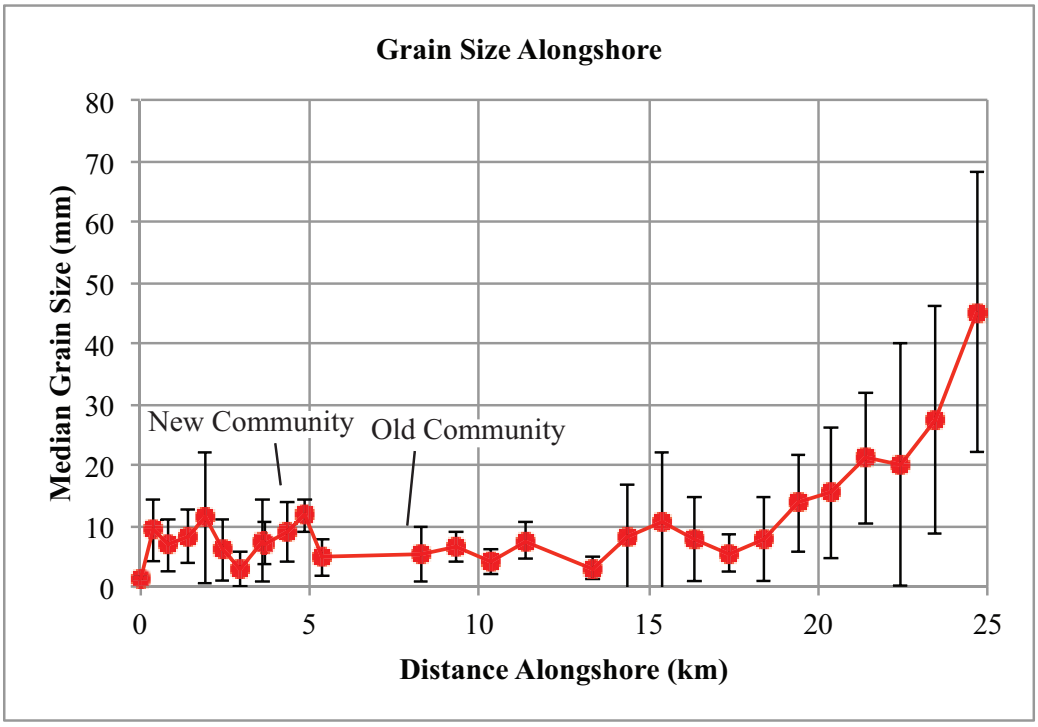

Figure 2.11. Grain size along Shaktoolik's spit. Distance along spit is the distance laterally from Profile 10. Error bars represent the standard deviation of the each dataset. Locations of the community and old community are also noted.

Chapter Summary: The fieldwork portion of this study was used to identify potential hazards, provide baseline data for the community of Shaktoolik, and to integrate into the modeling portion of the study. Offshore bathymetry and beach profiles in particular are important data used to calculate overall storm surge and wave runup elevations. The location of the debris lines is useful to evaluate historical flooding extent and the recurrence intervals for floods can be compared to identify the magnitude of the storm that deposited the debris. Grain size has an impact on wave runup elevation causing greater water infiltration with larger grains, which acts as a damping effect. These field data make up an important component of the overall storm surge and wave runup results.

Chapter 3

Storm Surge

3.1 Development of Analytical Model for Storm Surge

Historical sea level pressure data from four different GCMs from the Coupled Model Intercomparison Project (CMIP5) were compared in order to choose the best one for this analysis. The four GCMs included MIROC5 (MIROC) from the Atmosphere and Ocean Research Institute at The University of Tokyo, INM-CM4 (INMCM) from the Institute for Numerical Mathematics, GFDL-ESM2M (GFDL) from the NOAA Geophysical Fluid Dynamics Laboratory, and BCC-CSM1.1 (BCC) from the Beijing Climate Center. These models were chosen based on the inclusion of historical model runs and availability of modeled data at the time of this study.

The reference data for sea level pressure used to assess the accuracy of each model came from the North American Regional Reanalysis (NARR). NARR provides high resolution and high frequency atmospheric and land surface hydrology data for the years 1979 to the present (Mesinger et al., 2006). NARR is also considered to be the most accurate and highest resolution reanalysis of historical meteorological data.

Three-hourly climatologies for sea level pressure from each GCM and the NARR for the years 1996-2005 were utilized for the comparison (Mesinger et al, 2006). Since the GCMs have lower resolution, the pressure data were interpolated onto the higher resolution NARR grid. Table 3.1 shows the spatial resolution for each model. The grid extended from 44 to 76°N latitude and 170 to 230° longitude so

that only the Alaska region was included in the analysis. Sea level pressures for each GCM and the NARR data were averaged at each grid point annually from 1996-2005, across the 10-year time span, and monthly from July through October over the 10 years of study.

Taylor Diagrams were used to analyze these means. Developed by Taylor (2001), these diagrams provide a statistical summary to compare how well patterns, in this case GCM runs, match a reference data frame, NARR. The statistical similarities are based on the correlation (R-value), root mean square difference (RMS), and standard deviation of each GCM compared to the NARR data. The results of the Taylor Diagrams are shown in Figures 3.1 to 3.4. The GCM MIROC5 was the most consistent in statistical similarity to the NARR reference data. MIROC5 also showed the closest correlation with the NARR during October, the month with the highest storm frequency out of the months analyzed (Figure 3.4D). MIROC5, therefore, was chosen to develop the analytical method and for calculating future flood level projections.

Table 3.1. Spatial resolution for each GCM and the NARR datasets.

Model	**Model Resolution (lon x lat) in degrees**
BCC-CSM1.1	2.8 x 2.8
INM-CM4	2.0 x 1.5
MIROC5	1.4 x 1.4
GFDL-ESM2M	2.5 x 1.5
NARR	0.25 x 0.25

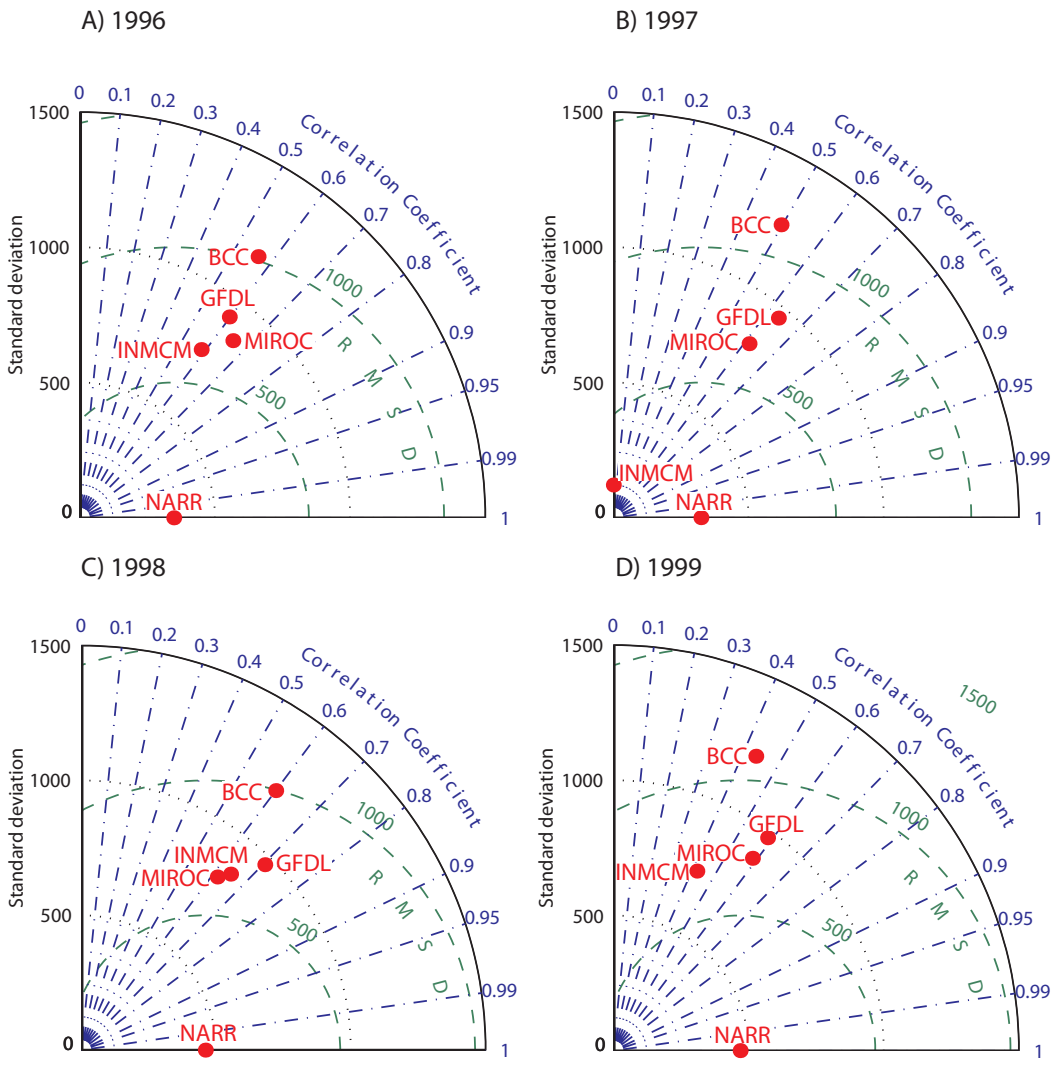

Figure 3.1. Taylor Diagrams for the years 1996-1999 (A-D). On the y-axis, the standard deviation in mean sea level pressures for the year, at each grid point in the Alaska grid, for each of the models is plotted. Radially, the correlation coefficient between each of the models and the NARR data reference frame is shown and the root mean squared deviation (RMSD) between each of the models and the NARR dataset is also plotted.

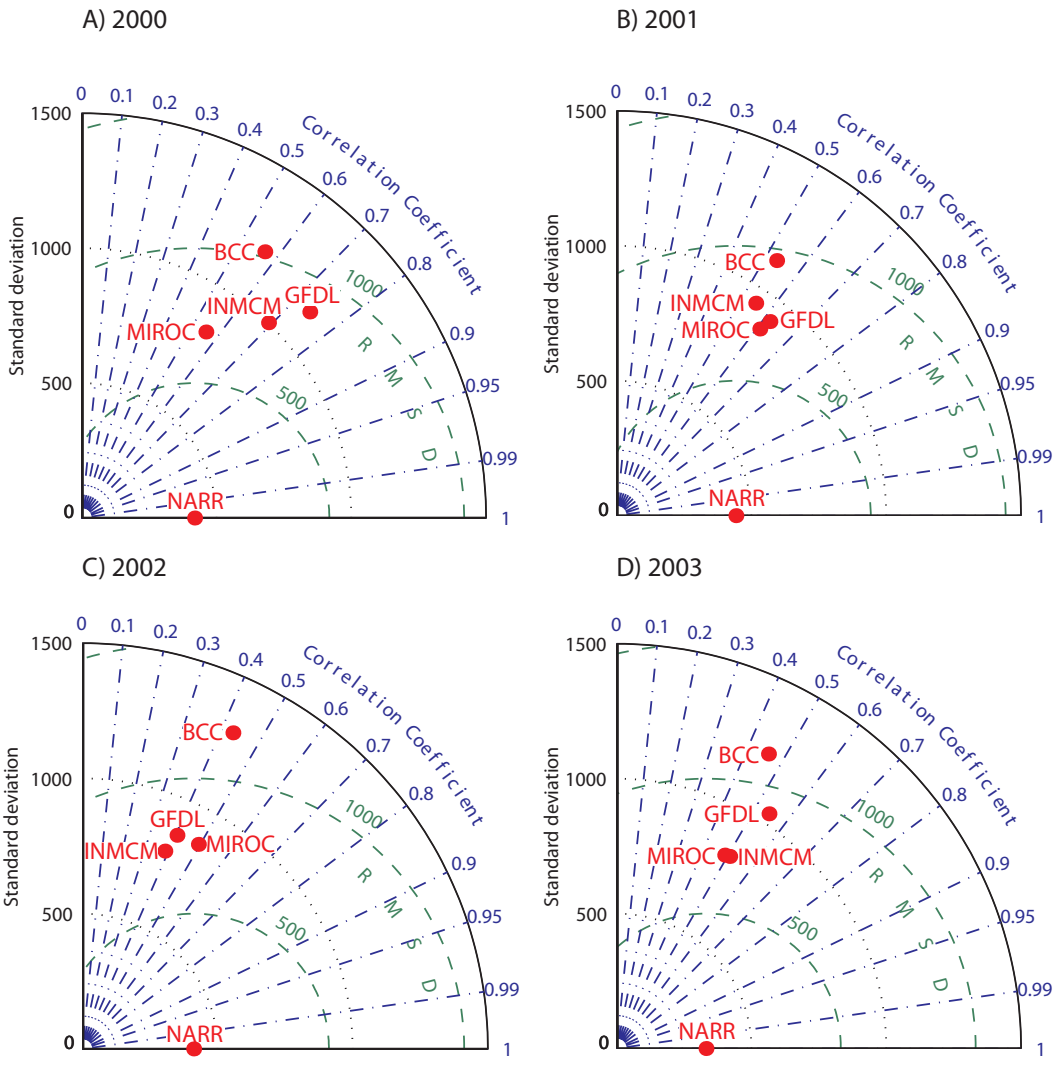

Figure 3.2. Taylor Diagrams for the years 2000-2003 (A-D) as described previously.

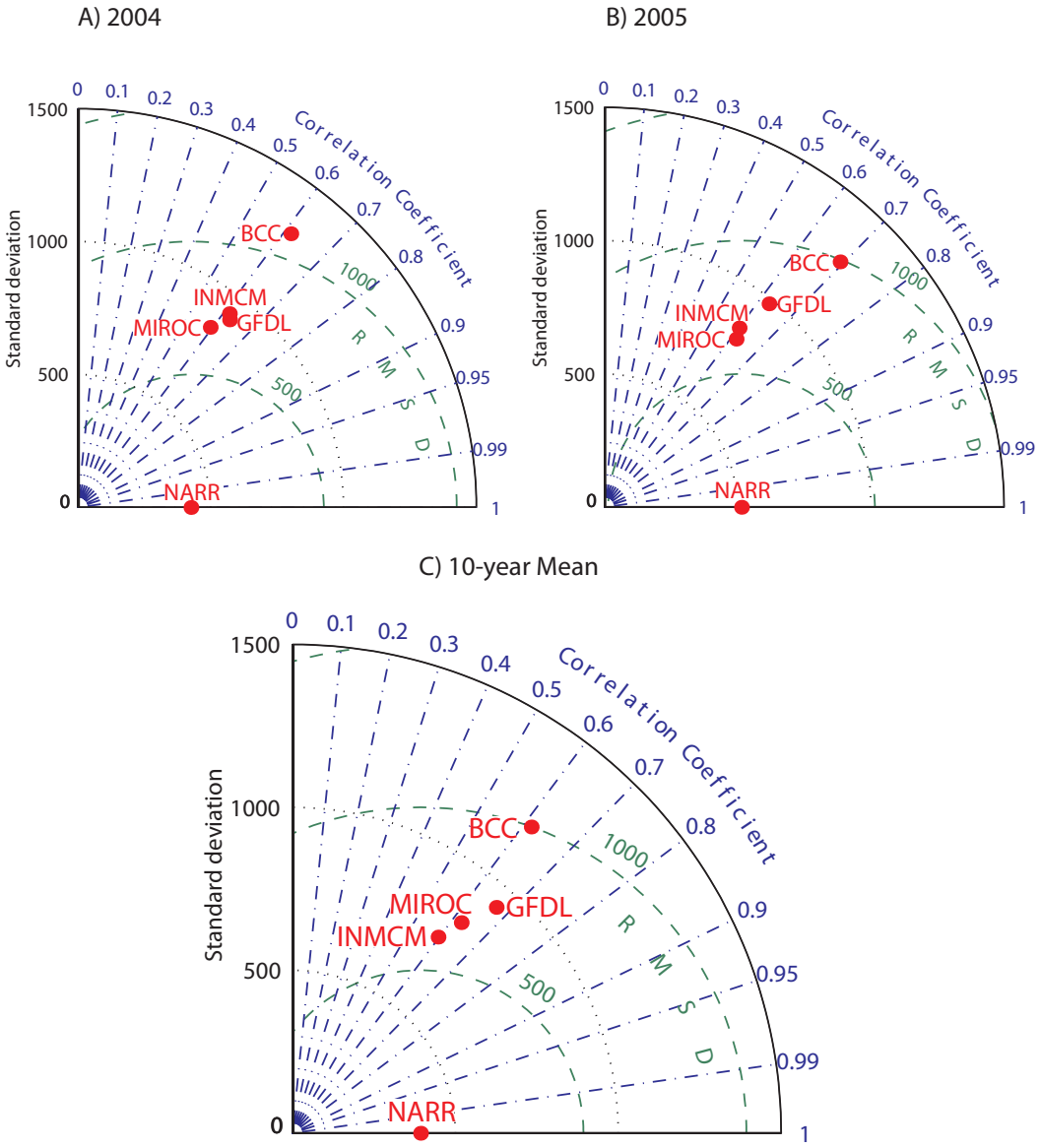

Figure 3.3. Taylor Diagrams for the years 2004-2005 (A-B) as described previously. Plot C shows the mean of sea level pressures across the 10-year times span, 1996-2005.

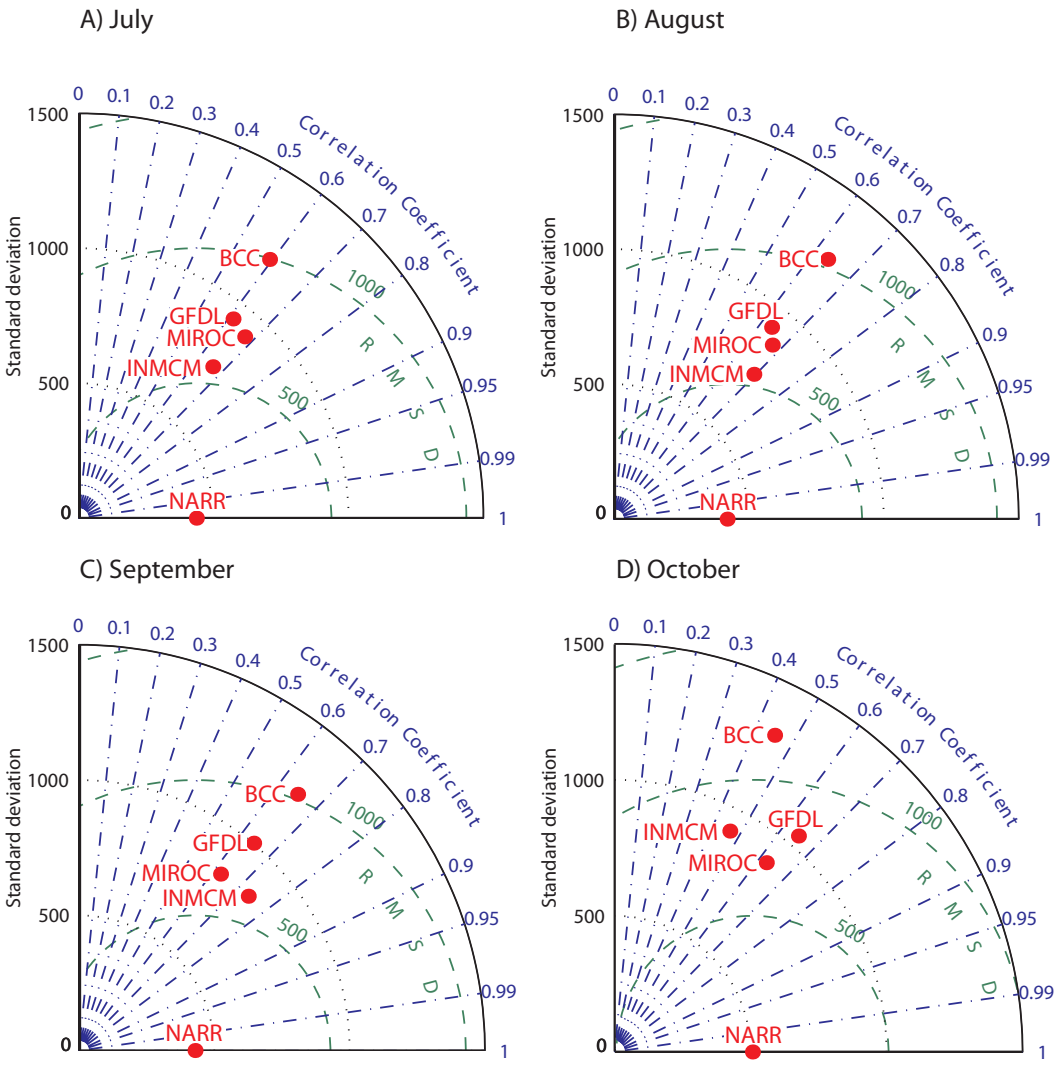

Figure 3.4. Taylor Diagrams for months July-October (A-D) as described previously. Monthly sea level pressure means were taken across the 10-year time span for each ice-free month of the year.

The next step in developing the analytical method was to quantify storm surge using NARR and MIROC5 data for the largest historic storm surge events, as identified and modeled by the USACE study in Shaktoolik (USACE, 2011)(Chapman et al., 2011). There are no observational data for storm surge heights in Shaktoolik so the USACE numerical modeling study was chosen for calibration of the analytical model in this study. The USACE study is the most extensive storm surge and wave

runup evaluation in Shaktoolik to date and uses some of the most sophisticated modeling techniques available currently.

Table 3.2 summarizes the flood levels calculated in the USACE study and used for calibration of the analytical model. Using historical data from NARR for sea level pressure (slp), north-south winds 10m above sea level (v_{as}), east-west winds 10m above sea level (u_{as}), and the equations for wind driven surge and pressure driven surge from Kamphuis (2000) discussed earlier, storm surge height was calculated for the top events. The USACE study uses storm events back to 1954, but the NARR data only extend back to 1979 so many of the top 10 events outlined in the USACE study could not be used for the analytical model validation. Therefore calibration with the NARR data was done with smaller surge events from the USACE study, for a total of 10 events to compare (see Table 3.2). Other inputs to the analytical model were offshore bathymetry collected in the field and from Smith and Sandwell (1997) measured along a shore normal southwest trending transect, out to deep water in the Bering Sea, for a maximum fetch of 797 km.

It is preferable to calibrate the analytical model using NARR as opposed to MIROC5 because the NARR wind and pressure data are the most accurate and highest resolution. They also rely on historical meteorological data. Therefore the results of the analytical model using NARR data should have the best correlation with the USACE results.

Table 3.2. Top storm surge events in Shaktoolik for the period 1954-2009. Storms identified in the USACE but excluded from this comparison were storms with duration longer than 10 days and storms occurring during months of extensive ice cover (December through June). Shaded boxes show storm events in which NARR data coverage is available. Modified from USACE (2011).

USACE Rank	Start Dates (in UTC)				Max surge (m)	Duration (days)
	Year	Month	Day	Hour		
1	1960	10	1	0	4.35	6.5
2	1974	11	10	0	3.80	6.5
3	1970	11	26	0	3.27	6.5
4	1966	11	14	0	3.20	6.5
5	1978	11	8	0	3.08	6.5
6	1975	8	21	15	2.80	6.5
7	2004	10	15	0	2.79	6.5
8	2005	9	18	0	2.68	7.5
9	1965	11	12	0	2.64	6.5
10	1996	10	25	0	2.63	6.5
13	1990	9	1	0	2.40	9.7
14	1991	10	18	0	2.20	6.5
17	1990	11	16	0	2.14	6.5
20	1985	11	6	0	2.07	6.5
24	1983	10	3	0	1.84	8.5
25	1994	8	12	0	1.75	10
27	1992	10	2	0	1.70	6.5

In the analytical model, pressure driven surge due to the inverse barometric effect is calculated by finding the change in sea level pressure between the location of maximum fetch, 797 km offshore at 60° N latitude and 171° 30’ W longitude, and at Shaktoolik’s location for each 3-hourly time step. If the sea level pressure is higher offshore than at the coast then there will be a rise in water level at the coast according to Kamphuis’s (2000) equation (Equation 1.2).

For the wind driven surge component in the analytical model, wind speed and direction are calculated from the u_{as} and v_{as} wind vectors (east-west component and north-south component, respectively) at the location of maximum fetch. The offshore grid cell at the location of maximum fetch was used because many of the storms do not track completely into Norton Sound; therefore the offshore wind speed that builds up surge heading toward Shaktoolik is not necessarily represented at the coastline. The analytical model surge heights also showed much better correlation with the USACE study results when using an offshore grid cell for wind speed and direction than when using the grid cell closest to Shaktoolik's location.

The wind directions are altered so that they are oriented correctly for Shaktoolik's location with a maximum value of 180° for an onshore wind, where the shoreline trends northwest 320° and southeast 140°. Therefore a wind direction of 230° is directly onshore so the new wind direction is 180°. These values decrease to zero for a directly offshore wind, which in Shaktoolik has a 50° initial azimuth direction. The wind direction and speed for each time step, along with distances offshore and depths from the bathymetric data are used to calculate storm surge height at the coast using the one-dimensional storm surge equation from Kamphuis (2000).

Wind duration is also incorporated into the storm surge equation. Winds of the same origin are defined as having a wind direction with a less than 15° difference, wind speed less than 5 ms^{-1} difference, organized into 5 ms^{-1} bins starting at a wind magnitude of 10ms^{-1}. In the analytical model, the wind direction and speed from one

time step are compared against the previous time record to see if they match these criteria. If the winds do, then the duration of the same wind is continued and increases by 3 hours with each time step until they no longer match the criteria, in which case the duration goes back to zero. The duration component is included as a coefficient in the wind-driven surge equation and divided by 33 hours so the coefficient is dimensionless. The 33 hours was chosen because it is the average wind duration for wave growth, based on wind speed and fetch distance, from the wave analysis and forecasting nomogram (Bretschneider, 1970).

In addition to including the wind duration during storm events, the track of the storms was also found to be an important factor. Figure 3.5 shows the typical storm tracks that impact the area. The largest storm surges in Shaktoolik are caused by storms tracking eastward from the North Pacific and then turning and tracking north through the Bering Sea. In the analytical model, low-pressure systems traveling eastward through the Aleutians or over land also produced storm surges in Shaktoolik. These storm events were not included in the USACE storm population because they either occurred farther East over the Alaskan continent or farther offshore so they did not produce water level setup in the study area (USACE, 2011)(Chapman et al., 2011). Therefore these storm tracks were also filtered out in the analytical model because they did not produce significant surge at the coastline historically. From Figure 3.5 only the tracks BS1 and BS2 storm tracks were recognized to produce surge in the analytical model, storms following all other tracks were assumed not to produce storm surge in Shaktoolik. Historical low-pressure

systems were tracked manually and storms not travelling north through the Bering Sea were filtered out so that only the dates of storm events in the Bering Sea were used for the storm surge calculations.

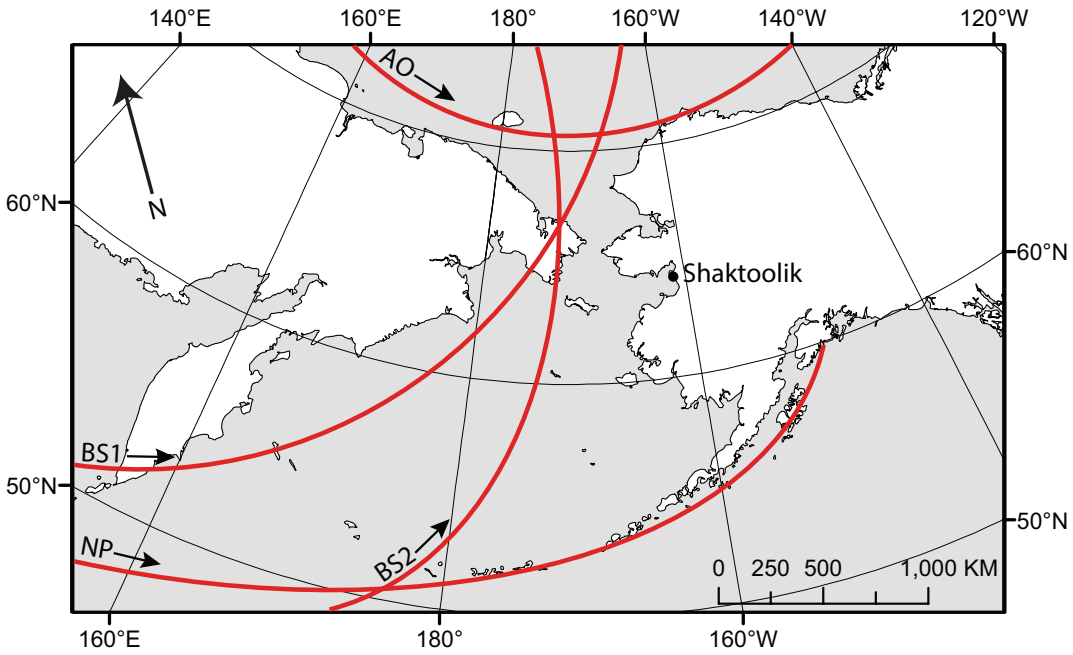

Figure 3.5. Map of typical storm tracks in the Alaska region. Tracks BS1 and BS2 represent storms that travel North through the Bering Sea and cause substantial water level setup in Shaktoolik. Tracks in the Arctic Ocean (AO) and North Pacific (NP) were filtered out of the analytical model, as they do not cause significant surge along the Shaktoolik coastline.

Storm surge heights from the top events outlined in the USACE study were used to calibrate the analytical model. In the analytical model, for each storm, the length of the model run was extended to 7 days before the start date of the storm event in order to allow sufficient time for the wind duration to build up. The model was then run for each of the storm events and the highest surge height during the event was plotted against the USACE maximum surge height. The relationship between the two was linear so the equation of the best-fit line between the two

datasets was found and incorporated into the analytical model. This calibration process makes the analytical model more accurate because the analytical approach cannot take into account all the components of storm surge that can be incorporated in a numerical model. Using a best-fit line to calibrate the data factors in these storm surge components that were missed in the one-dimensional storm surge calculation.

3.2 Model Validation Results

The linear best-fit line equation was found to further calibrate the NARR data against the USACE storm surge height results. The correlation between the results of the analytical model using the NARR data and the USACE study has an R^2=0.69. Furthermore the analytical model results show a similar relationship to the USACE study because they both have similar standard deviations and a small root mean squared deviation (RMSD). The analytical model is compared to the USACE results in Table 3.3 and Figure 3.6.

Table 3.3. Historical NARR storm surge estimates validated against the USACE results for storm surge height. Statistical results highlighted in grey where Std Dev is the standard deviation of each model result, RMSD is the root mean squared deviation between the model and the USACE results, and R^2 is the correlation coefficient squared. Events that fall in the top 10 USACE surge events are outlined in bold.

Event Year	NARR surge height (m above MLLW)	USACE surge height (m above MLLW)
1983	2.45	2.44
1985	2.56	2.67
1990	2.65	2.74
1990	3.15	3.00
1991	3.15	2.80
1992	2.44	2.30
1994	2.77	2.35
1996	3.08	3.23
2004	3.35	3.39
2005	3.02	3.28
Std Dev (m)	0.31	0.37
RMSD (m)		0.21
R^2		0.69

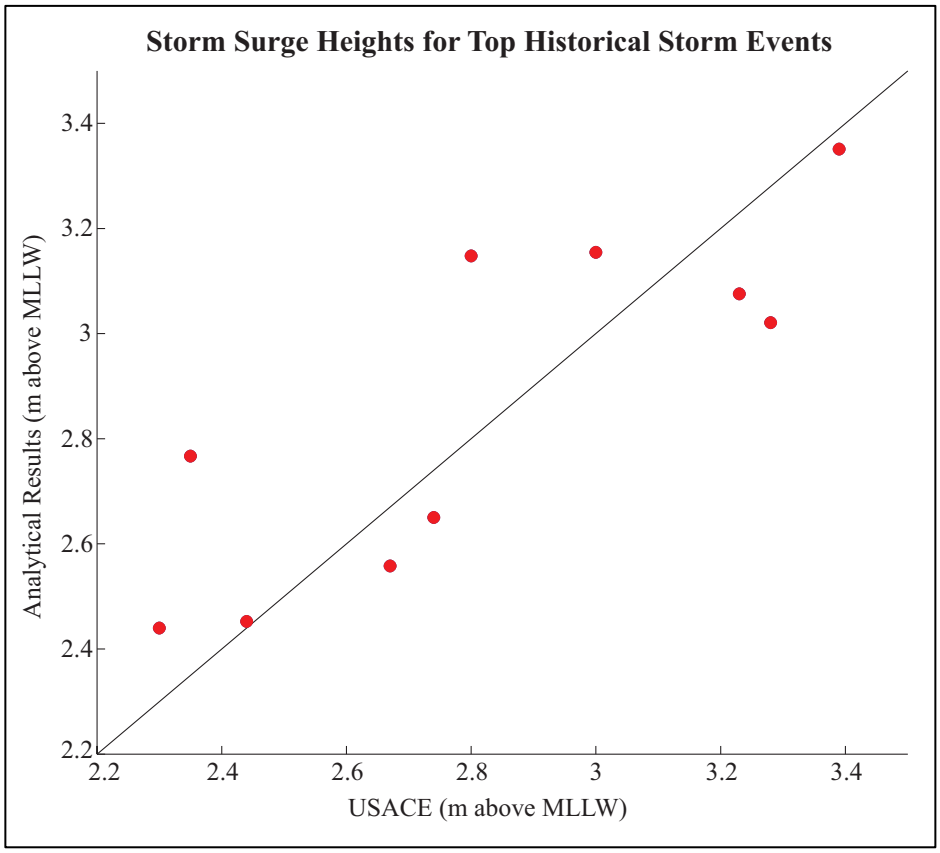

Figure 3.6. Graph of the analytically produced storm surge heights, for the NARR and dataset, versus the modeled storm surge height from the USACE study.

According to Taylor (2001) a strong fit for the analytical model is based on the small root mean squared difference between the two datasets, the similarity in standard deviations, and the high correlation coefficient. Therefore there is a correlation between the NARR and the USACE results. Since the analytical model is calibrated against the previous study of historical storm surge levels in the region, the analytical model can be used to evaluate projected storm surge heights for the mid- to late-21st century using MIROC5 projected model runs.

Chapter Summary: Development of an analytical model for storm surge included choosing the most accurate model for meteorological forcing by comparing multiple GCMs to the NARR data, using field data and storm surge equations from Kamphuis (2000) to create the model, and calibrating that storm surge model against the USACE historical surge results, which are the best available data. The storm surge model shows a close correlation with the USACE results and therefore the model is sufficiently validated for use in calculation of projected storm surges for storm events in the mid- to late-21st century.

Chapter 4

Wave Runup

4.1 Offshore Wave Height and Period

To predict wave runup, offshore significant wave height and peak wave period were modeled with the MIROC5 wind magnitude and direction data using the WAVEWATCH III (WWIII) numerical wave model, developed by the National Oceanic and Atmospheric Administration (NOAA) and the National Centers for Environmental Protection (NCEP) (Tolman, 2009). The governing equation of the model is the random phase spectral action density balance, which assumes that both ocean properties, such as water depth and current, and the wave field, vary spatially and through time on much larger scales than an individual wave. Defining parameters of physical processes include wave growth and decay as a result of the actions of wind, nonlinear interactions, dissipation, bottom friction, and scattering due to wave-bottom influences.

The WWIII model was run for the global grid (NWW3) with a resolution of 1.25° latitude by 1.00° longitude, a minimum water depth of 25 m, and a 1 hour time step (Erikson, personal communication). WWIII was forced with MIROC5 10 m height winds under two greenhouse gas emissions scenarios. The two scenarios chosen were a medium and a high emissions scenario, RCP 4.5 and the RCP 8.5 respectively, as outlined in the 2007 Intergovernmental Panel on Climate Change (IPCC) report (Solomon et al., 2007). The primary difference in these two scenarios is that RCP 4.5 corresponds to a radiative forcing of 4.5 Wm^{-2} by the year 2100 while

RCP 8.5 corresponds to a radiative forcing of 8.5 Wm^{-2} by the year 2100, which is almost double the medium emissions scenario.

The WWIII model outputs used in the wave runup analysis were significant wave height (H_s) and peak wave period (T_p). For the purposes of this study only results from one location closest to Shaktoolik, identified as Station NAWC8, were used. Station NAWC8 is located at 61° 34' 33.18" N latitude and 169° 5' 22.21" W in the Bering Sea.

WWIII output using the MIROC5 wind data was evaluated against wave measurements collected by the National Data Buoy Center (NDBC). One of the closest buoys, Station 46073, was chosen for the comparison with the MIROC5 outputs from WWIII to check that MIROC5 gives reasonable results. NDBC Station 46073 is located at 55°00'44" N and 171°58'50" W, which is 1,200 km away, southeast of Norton Sound and off the continental shelf of the Bering Sea. NAWC8, the closest WWIII virtual buoy to Shaktoolik, was not used in this comparison because of its distance from the NDBC buoy (~740 km away). Its location on the continental shelf may affect the wave heights when compared to a buoy in deeper water. Therefore WWIII outputs from station NAWC11 were used instead because of this station's proximity to NDBC Station 46073, approximately 233 km away, and it's location on the continental slope, 55°20'37.51"N and 168°20'24.31"W, as opposed to the shallower continental shelf (Figure 4.1).

Hourly outputs for significant wave height for the months of assumed no sea ice cover, July through October, from both NAWC11 and Station 46073 were

compared using graphs of mean wave height, standard deviation, and maximum and minimum values. The plots from each station are shown in Figure 4.2. The means, standard deviations, and most importantly, extreme values, are consistently similar between the WWIII output and measured significant wave heights at the buoy location. There is a strong correlation between the WWIII significant wave heights using the MIROC5 meteorological data and measured historical values; therefore it is reasonable to use the WWIII data for the projected significant wave heights during storm events in the Bering Sea.

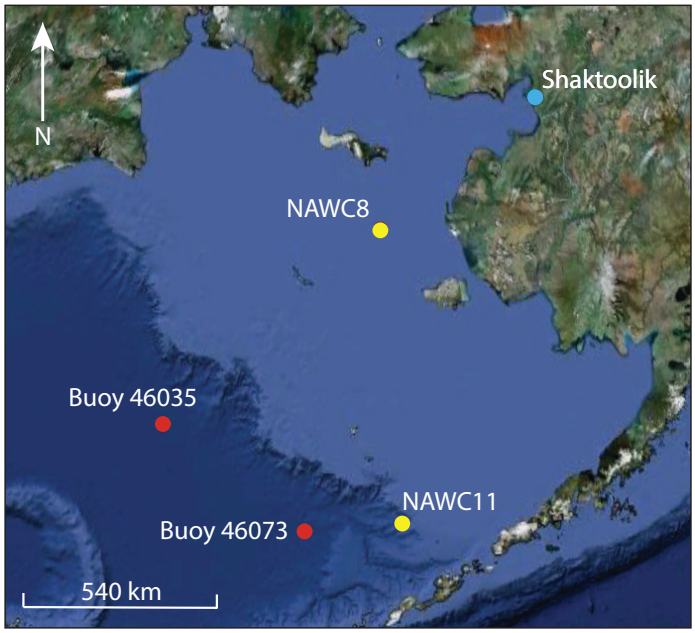

Figure 4.1. Buoy locations in the Bering Sea (imagery from Terrametrics, 2012).

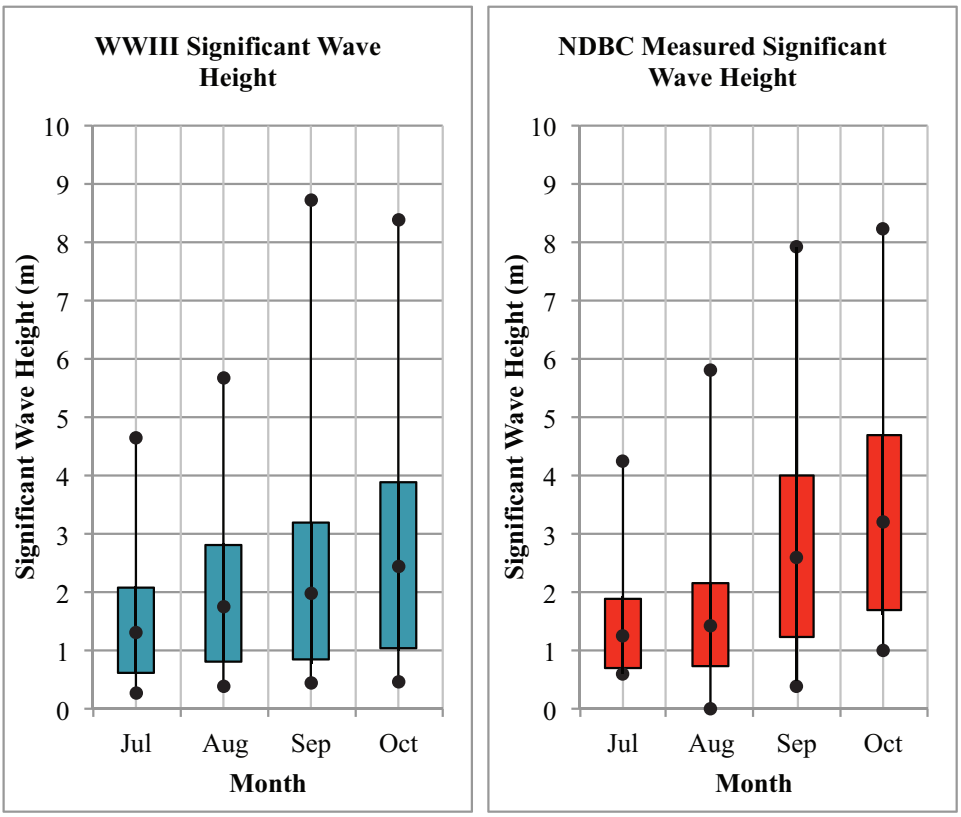

Figure 4.2. Monthly significant wave heights for WWIII outputs and verified buoy measurements. Maximum and minimum values plotted at the ends of the lines, mean in the middle of the box and standard deviation on extent of the box. Data for WWIII is from the years 1996-2005 and NDBC data is from the years 2005-2008.

For further validation, the MIROC5 wave height data calculated using WWIII and MIROC5 winds for the mid- to late-21st century, were compared with other GCM WWIII wave height data. The other three GCMs used for comparison included BCC, GFDL, and INMCM, as discussed previously. Cumulative distribution functions of significant wave height for each model were compared in both the RCP 4.5 and RCP 8.5 emissions scenarios. These resulting cumulative distribution functions are plotted in Figures 4.3 and 4.4. The MIROC5 shows the largest significant wave heights for any given probability in both the RCP 4.5 and RCP 8.5 scenarios. As seen in the

validation against actual wave height measurements from offshore buoys, MIROC5 shows very close similarities with the verified buoy data and is therefore the best model to use for calculating wave runup.

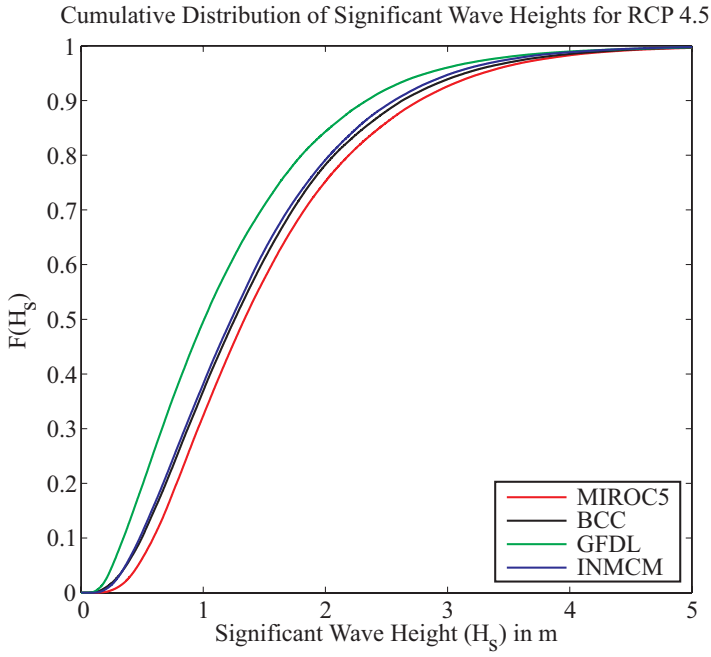

Figure 4.3. Cumulative distribution function of significant wave height for each GCM RCP 4.5 WWIII simulation. For the mid- and late-21st century.

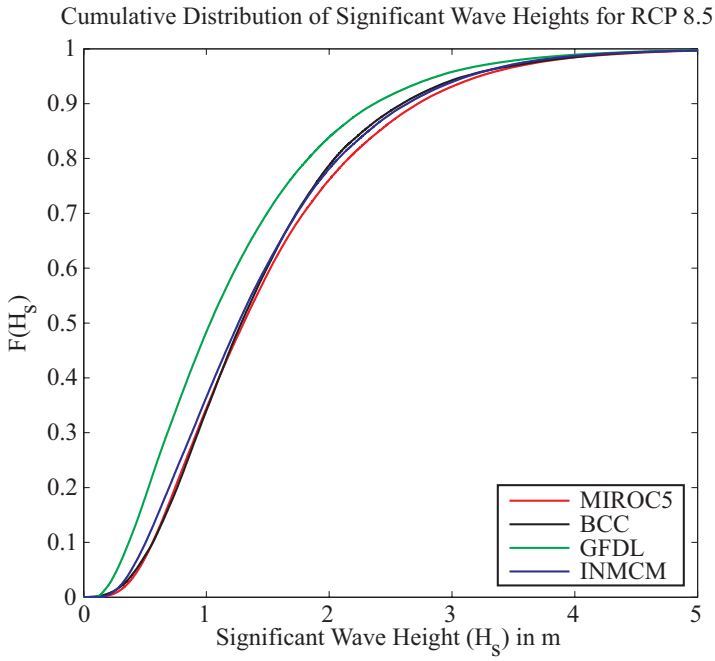

Figure 4.4. Cumulative distribution function of significant wave height for each GCM RCP 8.5 WWIII simulation. For the mid- and late-21st century.

4.2 SBEACH Wave Runup Analysis

To calculate wave runup in Shaktoolik using the WWIII outputs, SBEACH, a numerical model for simulating storm induced beach change, was used. SBEACH was developed by the USACE Coastal and Hydraulics and Laboratory and transforms offshore storm conditions, including storm surge and significant wave height and period, to total flooding at the coastline (Larson and Kraus, 1989). SBEACH estimates maximum wave runup elevation at the shoreface by assuming that a wave will continue to runup until it runs out of momentum, which is determined by the offshore wave conditions, slope and elevation of the shoreface, and different beach parameters that can be edited within the SBEACH model. The SBEACH model

operates in the Coastal Engineering Design and Analysis System (CEDAS) graphical user interface to assist in data input.

Model inputs for Shaktoolik included two reaches perpendicular to the shoreline, one at the present day village site in front of the school (Profile 18) and one at the old village site further south along the spit (Profile 29). The reaches included onshore profiles that extended 60 m onshore at Profile 18 and 87 m onshore at Profile 29. Offshore depth profiles from bathymetry collected in the field and from Smith and Sandwell (1997) extended to 358 km offshore where depth reached 30 m below MLLW and was sufficient depth for deep water waves to occur.

The grid sizes designated for the reaches in SBEACH ranged from a highest resolution of 1.00 m width onshore and in the nearshore, and progressively increased offshore to a maximum of grid cell width of 1000 m at the furthest offshore grid cells. Median grain size is 5 to 8 cm along the inhabited portion of the spit in Shaktoolik. The SBEACH model however cannot account for these coarse grain sizes so an effective grain size of 1.0 mm (the largest grain size SBEACH will run) and an overwash transport parameter of 0.001 were used. These parameters are consistent with the parameters used in the USACE study in Shaktoolik (USACE, 2011) (Chapman et al., 2011).

For the projected storms each event was individually input into SBEACH. Each storm also included a time series of hourly significant wave height and peak wave period data from the WWIII outputs as well as maximum water elevation, in meters above MLLW, from the storm surge calculations and a time series of wind

speed and direction from the MIROC5 meteorological data. Each storm event was then run in SBEACH for both reaches. The SBEACH output used for the purposes of this project was maximum water elevation, which includes maximum storm surge, wave setup, and wave runup. The total water level results, including wave runup elevation, are given in Chapter 5.

Chapter Summary: To calculate wave runup, offshore wave height and period were modeled using WWIII forced by the MIROC5 model, as in the storm surge calculations. Then, the MIROC5 offshore wave data were validated against observed measurements from the Bering Sea, and the MIROC5 data showed a close correlation to historical observations. Next the wave runup model SBEACH was setup to calculate total storm water levels for projected storm events. The projected results for storm surge and wave runup (Chapters 3 and 4) are reported in Chapter 5.

Chapter 5

Total Water Levels

5.1 Projected Storm Surge and Wave Runup

To find projected storm surge and wave runup heights in Shaktoolik for the mid- to late-21st century, MIROC5 projected model runs were used for the RCP 4.5 and RCP 8.5 greenhouse gas emissions scenarios, as discussed earlier.

The MIROC5 model runs from each of these scenarios cover the mid-21st century, years 2026 to 2045, and the late-21st century, years 2081 to 2100. For both scenarios and each of the years included in the projected model runs, storm events in the Bering Sea were identified as areas in which sea level pressures were below 980 mb. These events were tracked manually and the dates were recorded so that only those periods of storms in the Bering Sea were used (following tracks BS1 and BS as shown previously in Figure 3.5). The duration of each storm event was extended three days before the event reached the Alaska grid (44-76°N latitude and 170-230° longitude) and three days after the storm dissipated in order to allow the effects of wind duration to build up. Additionally, only the ice-free months, July through October, were used in the surge and runup calculations, and therefore only storms from those months were tracked. A table of the projected storm dates and durations is given in Appendix C. For the RCP 4.5 scenario, a total of 149 Bering Sea storms were identified, 76 events in the mid-21st century and 73 events in the late-21st century. For the RCP 8.5 scenario a total of 88 storms were identified, 42 events in

the mid-21st century and 46 in the late-21st century. The RCP 8.5 scenario had fewer storm events in the Bering Sea than the RCP 4.5 scenario.

The top ten largest storm surge events from both the RCP 4.5 and RCP 8.5 scenarios are outlined in Table 5.1. The largest storm surge elevation reached by projected storm conditions in the RCP 4.5 emissions scenario is 5.5 m above MLLW and 4.8 m above MLLW in the RCP 8.5 emissions scenario. The highest historical surge, as modeled by the USACE, occurred in 1960 had a surge of 4.35 m above MLLW and the historical 100-yr storm surge flood level is 5.82 m above MLLW (USACE, 2011) (Chapman et al., 2011).

When the maximum storm surge for each event is combined with the maximum wave runup and setup heights, the result is the total water level or maximum vertical extent of flooding. Table 5.2 outlines the highest total water level events and maximum wave runup heights from those events for both RCP 4.5 and RCP 8.5. The highest total water level reached by projected storm conditions in the RCP 4.5 emissions scenario is 8.9 m above MLLW and 6.5 m above MLLW in the RCP 8.5 emissions scenario at the new village site. At the old village site the highest total water levels are projected to reach 8.1 m for RCP 4.5 and 6.4 m for RCP 8.5. Historically, the highest total water level was estimated at the old village site to be 8.39 m above MLLW as modeled by the USACE study (USACE, 2011) (Chapman et al., 2011).

Table 5.1. Top projected storm surge events in Shaktoolik for each greenhouse gas emissions scenario. Date corresponds to mid-21st century (Mid) or late-21st century (Late).

Event Rank	RCP 4.5		RCP 8.5	
	Date	Surge Height (m above MLLW)	Date	Surge Height (m above MLLW)
1	Mid	5.5	Mid	4.8
2	Late	5.0	Mid	3.7
3	Mid	4.9	Mid	3.2
4	Mid	4.9	Late	3.2
5	Mid	4.1	Late	3.2
6	Late	3.7	Mid	3.2
7	Mid	3.4	Mid	3.2
8	Late	3.3	Mid	3.1
9	Late	3.3	Late	3.0
10	Mid	3.2	Mid	3.0

Table 5.2. Top projected total water level events in Shaktoolik at Profile 18 for each greenhouse gas emissions scenario. All heights are in meters above MLLW and the Date field corresponds to mid-21st century (Mid) or late-21st century (Late).

Event Rank	RCP 4.5			RCP 8.5		
	Date	Total Water Level (m)	Runup Height (m)	Date	Total Water Level (m)	Runup Height (m)
1	Mid	8.9	3.4	Mid	6.5	3.4
2	Mid	8.0	3.1	Late	6.3	4.3
3	Late	7.2	3.5	Mid	6.3	4.2
4	Mid	6.5	4.1	Mid	6.2	1.4
5	Late	6.3	1.4	Late	6.2	4.2
6	Mid	6.2	3.4	Mid	5.7	3.3
7	Late	6.1	2.9	Mid	5.6	2.4
8	Mid	6.0	1.9	Mid	5.5	2.3
9	Mid	5.9	2.8	Mid	5.5	3.1
10	Mid	5.8	1.0	Mid	4.9	1.2

5.2 Return Periods of Flooding

The Ranked Plotting Method approach for extreme value analysis outlined in Makkonen (2006) was used to predict return periods of flooding for both storm surge and total water levels. The simple formula employed by this method, shown in equations 5.1 and 5.2, is one of the most accurate methods for estimating the probability of extreme events.

$$P = \frac{m}{(N + 1)} \tag{5.1}$$

where

P is the probability of not exceeding the given event

N is the number of data (in this case largest storm event per year of record)

m is the rank of the data from 1 to N

$$R = \frac{1}{(1 - P)} \tag{5.2}$$

where

P is the probability of not exceeding the given event

R is the recurrence interval, in years

This method relates the recurrence interval R to the probability P of not exceeding that event in any given year. First the data is ranked from smallest to largest, in this case each storm event is ranked from lowest (m=1) to highest (m=N) water elevation, and the probability of each event is calculated using Equation 5.1. Then, the recurrence interval for each event is calculated with Equation 5.2.

The Ranked Plotting Method assumes that future events will be statistically similar to past events in frequency and magnitude. Therefore the RCP 4.5 and RCP 8.5 scenarios were analyzed for the entire 21st century, as well as divided into mid- and late-21st century for separate analysis of each. This extreme value analysis method predicts shorter recurrence intervals than other traditionally used methods, so the Ranked Plotting Method will predict storm water levels to occur more frequently than when using other extreme value analysis methods.

Additionally, the Ranked Plotting Method was used in the USACE study in Shaktoolik so the results of this study can be directly compared (USACE, 2011) (Chapman et al., 2011). Due to the nature of the analytical model for storm surge, the highest flooding event for each year was chosen for the recurrence interval analysis as opposed to using every storm event. This eliminates any smaller surge events that may be overestimated in the model.

The USACE study used every event on record, not the highest yearly flood level. From the raw storm surge data provided in the USACE study for 56 storms between the years 1954-2009, the same method was employed to choose the largest storm surge event per year for recurrence interval analysis. Figure 5.1 shows the results of this analysis compared with the original recurrence intervals for storm surge published in the USACE study (Chapman et al., 2011). The yearly maximum event recurrence intervals differ from the original results published by the USACE by about 0.8 to 1 m across the 1- to 100-yr recurrence interval and report a decrease in the frequency of occurrence of storm surge levels. Since they differ from the original

published results and the yearly maximum event method matches the method used for the projected recurrence intervals, these new values were used for comparison against the MIROC5 surge results.

Storm surge events used in the Ranked Plotting Method are plotted for RCP 4.5 and RCP 8.5 in Figures 5.2 and 5.3, respectively. Also plotted are the historical recurrence intervals for storm surge from the USACE study. Table 5.3 outlines the recurrence intervals from Figures 5.2 and 5.3 and shows the correlation coefficients for the best-fit lines through the data.

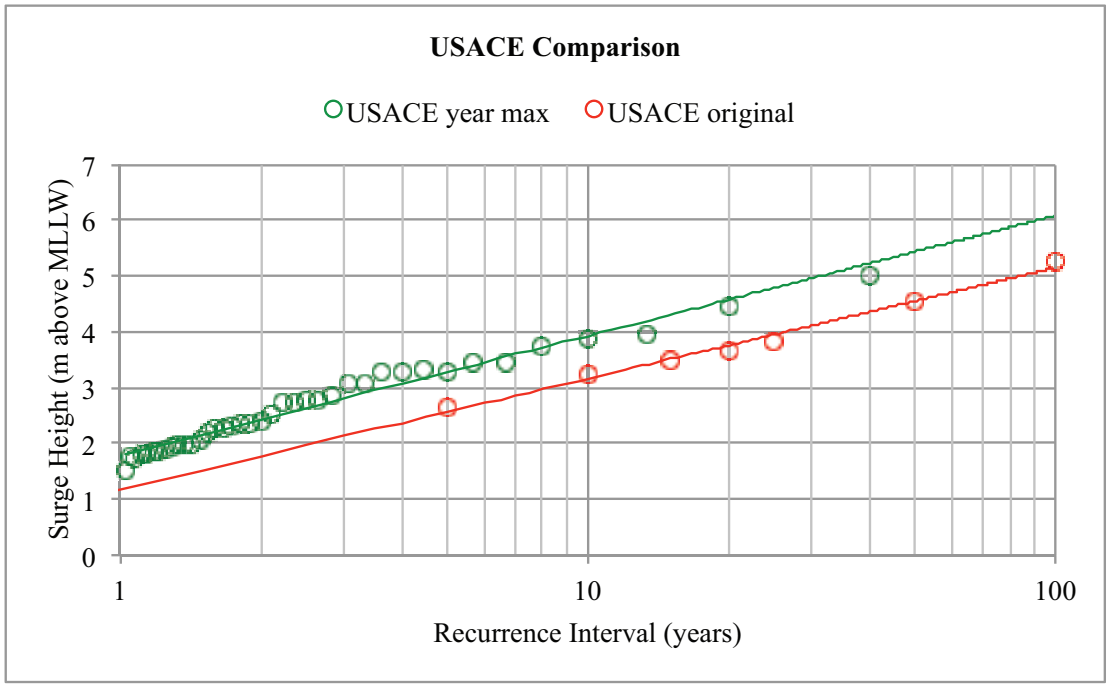

Figure 5.1. Comparison of original USACE published recurrence intervals (red) and yearly maximum surge event recurrence intervals (green). The R^2 value of the best-fit line for the yearly maximum surge event method is 0.97.

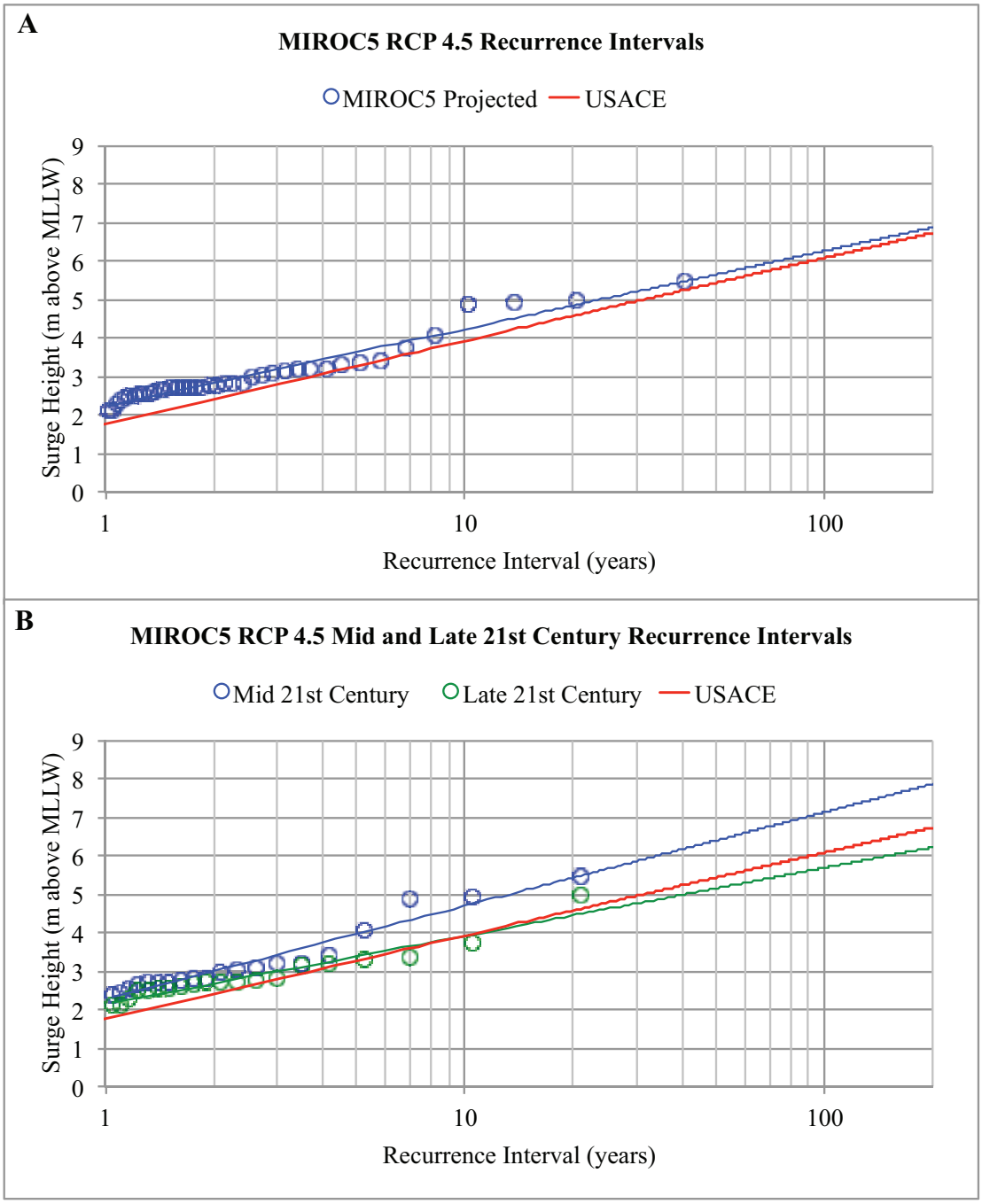

Figure 5.2. Storm surge height (above MLLW) recurrence intervals for the projected MIROC5 RCP 4.5 model runs compared to the historical return periods of flooding from the USACE study (in red). Figure A shows the combined mid- and late-21st century surge heights (in blue) and Figure B shows the surge heights for the mid-21st century (in blue) and the late-21st century (in green). The corresponding lines are the best logarithmic fit lines to the data.

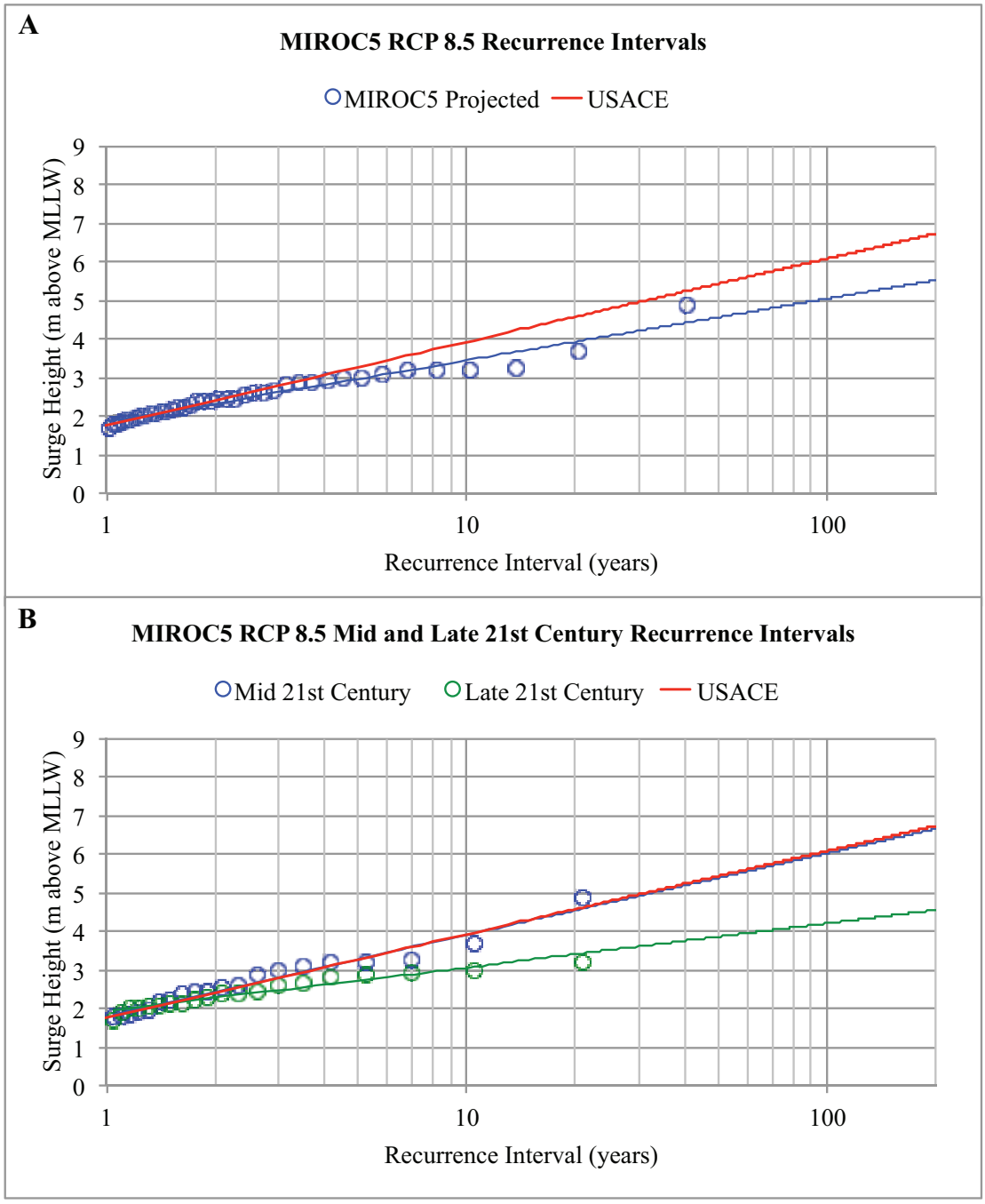

Figure 5.3. Storm surge height (above MLLW) recurrence intervals for the projected MIROC5 RCP 8.5 model runs compared to the historical return periods of flooding from the USACE study (in red). Figure A shows the combined mid- and late-21st century surge heights (in blue) and Figure B shows the surge heights for the mid-21st century (in blue) and the late-21st century (in green). The corresponding lines are the best logarithmic fit lines to the data.

Table 5.3. Return periods of storm surge flooding for RCP 4.5 and RCP 8.5 MIROC5 model runs.

Recurrence Interval (years)	RCP 4.5 Surge Height (m above MLLW)			RCP 8.5 Surge Height (m above MLLW)			USACE Surge Height (m above MLLW)
	Mid	Late	Both	Mid	Late	Both	
1	2.3	2.2	2.2	1.8	1.9	1.9	1.8
5	4.0	3.4	3.6	3.3	2.7	3.0	3.3
10	4.7	3.9	4.2	3.9	3.1	3.5	3.9
50	6.4	5.2	5.7	5.4	3.9	4.6	5.4
100	7.1	5.7	6.3	6.0	4.2	5.0	6.1
R^2 best-fit line	0.95	0.93	0.95	0.96	0.93	0.95	

Total water level results, surge height plus wave setup and runup, published in the USACE study were compared to the projected total water levels. The raw data were for wave setup and runup were not included in the USACE report and therefore the yearly maximum flood level could not be extracted. It is expected that if the yearly maximum flood recurrence intervals were available, they would produce increased flood recurrence intervals compared to the published recurrence intervals, as seen with the storm surge comparison in Figure 5.1. Additionally, the beach profile used by the USACE at the new community site, directly in front of the school, matches the location of the beach profile collected for this study but at the old community site they profile locations may not match up. The USACE profiles were collected a year prior to profile surveys for this study and both surveys were conducted during the summer season. Differences in the beach profile cross-sections can cause significant changes in the wave runup heights.

Total water levels for the mid- and late-21st century are shown in Figures 5.4 and 5.5 for the present day community site (Profile 18) and in Figures 5.6 and 5.7 for the old community site (Profile 29). Due to the steeper sloping nearshore at the old community site, larger waves break closer to the shoreline and cause a higher maximum wave runup than seen at the new community site. The USACE runup values do not follow the same pattern between the new and old community sites, suggesting that their beach profile and bathymetric data differ from the data collected for this study. Summary tables with return periods of flooding are shown in Table 5.4 for the present day community and 5.5 for the old community.

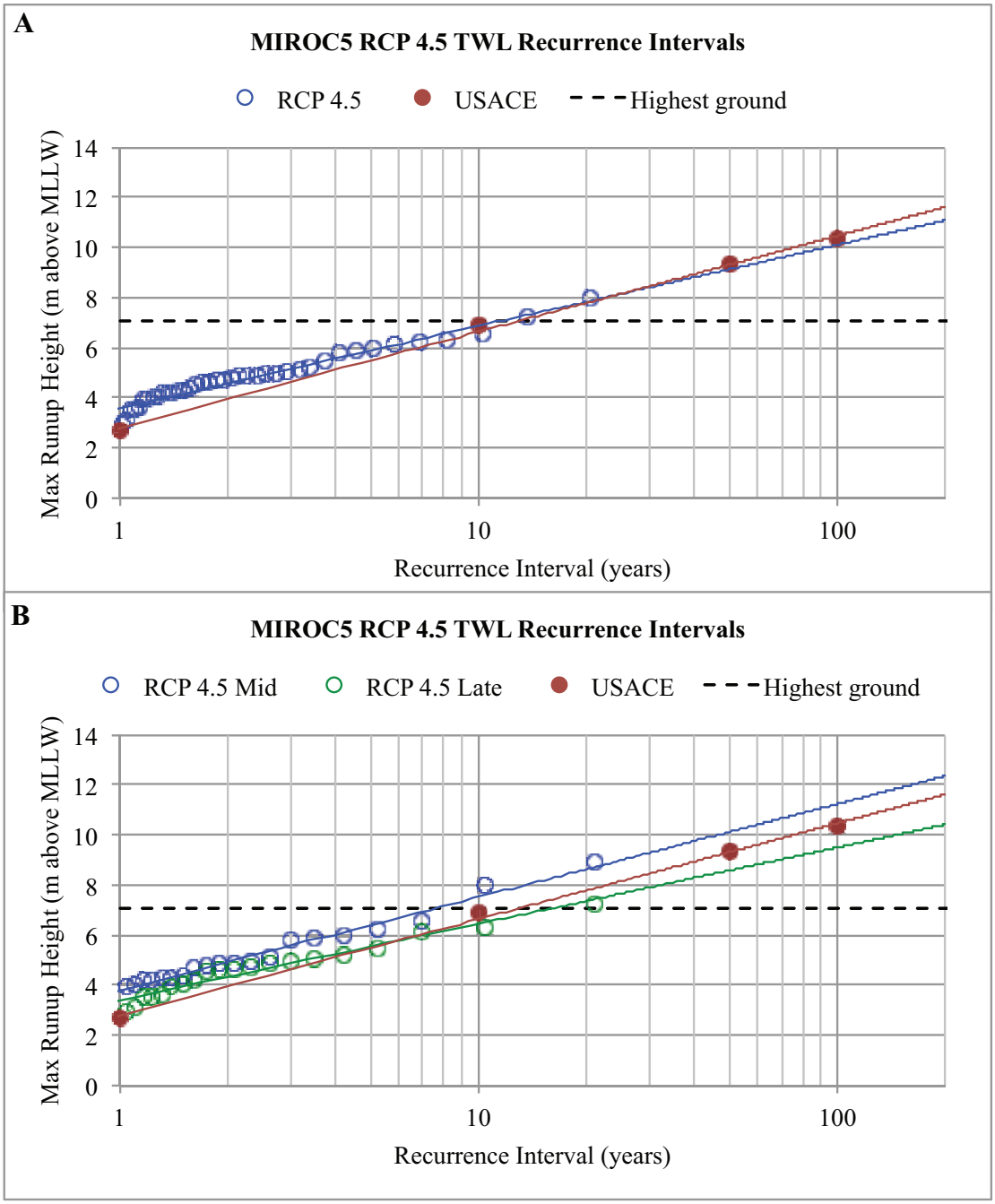

Figure 5.4. Total water level (above MLLW) recurrence intervals in the community for projected MIROC5 RCP 4.5 model runs as described previously. The black dotted line represents the highest ground elevation of the spit along the transect through the new community.

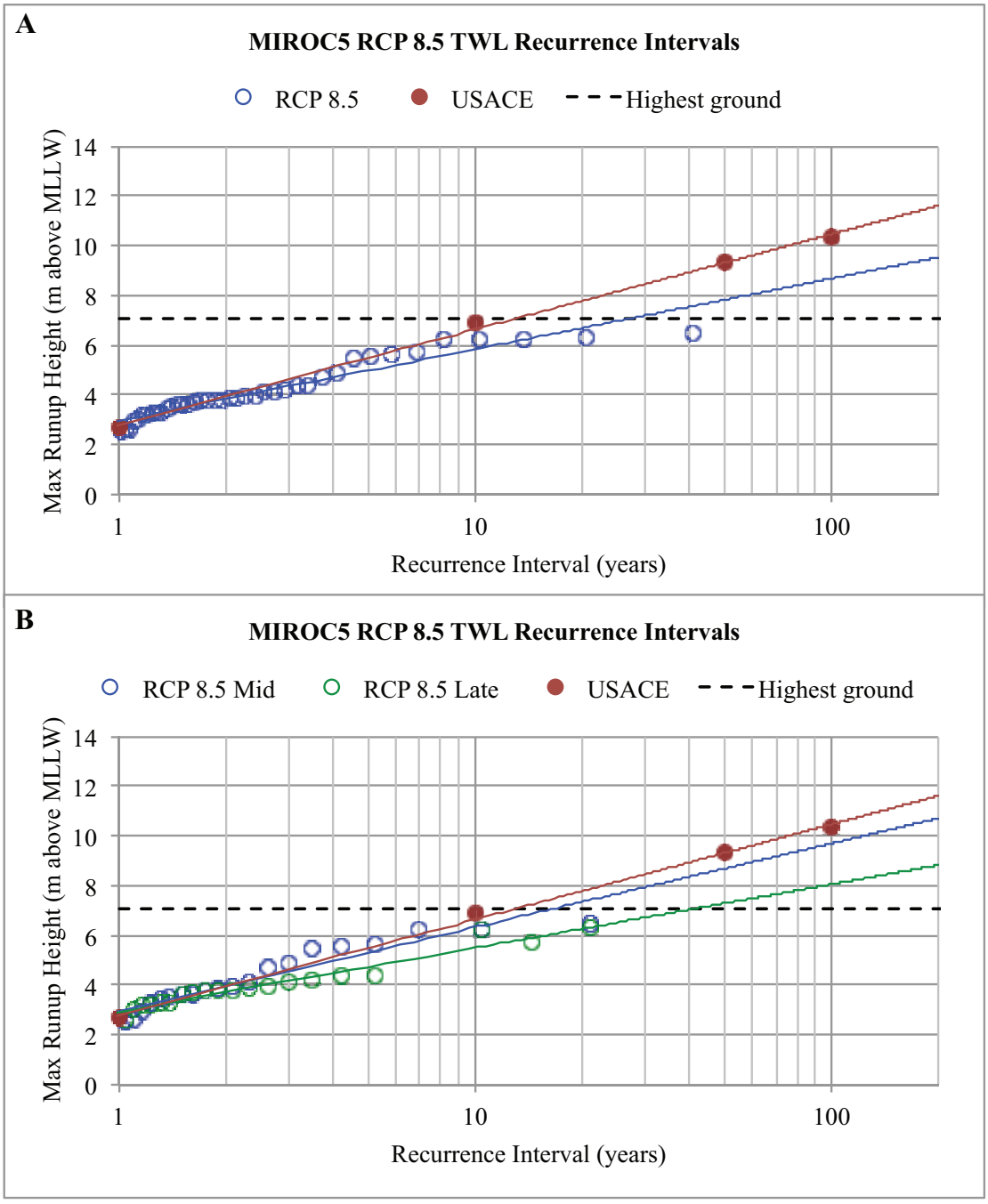

Figure 5.5. Total water level (above MLLW) recurrence intervals in the community for projected MIROC5 RCP 8.5 model runs as described previously. The black dotted line represents the highest ground elevation of the spit along the transect through the new community.

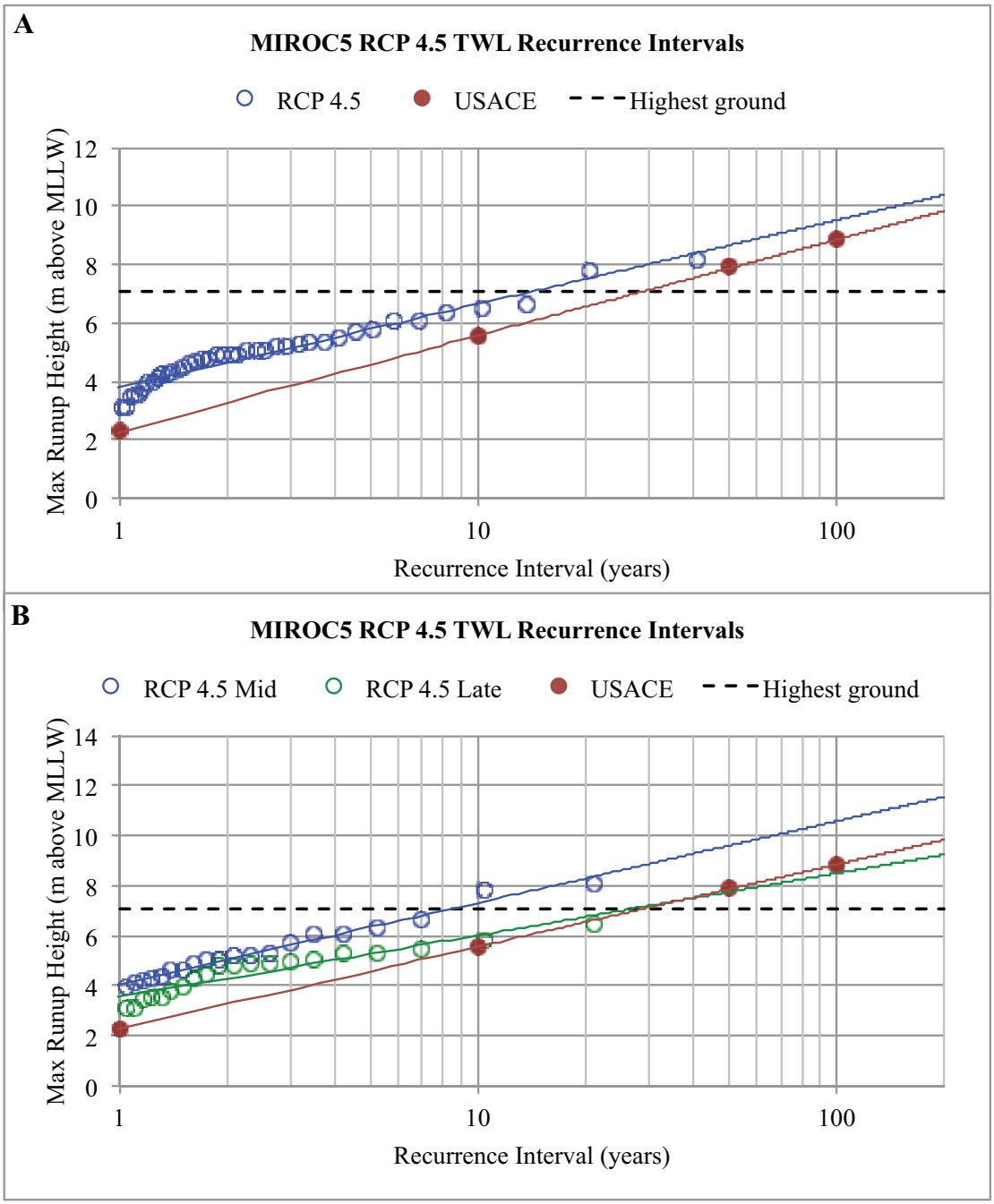

Figure 5.6. Total water level (above MLLW) recurrence intervals at the old community site for projected MIROC5 RCP 4.5 model runs as described previously. The black dotted line represents the highest ground elevation of the spit along the transect through the old community site.

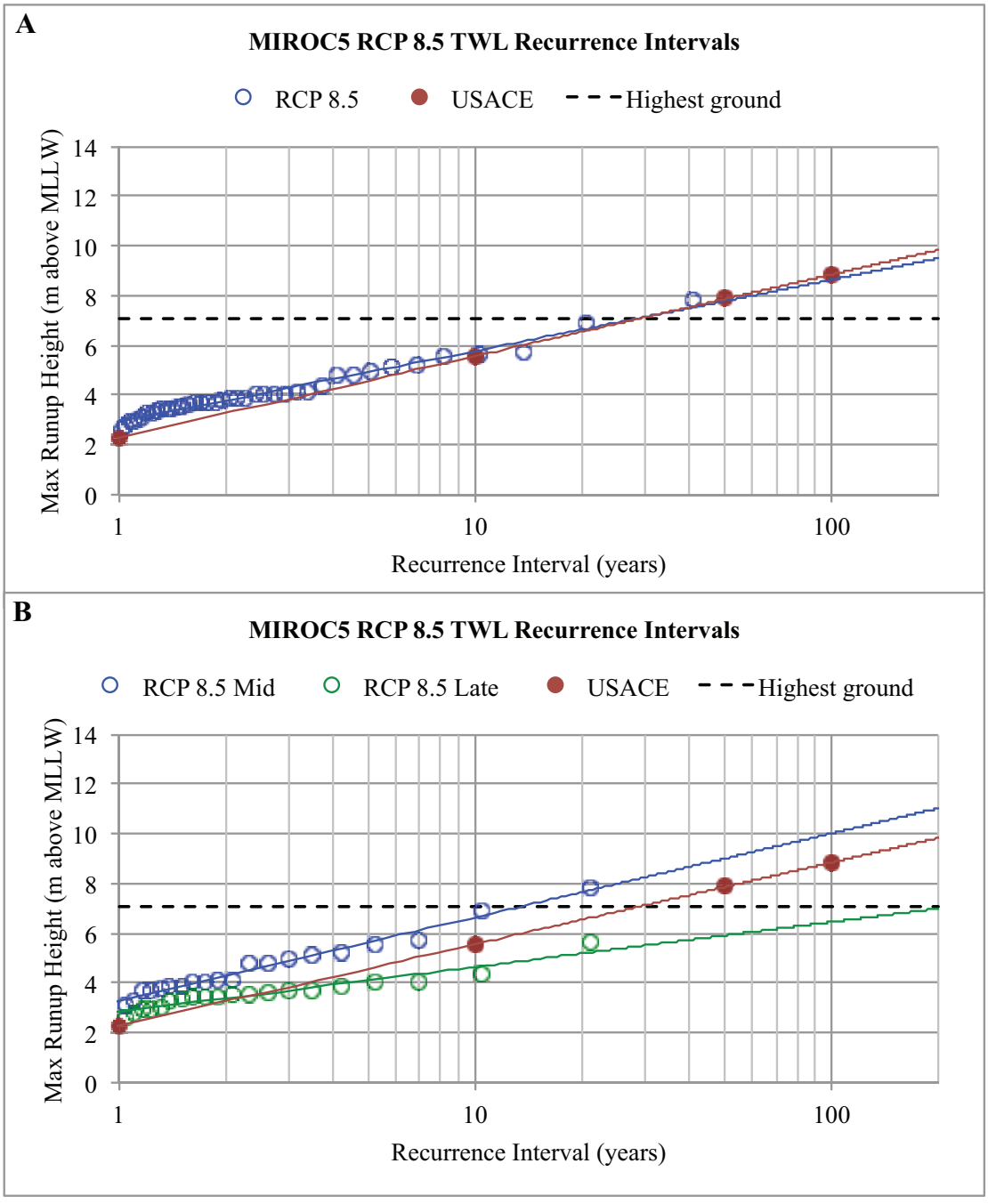

Figure 5.7. Total water level (above MLLW) recurrence intervals at the old community site for projected MIROC5 RCP 8.5 model runs as described previously. The black dotted line represents the highest ground elevation of the spit along the transect through the old community site.

Table 5.4. Return periods of total water level flooding for RCP 4.5 and RCP 8.5 MIROC5 model runs at Profile 18.

Recurrence Interval (years)	RCP 4.5 Flood Height (m above MLLW)			RCP 8.5 Flood Height (m above MLLW)			USACE Flood Height (m above MLLW)
	Mid	Late	Both	Mid	Late	Both	
1	3.8	3.4	3.6	3.0	3.0	3.0	2.7
5	6.4	5.5	5.9	5.3	4.7	5.0	5.5
10	7.5	6.5	6.9	6.3	5.5	5.8	6.9
50	10.1	8.6	9.1	8.7	7.3	7.8	9.3
100	11.2	9.5	10.1	9.7	8.1	8.7	10.4
R^2 best-fit line	0.98	0.95	0.96	0.91	0.95	0.92	

Table 5.5. Return periods of total water level flooding for RCP 4.5 and RCP 8.5 MIROC5 model runs at Profile 29.

Recurrence Interval (years)	RCP 4.5 Flood Height (m above MLLW)			RCP 8.5 Flood Height (m above MLLW)			USACE Flood Height (m above MLLW)
	Mid	Late	Both	Mid	Late	Both	
1	4.1	3.6	3.8	3.3	2.9	2.9	2.3
5	6.4	5.3	5.8	5.6	4.1	4.9	4.6
10	7.3	6.0	6.6	6.6	4.7	5.8	5.5
50	9.6	7.8	8.7	9.0	5.9	7.8	7.9
100	10.6	8.5	9.5	10.0	6.5	8.6	8.8
R^2 best-fit line	0.98	0.88	0.94	0.98	0.92	0.98	

The total water levels from Tables 5.4 and 5.5 were then plotted on the beach profile cross-sections for both the new and old community sites. The values for the mid- and late-21st century combined were used for plotting the flood levels. Figures 5.8 to 5.10 show the results for the USACE study, RCP 4.5, and RCP 8.5 respectively. The 50- and 100-yr flood levels overtop the spit at each location historically and for both the RCP 4.5 and RCP 8.5 emissions scenarios. Therefore only the 1-, 5-, and 10-yr flood levels are shown.

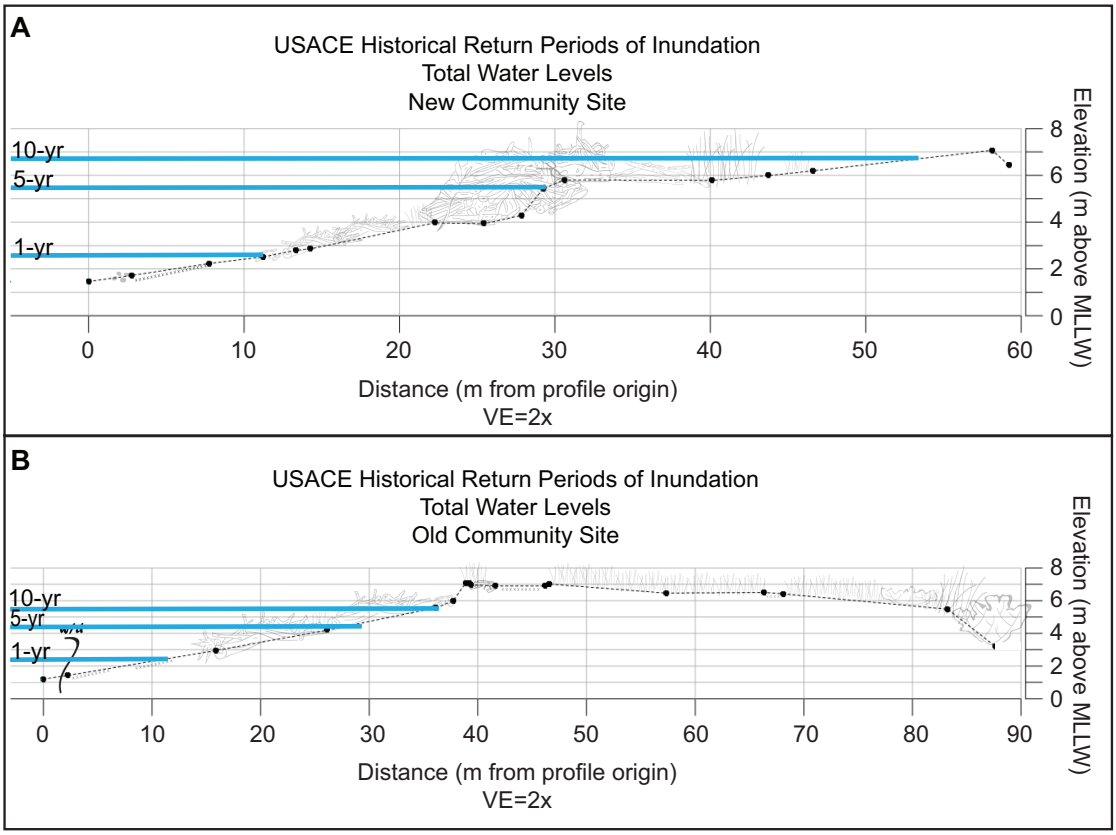

Figure 5.8. Return periods of flooding for the USACE study superimposed on beach profiles at the new community site (A) and old community site (B). The 50- and 100-yr floods are not shown because they overtop the spit. Also included are sketches of debris lines and vegetation locations, w/d is the wet-dry line and VE is vertical exaggeration. Modified from an unpublished figure by N. Kinsman and J. Smith, DGGS, 2012. Adapted with permission.

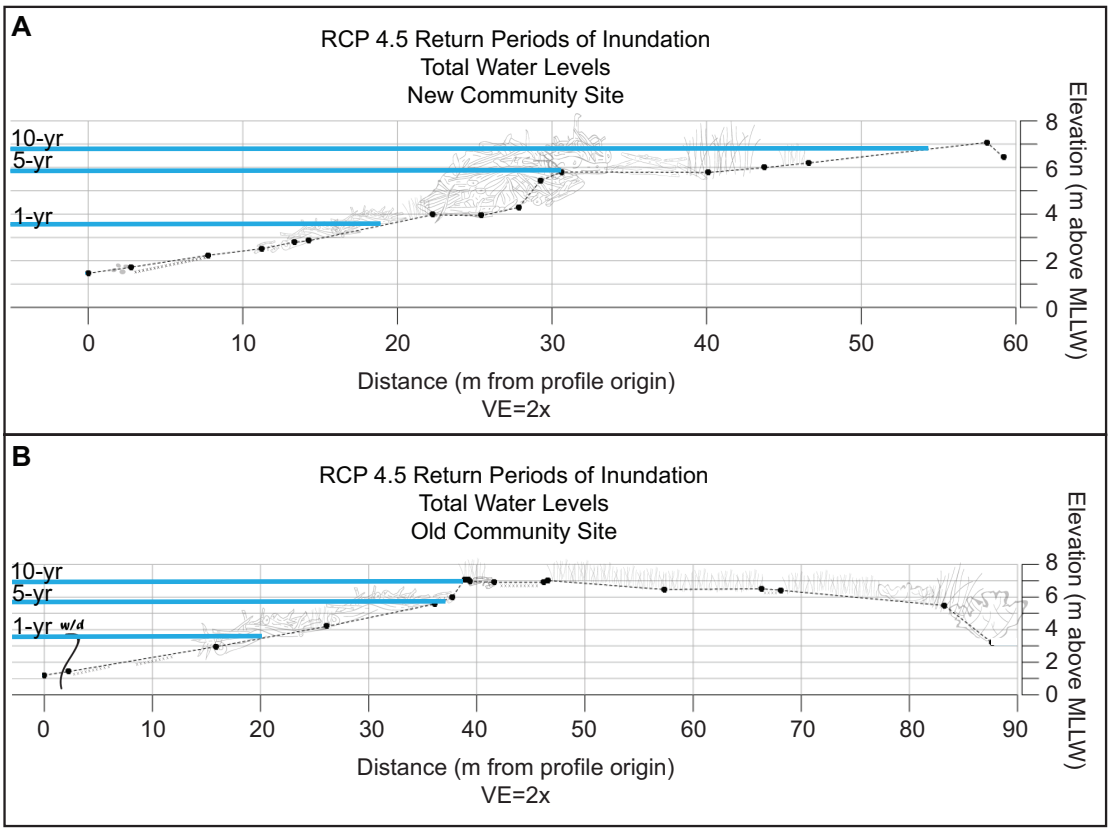

Figure 5.9. Return periods of flooding for the RCP 4.5 emissions scenario superimposed on beach profiles at the new community site (A) and old community site (B). The 50- and 100-yr floods are not shown because they overtop the spit. Also included are sketches of debris lines and vegetation locations, w/d is the wet-dry line and VE is vertical exaggeration. Modified from an unpublished figure by N. Kinsman and J. Smith, DGGS, 2012. Adapted with permission.

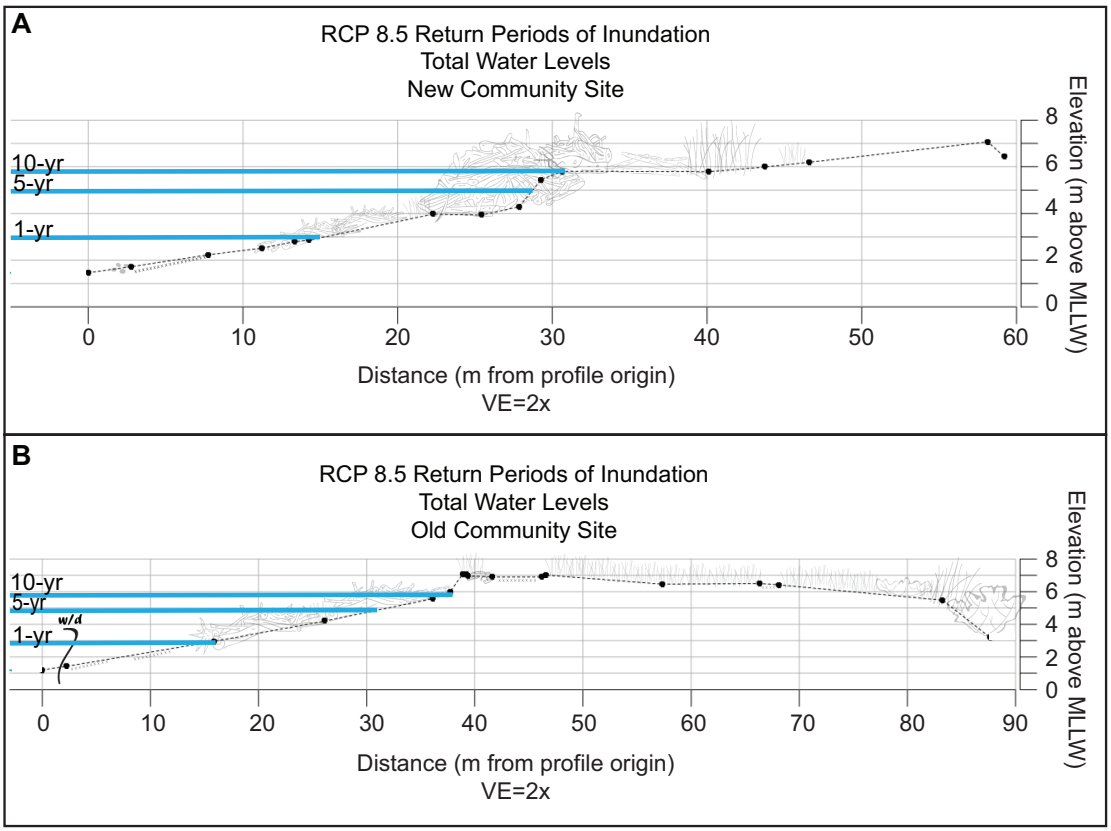

Figure 5.10. Return periods of flooding for the RCP 8.5 emissions scenario superimposed on beach profiles at the new community site (A) and old community site (B). The 50- and 100-yr floods are not shown because they overtop the spit. Also included are sketches of debris lines and vegetation locations, w/d is the wet-dry line and VE is vertical exaggeration. Modified from an unpublished figure by N. Kinsman and J. Smith, DGGS, 2012. Adapted with permission.

Chapter Summary: This chapter gives results for storm surge and total water level for the MIROC5 projected Bering Sea storm events, including the mid- to late-21st century for both the moderate (RCP 4.5) and high (RCP 8.5) greenhouse gas emissions scenarios. Recurrence intervals were calculated with the Ranked Plotting Method using largest events for each year of model output. The mid- and late-21st century recurrence intervals were compared to the historical recurrence intervals.

Flood elevations for these recurrence intervals are shown on cross-sectional views of the beach, including debris line position.

Chapter 6

Conclusions

6.1 Discussion

Shaktoolik, at its present day location, is highly susceptible to flooding on both the Norton Sound and lagoon sides of the spit. The analytical model for storm surge shows a close correlation with historical surge heights modeled by the USACE study and provides a quick way for people in Shaktoolik and other coastal communities of Northwest Alaska to predict flooding levels from an oncoming storm. The results also show that wave setup and runup also cause a significant increase in flood level during storm events and the force of these waves can cause additional damage to infrastructure in the community.

Surprisingly, for the projected storm surge and wave runup events the moderate greenhouse gas emissions scenario (RCP 4.5) produces larger flood levels and more frequent flooding than the high greenhouse gas emissions scenario (RCP 8.5). These results are consistent with recent studies off the California coast using GCM data for the mid- and late-21st century (Erikson, personal communication). The frequency of projected storm events in the Bering Sea region is also substantially larger in the RCP 4.5 scenario (149 total storms) versus the RCP 8.5 scenario (88 total storms) for both the mid- and late-21st century. It appears that there is a change in ocean and atmospheric circulation in the North Pacific causing increased

storminess in this region with the RCP 4.5 scenario. As seen in the recurrence interval plots, when the projected storm surge results are compared to historical surge levels, the moderate emissions scenario (RCP 4.5) has higher storm surge levels at each return period of flooding than seen historically. For the mid-21st century, surge levels are higher at lower recurrence intervals than seen historically but for the late-21st century surge recurrence intervals are similar to those seen historically. The high emissions scenario (RCP 8.5), however, projects lower surge levels than the moderate emissions scenario. The mid-21st century recurrence intervals for the high emissions scenario are similar to the historic and the late-21st century projects lower surge heights at the same recurrence intervals as seen historically.

For the total storm water levels, there are significant differences between the new community and old community sites, specifically when compared to historical values. Since there is a steeper slope in the nearshore at the old community site it is expected that there is a higher wave runup extent during storm events than there is at the new community site. In the RCP 4.5 and RCP 8.5 scenarios at the old community site, results are consistent with the storm surge results; that is RCP 4.5 has higher flood levels than the historical values and the RCP 8.5 produces similar values to historical data. At the new community site however there is a shift. The RCP 4.5 scenario return periods of flooding water levels are similar to the historical return periods of flooding, and the RCP 8.5 scenario produces total storm water levels that are significantly lower than the historical storm water levels. These differences are likely due to the different beach profile and offshore bathymetry datasets used for in

this experiment versus in the USACE modeling study, which is assumed to be the best historical data available for Shaktoolik. Because the yearly maximum flood levels were used for the projected total water level recurrence intervals but not for the historic, there may also be variances in the historic flood recurrence intervals when compared to the projected results.

Additionally, the mid-21st century produces higher flooding events than the late-21st century for both emissions scenarios in both storm surge and total flooding levels. This may be a result of both global climate change effects as well as influences by decadal oscillations. If MIROC5 is accurately predicting future climate, it can be expected that storminess will increase into the mid-21st century and then start to decrease again into the late-21st century.

When these results are plotted on the beach profiles at the new and old community sites, overtopping of the spit occurs at the 50- and 100-yr flood levels both historically and for both projected scenarios. From the USACE study the two distinct debris line locations match up with the 5- and 10-yr flood levels indicating that these large debris-depositing events occur fairly often. This correlation can be seen in Figure 5.7. Based on the projected changes in return periods of flooding for the RCP 4.5 scenario, debris lines remain at the same location in the new community and will be deposited farther onshore at the old community site. For the RCP 8.5 scenario, however, debris lines shift seaward at the new site and remain stationary at the old site.

6.2 Limitations and Future Work

The lack of historical water level data in Shaktoolik, or in the surrounding region, is the primary limiting factor of this study. The analytical model for storm surge was validated against results from another modeling study as opposed to measured historical storm surge heights and therefore the magnitude of error in the storm surge estimates is greater. This is not only a limiting factor in this study, many coastal communities in Northwest Alaska do not have water level records so it is difficult to predict future surge heights and return periods of flooding for flood events in these areas highly susceptible to flooding.

Another limitation of this study is the scale of resolution in both the GCMs and WWIII output. MIROC5 has a resolution of 1.4° longitude by 1.4° latitude and had the finest resolution of the four GCMs compared in this study. A higher resolution version of the MIROC model, MIROC4h, has an average resolution of 0.562° longitude by 0.562° latitude and when the historical sea level pressure data for MIROC4h are compared to the NARR data there is a much stronger correlation than with the lower resolution models. Unfortunately the projected model runs for MIROC4h were not completed at the time of this study, and therefore this model could not be used to analyze projected surge and runup events.

For the offshore wave modeling using WWIII, the global scale model, NWW3, was used for these analyses. The wave heights modeled using MIROC5 and

the WWIII data show a close correlation with measured wave heights in the Bering Sea using the lower resolution NWW3. However, a higher resolution WWIII model for the Alaska region, AKW, is also available that may produce more accurate offshore wave heights and consequently more accurate wave runup estimates.

Future work in Shaktoolik includes using the higher resolution MIROC4h GCM and the higher resolution Alaska regional WWIII model to force the analytical storm surge model and the wave runup calculations in SBEACH. This will help improve the analytical model and reduce the error in the estimates of storm surge and wave runup. Additional research could also look at using the analytical storm surge model in other Alaskan coastal communities to test how robust the model is and improve it further.

Shaktoolik's beaches are very coarse grained as stated previously in the grain size analysis section. SBEACH only allows for a maximum of 1 mm grain size diameter to be used in its wave runup simulations. Since the majority of sediments in Shaktoolik exceed 1 mm in diameter, future work could also analyze the impacts of the coarse grains on wave runup extent. Since the mean grain size increases from the end of the spit to the base of the spit, wave runup extent may correlate with grain size and differ laterally along the beach. Hughes (1995) has shown that large grain size contributes to the friction component of wave uprush. On very coarse-grained beaches, the grains may act as a damping effect for wave runup by reducing available water due to infiltration thus reducing the maximum extent of runup at the coastline.

For the projected storm surge and runup results using MIROC5 it is interesting that the RCP 4.5 emissions scenario causes the highest frequency and most intense storms in the region. Future studies could look at if other GCMs show similar results and if they do, analyze why the North Pacific sees a dramatic change only during a moderate greenhouse gas emissions scenario. This could also be done on a global scale using GCMs to see how other regions are affected in terms of storminess under the same, modeled conditions.

The analytical approach for storm surge calculation used in this study did not include the effects of ice cover on overall storm surge and therefore, only ice-free months were analyzed. Most of the storm damage occurs during the ice-free months when the coast is exposed and there is greater fetch. However, further investigation of projected storm surge and wave runup could also examine the intricate effects of sea ice on storm surge during ice cover months. Particularly, how the impacts of ice affect flooding at the coastline and also how the diminishing sea ice every year will change these affects as a result of global warming.

Appendices

Appendix A: Bathymetry Data

New Community (Transect B)		Old Community (Transect C)		Smith and Sandell Offshore Bathymetry	
Distance Offshore (m)	Depth (m)	Distance Offshore (m)	Depth (m)	Distance Offshore (km)	Depth (m)
0.0	1.3	0.0	2.4	0.00	25.5
54.6	1.2	6.9	2.4	3.00	16.3
64.9	1.3	10.2	2.5	6.01	9.4
75.6	1.4	15.8	2.4	9.01	9.7
130.5	1.5	20.8	2.5	12.01	11.3
140.8	1.5	25.4	2.5	15.01	13.8
152.4	1.5	34.8	2.5	18.02	15.1
163.7	1.6	42.0	2.5	21.02	14.8
802.8	3.1	49.8	2.5	24.02	17.0
814.1	3.1	55.0	2.5	27.02	17.0
825.1	3.2	63.7	2.5	30.03	17.0
1078.6	3.9	67.8	2.6	33.03	16.6
1085.1	3.8	74.6	2.6	36.03	15.9
1093.5	3.8	82.9	2.7	39.03	16.0
1100.9	3.8	86.9	2.7	42.04	15.7
1106.8	3.7	93.9	2.7	45.04	14.9
1112.3	3.7	99.7	2.8	48.04	16.1
1117.9	3.8	106.7	2.7	51.04	16.3
1125.3	3.7	112.4	2.8	54.05	15.0
1128.8	3.7	118.0	2.9	57.05	16.6
1134.8	3.8	123.8	2.7	60.05	18.1
1142.4	3.7	132.7	2.9	63.05	16.8
1147.0	3.7	136.7	2.9	66.06	16.4
1147.8	3.7	144.3	2.8	69.06	17.4
1152.7	3.7	146.7	2.9	72.06	18.2
1156.5	3.7	152.5	2.9	75.06	16.5
1162.5	3.7	156.6	2.8	78.07	16.1
1166.6	3.6	160.0	2.9	81.07	15.6
1171.5	3.7	168.0	2.8	84.07	17.8
1174.5	3.7	171.7	2.9	87.07	16.8
1180.4	3.7	179.2	2.9	90.08	15.2
1185.6	3.6	183.2	2.9	93.08	16.0
1191.3	3.6	190.6	2.9	96.08	14.9
1194.8	3.7	194.3	2.9	99.08	14.9
1198.6	3.6	202.1	3.0	102.09	15.2

1203.3	3.6	209.0	2.9	105.09	15.9
1207.3	3.6	213.9	2.9	108.09	17.1
1213.0	3.6	217.3	3.0	111.09	14.7
1218.5	3.6	220.7	3.0	114.10	14.6
1222.2	3.5	227.4	3.0	117.10	16.0
1226.6	3.7	231.1	3.0	120.10	14.1
1233.7	3.6	238.9	3.0	123.10	13.8
1238.8	3.5	244.2	3.0	126.11	14.1
1242.1	3.6	248.1	3.0	129.11	10.6
1248.3	3.6	254.6	3.2	132.11	12.0
1257.6	3.5	258.4	3.0	135.11	14.0
1266.0	3.6	262.1	3.1	138.12	11.1
1274.4	4.0	266.5	3.1	141.12	10.7
1276.6	3.5	271.0	3.1	144.12	10.0
1284.2	3.5	277.4	3.2	147.12	9.2
1290.7	3.4	284.0	3.2	150.13	9.0
1301.3	3.5	289.5	3.2	153.13	9.1
1312.2	3.5	294.4	3.2	156.13	8.2
1317.6	3.5	297.4	3.3	159.13	7.0
1326.0	3.5	301.1	3.3	162.14	6.7
1334.4	3.3	304.7	3.3	165.14	7.0
1342.0	3.4	308.5	3.2	168.14	7.0
1349.1	3.4	313.8	3.4	171.14	6.8
1360.0	3.4	318.5	3.4	174.15	5.5
1368.4	3.3	322.0	3.4	177.15	8.2
1374.4	3.4	326.0	3.4	180.15	8.9
1382.5	3.3	330.7	3.5	183.15	9.9
1388.2	3.3	334.8	3.4	186.16	10.1
1398.3	3.4	339.9	3.5	189.16	10.0
1408.6	3.3	342.9	3.6	192.16	10.1
1411.2	4.4	344.5	3.7	195.17	8.2
1413.2	3.2	347.1	3.5	198.17	6.8
1420.5	3.3	349.0	3.6	201.17	6.0
1426.8	3.3	352.1	3.6	204.17	5.2
1432.5	3.2	354.8	3.7	207.18	3.7
1436.0	3.4	356.3	3.6	210.18	1.7
1441.7	3.2	360.3	3.6	213.18	2.9
1443.8	4.6	364.8	3.7	216.18	4.8
1446.6	3.3	370.3	3.6	219.19	6.5
1450.2	3.3	373.8	3.7	222.19	7.9
1451.7	3.2	377.0	3.6	225.19	8.0

1453.6	3.2	381.2	3.7	228.19	8.0
1456.4	3.2	385.1	3.7	231.20	8.1
1458.7	3.3	388.8	3.7	234.20	11.8
1458.8	3.2	395.2	3.8	237.20	13.2
1462.5	3.1	399.3	3.7	240.20	13.0
1466.4	3.2	402.4	3.7	243.21	13.8
1473.3	3.2	405.2	3.8	246.21	14.8
1480.8	3.2	409.6	3.8	249.21	14.7
1490.5	3.2	415.8	3.8	252.21	14.7
1501.4	3.1	420.0	3.8	255.22	15.5
1508.9	3.2	424.9	3.9	258.22	14.7
1520.3	3.1	430.8	3.9	261.22	16.6
1530.6	3.1	438.6	3.9	264.22	18.8
1541.5	3.1	447.7	4.1	267.23	20.2
1551.4	3.0	458.7	4.2	270.23	18.4
1563.5	3.1	469.7	4.1	273.23	18.2
1571.6	3.0	491.0	4.4	276.23	19.4
1581.0	3.1	513.9	4.3	279.24	17.7
1588.2	3.0	524.3	4.5	282.24	17.1
1595.5	3.0	535.8	4.5	285.24	16.0
1604.8	5.5	547.1	4.5	288.24	15.5
1606.9	3.0	569.7	4.6	291.25	16.9
1615.4	5.4	580.6	4.7	294.25	18.7
1615.7	3.0	591.6	4.9	297.25	17.4
1623.5	3.0	603.2	4.8	300.25	17.7
1626.4	5.4	614.8	4.9	303.26	20.5
1633.2	2.9	626.4	4.8	306.26	21.7
1641.3	2.9	648.9	4.9	309.26	20.7
1649.2	2.9	660.5	5.0	312.26	22.6
1654.0	3.0	671.5	5.1	315.27	21.6
1658.8	2.9	682.8	5.2	318.27	21.2
1659.8	2.8	692.5	5.1	321.27	21.0
1661.1	2.9	703.2	5.2	324.27	22.2
1663.0	2.8	714.5	5.2	327.28	21.5
1664.9	2.9	734.6	5.1	330.28	23.8
1667.6	2.9	744.9	5.2	333.28	25.0
1669.3	2.9	764.4	5.3	336.28	25.2
1672.3	2.9	776.0	5.3	339.29	25.6
1673.8	2.8	796.4	5.3	342.29	26.4
1675.3	2.8	808.0	5.3	345.29	28.8
1677.1	2.8	818.1	5.4	348.29	32.2

1679.0	2.9	828.1	5.5	351.30	33.0
1682.7	2.9	837.9	5.4	354.30	33.7
1685.3	2.8	848.0	5.4	357.30	34.9
1688.7	2.7	859.8	5.5	360.30	35.0
1691.3	2.8	870.8	5.5	363.31	35.7
1694.1	2.9	882.7	5.5	366.31	31.9
1695.9	2.8	904.3	5.6	369.31	31.6
1698.2	2.8	915.9	5.6	372.31	31.1
1702.0	2.7	927.5	5.6	375.32	27.1
1704.2	2.8	938.8	5.7	378.32	25.2
1704.4	5.8	950.4	5.7	381.32	25.1
1706.3	2.8	960.7	5.7	384.33	22.8
1708.2	2.8	971.7	5.7	387.33	21.0
1711.2	2.8	982.7	5.7	390.33	22.6
1715.1	2.8	993.3	5.7	393.33	24.5
1716.0	6.0	1003.4	5.8	396.34	28.0
1718.7	2.8	1014.7	5.8	399.34	23.7
1721.6	2.8	1026.0	5.8	402.34	16.6
1724.5	2.8	1036.9	5.7	405.34	15.7
1726.4	6.1	1059.5	5.7	408.35	17.5
1728.1	2.7	1070.8	5.9	411.35	17.4
1731.4	2.7	1082.0	5.9	414.35	16.3
1734.1	2.8	1093.3	5.9	417.35	17.9
1736.4	5.9	1116.5	5.8	420.36	20.5
1738.0	2.7	1127.5	5.9	423.36	21.0
1742.5	2.7	1138.4	5.9	426.36	22.2
1745.9	2.7	1149.4	5.9	429.36	23.5
1746.8	6.0	1160.7	5.9	432.37	25.5
1749.7	2.7	1171.7	6.1	435.37	25.4
1753.6	2.7	1182.6	6.1	438.37	27.4
1755.5	2.7	1193.6	6.1	441.37	26.5
1757.8	2.6	1205.5	6.2	444.38	29.1
1757.8	6.1	1216.5	6.2	447.38	26.2
1760.5	2.7	1248.2	6.1	450.38	25.9
1762.7	2.7	1258.5	6.1	453.38	26.9
1766.6	2.7	1269.2	6.1	456.39	27.0
1768.4	6.1	1280.2	6.1	459.39	27.5
1769.6	2.6	1291.1	6.1	462.39	31.4
1771.9	2.6	1313.1	6.2	465.39	34.1
1774.7	2.7	1324.1	6.2	468.40	35.6
1778.5	6.2	1334.7	6.1	471.40	39.6

1778.8	2.7	1354.8	6.1	474.40	42.4
1783.0	2.6	1365.2	6.3	477.40	43.2
1786.6	2.6	1385.6	6.2	480.41	44.9
1788.9	6.1	1396.3	6.2	483.41	45.9
1789.7	2.6	1406.7	6.3	486.41	43.6
1791.8	2.6	1417.0	6.3	489.41	42.1
1795.8	2.6	1427.7	6.3	492.42	44.0
1798.1	2.6	1438.4	6.3	495.42	42.9
1799.8	6.2	1449.3	6.4	498.42	43.0
1800.0	2.6	1459.7	6.4	501.42	43.6
1802.8	2.5	1470.1	6.4	504.43	45.9
1803.6	2.5	1480.4	6.2	507.43	46.3
1806.6	2.6	1511.8	6.3	510.43	43.0
1810.1	2.5	1522.2	6.4	513.43	39.7
1810.8	6.3	1532.8	6.4	516.44	37.4
1813.5	2.5	1543.5	6.4	519.44	37.1
1816.7	2.5	1554.5	6.3	522.44	34.0
1818.1	2.5	1575.5	6.4	525.44	31.7
1819.8	2.6	1585.9	6.5	528.45	28.1
1821.8	6.3	1595.9	6.5	531.45	26.4
1822.6	2.5	1606.6	6.6	534.45	25.9
1825.4	2.5	1617.0	6.6	537.45	26.8
1828.0	2.5	1627.0	6.6	540.46	31.0
1831.8	6.4	1637.4	6.5	543.46	35.5
1831.9	2.5	1647.7	6.7	546.46	38.6
1836.9	2.5	1658.1	6.6	549.46	40.1
1840.2	2.5	1669.1	6.6	552.47	40.7
1842.1	2.4	1679.4	6.5	555.47	41.5
1845.8	2.5	1689.8	6.7	558.47	42.8
1849.2	2.6	1700.2	6.6	561.48	43.8
1851.9	2.5	1710.8	6.6	564.48	46.1
1855.9	2.4	1722.1	6.6	567.48	49.5
1857.9	2.4	1744.1	6.7	570.48	50.7
1860.3	2.5	1754.1	6.7	573.49	50.4
1862.5	2.4	1764.2	6.7	576.49	50.8
1864.5	2.5	1775.2	6.7	579.49	52.0
1868.1	2.4	1786.4	6.8	582.49	51.0
1869.7	2.4	1797.4	6.8	585.50	48.7
1871.3	2.4	1808.7	6.7	588.50	46.0
1874.9	2.3	1819.7	6.8	591.50	46.2
1877.9	2.4	1830.3	6.8	594.50	48.1

1881.1	2.4	1841.0	6.8	597.51	49.5
1885.2	6.6	1852.3	6.7	600.51	51.5
1886.2	2.4	1863.5	6.9	603.51	53.8
1890.7	2.4	1873.9	6.7	606.51	56.0
1895.0	2.4	1884.9	6.7	609.52	57.5
1900.6	2.3	1895.9	6.8	612.52	59.2
1903.7	2.3	1906.8	6.8	615.52	60.4
1907.7	2.3	1917.5	6.9	618.52	61.9
1910.7	2.3	1928.5	6.7	621.53	62.2
1914.6	2.2	1938.5	6.9	624.53	60.0
1918.7	2.3	1949.8	6.8	627.53	58.6
1921.1	2.3	1959.9	6.7	630.53	58.9
1924.9	2.2	1970.2	6.8	633.54	57.3
1928.3	2.3	1981.2	6.9	636.54	51.4
1930.9	2.3	2001.9	6.8	639.54	51.7
1934.4	2.3	2012.0	6.9	642.54	59.0
1936.5	2.3	2032.1	6.8	645.55	62.3
1941.2	2.2	2042.5	6.8	648.55	54.1
1948.0	2.2	2053.4	7.0	651.55	43.1
1954.9	2.2	2064.1	7.0	654.55	39.5
1959.6	2.2	2074.5	7.0	657.56	37.3
1967.0	2.2	2083.6	6.9	660.56	34.6
1973.8	2.2	2093.1	6.7	663.56	33.5
1973.9	6.7	2135.7	6.8	666.56	34.4
1980.4	2.2	2141.2	7.0	669.57	35.6
1985.8	6.8			672.57	36.5
1985.9	2.1			675.57	37.4
1989.6	2.1			678.57	37.3
1994.1	2.1			681.58	38.2
1996.4	6.9			684.58	39.0
1998.4	2.1			687.58	47.9
2001.5	2.1			690.58	54.0
2005.8	2.1			693.59	48.5
2007.1	6.8			696.59	56.1
2010.4	2.0			699.59	62.8
2014.5	2.0			702.59	63.9
2017.5	6.8			705.60	60.6
2020.3	2.1			708.60	58.6
2024.8	2.1			711.60	60.5
2028.0	2.0			714.60	61.6
2028.1	6.9			717.61	61.2

2032.1	2.0
2035.6	2.1
2039.4	2.0
2042.9	1.9
2047.9	1.9
2052.6	2.0
2054.4	1.9
2057.5	1.9
2060.5	1.9
2064.2	2.0
2066.6	1.9
2069.5	1.9
2072.4	1.9
2075.0	1.9
2077.7	1.8
2079.6	1.8
2082.1	1.9
2084.3	1.9
2086.6	1.9
2089.5	1.9
2091.8	1.8
2093.8	1.8
2095.7	1.8
2096.8	1.8
2099.3	1.8
2101.1	1.9
2103.7	1.8
2106.8	1.7
2109.2	1.6
2111.7	1.7
2131.2	7.1
2142.4	7.2
2154.3	7.2
2166.5	7.3
2179.0	7.1
2236.3	7.3
2250.3	7.3
2275.2	7.3

720.61	59.1
723.61	55.9
726.61	52.2
729.62	51.4
732.62	53.3
735.62	58.8
738.62	69.8
741.63	81.0
744.63	82.5
747.63	73.8
750.64	55.7
753.64	35.5
756.64	25.4
759.64	27.2
762.65	42.3
765.65	63.2
768.65	78.5
771.65	92.9
774.66	109.1
777.66	115.1
780.66	97.7
783.66	97.8
786.67	123.1
789.67	129.3
792.67	129.6
795.67	128.4
798.68	125.5

Appendix B: Grain Size Data

Beach Profile Samples	Grain Size in mm									
Sample Name	**Mean**	**d05**	**d10**	**d16**	**d25**	**d50**	**d75**	**d84**	**d90**	**d95**
SKK_10_314_NK	1.2	0.2	0.4	0.6	0.8	1.2	1.6	1.8	1.9	2.2
SKK_10_314b_NK	1.5	0.5	0.7	0.9	1.1	1.5	1.9	2.1	2.2	2.5
SKK_11_JS0008	3.0	0.5	0.8	1.1	1.5	2.3	3.1	3.4	3.8	4.2
SKK_11_JS0008_2	13.1	3.7	5.6	7.2	9.0	13.1	17.2	19.1	20.9	23.1
SKK_11_JS0010	15.2	4.0	6.3	8.2	10.3	15.1	20.0	22.3	24.3	27.0
SKK_11_JS0011	9.1	2.8	4.1	5.2	6.4	8.9	11.5	12.7	13.8	15.2
SKK_11_JS0012	7.0	2.0	3.0	3.8	4.8	7.0	9.1	10.2	11.1	12.3
SKK_12_042_JS	0.8	0.1	0.2	0.3	0.4	0.7	1.0	1.1	1.3	1.4
SKK_12_043b_JS	13.7	5.2	7.0	8.5	10.2	13.7	17.2	18.8	20.3	22.2
SKK_12_044_JS	9.5	2.3	3.7	4.9	6.4	9.7	13.0	14.6	16.0	17.9
SKK_12_044_JS_2	8.5	2.7	3.9	4.9	6.0	8.5	11.0	12.1	13.2	14.5
SKK_12_045_JS	13.7	4.1	6.0	7.7	9.6	13.7	17.9	19.9	21.7	24.0
SKK_12_046_JS	6.4	1.9	2.8	3.6	4.5	6.4	8.3	9.2	10.1	11.1
SKK_12_050_JS	3.2	1.1	1.5	1.9	2.3	3.1	4.0	4.4	4.8	5.2
SKK_12_054_JS	6.8	2.5	3.4	4.1	5.0	6.8	8.6	9.4	10.2	11.2
SKK_12_084_JS	5.1	1.5	2.3	2.9	3.5	5.0	6.4	7.1	7.8	8.5
SKK_12_090_JS	7.4	2.5	3.5	4.4	5.3	7.3	9.4	10.3	11.2	12.3
SKK_12_39_JS	2.4	0.3	0.6	1.0	1.4	2.4	3.5	4.0	4.5	5.1
SKK_12_39_JS_2	11.0	3.8	5.3	6.6	7.9	10.9	13.8	15.2	16.5	18.1
SKK_12_40b_JS	1.2	0.1	0.2	0.4	0.6	1.2	1.8	2.0	2.3	2.6
SKK_13_148_JS	9.0	4.1	5.2	6.0	6.9	8.9	10.9	11.8	12.6	13.7
SKK_13_149_JS	10.8	5.8	6.9	7.7	8.7	10.7	12.8	13.7	14.6	15.7
SKK_13_149_JS_2	14.9	8.2	9.6	10.8	12.1	14.8	17.5	18.8	20.0	21.5
SKK_13_151_JS	1.0	0.2	0.4	0.5	0.6	0.9	1.2	1.3	1.4	1.6
SKK_13_153_JS	2.8	0.3	0.7	1.2	1.7	3.1	4.7	5.5	6.2	7.1
SKK_13_157_JS	10.5	2.9	4.5	5.8	7.3	10.6	13.9	15.5	16.9	18.7
SKK_13_159_JS	8.5	2.0	3.2	4.4	5.7	8.6	11.7	13.1	14.4	16.1
SKK_13_166_JS	8.9	3.4	4.5	5.5	6.6	8.8	11.1	12.2	13.2	14.4
SKK_14_124_JS	2.8	0.3	0.7	1.2	1.7	3.1	4.6	5.3	6.0	6.8
SKK_14_127_JS	27.5	7.7	11.7	15.1	19.1	27.7	36.5	40.6	44.4	49.2
SKK_14_127_JS_2	21.2	11.8	13.9	15.5	17.3	21.2	25.0	26.8	28.5	30.6
SKK_14_128_JS	1.6	0.2	0.4	0.7	1.0	1.7	2.4	2.7	3.0	3.4
SKK_14_128_JS_2	3.5	0.7	1.2	1.7	2.3	3.6	5.0	5.6	6.2	7.0
SKK_14_135_JS	11.2	4.3	5.7	7.0	8.3	11.2	14.1	15.4	16.7	18.2
SKK_15_175_JS	15.8	7.6	9.4	10.8	12.4	15.8	19.1	20.7	22.1	23.9
SKK_15_175_JS_2	6.6	1.2	2.2	3.1	4.2	6.8	9.5	10.8	12.0	13.4
SKK_15_176_JS	4.0	1.3	1.9	2.3	2.8	3.9	5.0	5.6	6.0	6.6

SKK_15_176_JS_2	3.4	0.5	0.9	1.4	2.1	3.5	5.1	5.9	6.6	7.4
SKK_15_178_JS	8.3	2.4	3.6	4.6	5.8	8.3	10.8	12.0	13.1	14.4
SKK_15_180_JS	1.8	0.2	0.5	0.7	1.1	1.9	2.8	3.2	3.6	4.0
SKK_15_183b_JS	1.6	0.2	0.4	0.7	0.9	1.6	2.2	2.6	2.8	3.2
SKK_16_193_JS	0.9	0.0	0.2	0.3	0.5	0.9	1.3	1.5	1.7	1.9
SKK_16_194_JS	2.0	0.5	0.8	1.0	1.3	1.9	2.6	2.9	3.1	3.5
SKK_16_197_JS	7.1	1.7	2.7	3.6	4.7	7.2	9.6	10.8	11.9	13.3
SKK_16_198_JS	1.7	0.2	0.5	0.7	1.0	1.8	2.5	2.9	3.3	3.7
SKK_16_202_JS	3.5	0.8	1.3	1.7	2.3	3.4	4.6	5.2	5.7	6.4
SKK_18_217_JS	1.6	1.0	1.1	1.2	1.3	1.6	1.8	1.9	2.0	2.1
SKK_18_218_JS	12.4	6.1	7.4	8.5	9.7	12.3	14.9	16.1	17.2	18.6
SKK_18_219_JS	2.9	0.4	0.8	1.2	1.7	3.1	4.6	5.3	6.0	6.8
SKK_18_220_JS	16.9	5.7	8.1	10.0	12.2	16.9	21.6	23.8	25.8	28.3
SKK_19_240_JS	4.7	0.9	1.6	2.3	3.1	4.9	6.8	7.7	8.6	9.6
SKK_19_242_JS	8.4	3.3	4.4	5.3	6.2	8.4	10.5	11.5	12.4	13.5
SKK_19_243_JS	2.7	0.5	0.9	1.3	1.7	2.8	3.8	4.3	4.8	5.4
SKK_19_246_JS	8.2	0.2	2.8	3.9	5.3	8.4	11.6	13.2	14.6	16.4
SKK_19_247b_JS	5.9	0.9	2.2	3.0	3.9	5.9	7.9	8.9	9.7	10.8
SKK_19_248_JS	12.9	4.7	7.1	8.4	9.8	12.8	15.8	17.3	18.6	20.2
SKK_22_001_NK	6.5	5.5	3.6	4.3	5.0	6.5	8.0	8.7	9.3	10.1
SKK_22_002_NK	13.6	1.1	8.6	9.7	10.9	13.5	16.1	17.3	18.4	19.7
SKK_22_004_NK	1.5	1.2	0.7	0.9	1.0	1.4	1.8	2.0	2.2	2.4
SKK_22_007_NK	12.1	1.0	4.0	5.7	7.7	12.3	17.2	19.5	21.6	24.3
SKK_22_008_NK	11.2	2.9	4.9	6.2	7.8	11.2	14.7	16.4	17.8	19.7
SKK_24_001_NK	9.9	0.2	6.5	7.3	8.1	9.8	11.5	12.3	13.1	14.0
SKK_24_003b_NK	13.8	4.4	6.3	8.0	9.8	13.7	17.7	19.6	21.3	23.4
SKK_25_001_NK	7.0	2.9	3.8	4.5	5.3	6.9	8.5	9.3	10.0	10.8
SKK_25_001_NK_2	2.4	0.2	0.5	0.9	1.4	2.7	4.1	4.8	5.4	6.2
SKK_30_001b_NK	6.9	1.5	2.6	3.5	4.5	6.9	9.3	10.5	11.6	12.9
SKK_30_001b_NK_2	1.6	0.3	0.6	0.8	1.0	1.6	2.1	2.3	2.6	2.9
SKK_30_005b_NK	10.8	2.9	4.4	5.8	7.4	10.8	14.3	16.0	17.5	19.4
SKK_30_007C_NK	2.1	0.5	0.8	1.0	1.4	2.1	2.8	3.1	3.4	3.8
SKK_31_001_NK	6.4	1.1	2.0	2.9	4.0	6.6	9.3	10.5	11.7	13.2
SKK_01_014b_NK	2.7	0.5	0.9	1.3	1.7	2.7	3.7	4.2	4.6	5.2
SKK_01_017_NK	2.1	0.2	0.5	0.8	1.2	2.1	3.1	3.6	4.1	4.6
SKK_01_017_NK_2	1.4	NaN	0.2	0.4	0.7	1.4	2.1	2.5	2.8	3.2
SKK_03_001b_NK	1.8	0.2	0.5	0.7	1.1	2.0	3.0	3.5	4.0	4.6
SKK_03_001c_NK	34.6	6.4	11.3	16.2	22.3	36.5	51.6	58.9	65.5	73.9
SKK_03_002b_NK	8.5	1.6	2.8	4.0	5.4	8.8	12.3	14.0	15.5	17.4
SKK_06_006_NK	8.8	1.5	2.7	4.0	5.6	9.2	13.1	15.0	16.7	18.9
SKK_06_NK	1.4	0.2	0.5	0.6	0.8	1.3	1.8	2.0	2.2	2.4

SKK_17_013b_JS	15.6	6.1	8.1	9.8	11.6	15.5	19.4	21.2	22.9	25.0
SKK_21_017b_JS	24.4	10.4	13.4	15.8	18.5	24.1	29.8	32.5	34.9	38.0
SKK_23_b_JS	29.5	16.4	19.3	21.5	24.0	29.3	34.6	37.2	39.4	42.3
SKK_32_003B_NK	6.1	1.0	1.8	2.7	3.8	6.4	9.2	10.5	11.8	13.3
SKK_32_003B_NK_2	3.2	0.4	0.9	1.3	1.9	3.4	5.0	5.7	6.4	7.3
SKK_32_c_NK	2.5	0.8	1.1	1.4	1.7	2.4	3.1	3.5	3.8	4.1
SKK_33_001_NK	9.7	2.5	3.9	5.1	6.6	9.7	12.9	14.4	15.7	17.5
SKK_33_001_NK_2	5.6	1.6	2.4	3.1	3.9	5.5	7.1	7.9	8.6	9.5
SKK_35_001_JS	1.7	0.8	1.0	1.1	1.3	1.6	1.9	2.1	2.2	2.4
SKK_35_002_JS	5.3	0.9	1.7	2.4	3.4	5.6	7.9	9.0	10.0	11.3
SKK_35_003_JS	2.1	0.2	0.5	0.8	1.3	2.2	3.3	3.8	4.3	4.9
SKK_35_003_JS_2	1.6	0.2	0.5	0.7	1.0	1.6	2.3	2.7	3.0	3.4
SKK_35_004_JS	2.1	0.4	0.7	1.0	1.3	2.1	2.9	3.3	3.6	4.0
SKK_35_005_JS	2.7	0.9	1.2	1.5	1.9	2.6	3.4	3.7	4.0	4.4
SKK_35_006_JS	1.5	0.3	0.5	0.7	0.9	1.5	2.0	2.2	2.5	2.8
SKK_35_010_JS	3.9	0.9	1.5	2.0	2.6	3.9	5.2	5.8	6.4	7.1
SKK_35_010b_JS	3.0	0.6	1.0	1.4	1.9	3.0	4.2	4.7	5.2	5.8
SKK_35_011_JS	2.1	0.5	0.8	1.1	1.4	2.0	2.7	3.0	3.2	3.6
SKK_35_012_JS	6.9	1.8	2.8	3.7	4.7	6.8	9.1	10.1	11.1	12.3
SKK_36_001_JS	1.3	0.1	0.3	0.5	0.7	1.3	1.9	2.2	2.5	2.8
SKK_36_002_JS	17.6	8.0	10.1	11.7	13.6	17.5	21.4	23.3	24.9	27.0
SKK_36_002_JS_2	2.0	0.4	0.7	1.0	1.3	1.9	2.6	3.0	3.2	3.6
SKK_36_003b_JS	1.6	0.1	0.3	0.6	0.9	1.7	2.5	3.0	3.3	3.8
SKK_36_005_JS	4.1	0.5	1.1	1.7	2.5	4.6	6.9	8.0	9.0	10.3
SKK_36_006_JS	3.0	0.3	0.8	1.2	1.7	2.9	4.1	4.7	5.2	5.9
SKK_36_007_JS	23.0	6.5	9.9	12.7	16.0	23.2	30.5	34.0	37.2	41.1
SKK_36_009_JS	3.4	0.5	1.1	1.5	2.1	3.4	4.8	5.4	6.0	6.8
SKK_36_009_JS_2	23.2	5.6	9.0	12.0	15.6	23.5	31.6	35.5	39.0	43.5
SKK_36_013_JS	6.9	2.4	3.3	4.1	5.0	6.9	8.7	9.6	10.4	11.5
SKK_36_016_JS	1.4	0.2	0.4	0.6	0.9	1.4	1.9	2.2	2.4	2.7
SKK_37_001_JS	9.2	1.2	2.5	3.9	5.8	10.4	15.6	18.1	20.4	23.3
SKK_37_002_JS	8.2	1.8	3.0	4.1	5.4	8.2	11.1	12.5	13.8	15.4
SKK_37_002_JS_2	22.7	6.0	9.3	12.2	15.5	22.9	30.3	33.9	37.1	41.2
SKK_37_003_JS	4.3	0.5	1.1	1.8	2.6	4.6	6.8	7.9	8.9	10.1
SKK_37_004_JS	6.6	0.9	1.9	2.8	4.1	7.0	10.2	11.8	13.2	15.0
SKK_37_005_JS	3.0	1.0	1.4	1.7	2.1	2.8	3.6	3.9	4.3	4.7
SKK_37_006_JS	39.9	9.7	15.5	20.7	26.9	40.5	54.4	61.1	67.1	74.7
SKK_37_010_JS	6.5	2.2	3.1	3.8	4.7	6.4	8.2	9.0	9.7	10.7
SKK_37_012_JS	5.6	1.9	2.7	3.3	4.0	5.5	7.1	7.8	8.4	9.3
SKK_37_015_JS	3.3	0.5	0.9	1.4	2.0	3.5	5.0	5.8	6.4	7.3
SKK_37_c_NK	5.2	1.0	1.8	2.5	3.3	5.2	7.0	7.9	8.8	9.8

SKK_38_001_JS	1.8	0.1	0.4	0.6	1.0	1.8	2.7	3.1	3.5	4.0
SKK_38_002_JS	21.2	7.5	10.4	12.8	15.5	21.2	26.9	29.6	32.0	35.1
SKK_38_002_JS_2	2.4	0.6	1.0	1.3	1.6	2.3	3.0	3.3	3.6	4.0
SKK_38_003_JS	15.4	5.0	7.1	8.9	11.0	15.4	19.8	21.9	23.8	26.2
SKK_38_003_JS_2	2.2	0.2	0.6	0.9	1.3	2.4	3.5	4.0	4.5	5.2
SKK_38_004_JS	5.6	0.5	1.3	2.2	3.3	6.1	9.2	10.8	12.2	13.9
SKK_38_005_JS	4.1	0.5	1.1	1.7	2.5	4.2	6.1	6.9	7.8	8.8
SKK_38_006_JS	18.5	5.9	8.5	10.7	13.2	18.5	23.9	26.5	28.8	31.7
SKK_38_009_JS	2.3	0.3	0.6	0.9	1.3	2.4	3.5	4.1	4.6	5.2
SKK_38_011_JS	4.3	1.5	2.1	2.6	3.1	4.3	5.4	6.0	6.4	7.1
SKK_38_022b_JS	4.5	1.0	1.6	2.2	2.9	4.5	6.1	6.9	7.6	8.5
SKK_38_NK0061	11.0	3.1	4.7	6.0	7.6	11.1	14.5	16.2	17.7	19.6
SKK_39_001_JS	9.1	2.3	3.6	4.8	6.2	9.1	12.2	13.6	14.9	16.6
SKK_39_002_JS	3.4	0.4	0.9	1.5	2.2	4.0	6.0	7.0	7.9	9.1
SKK_39_004_JS	2.6	0.3	0.7	1.1	1.6	3.0	4.6	5.4	6.1	7.0
SKK_39_004_JS_2	8.0	4.2	5.0	5.6	6.4	7.9	9.5	10.2	10.9	11.7
SKK_39_006_JS	1.5	0.2	0.4	0.6	0.9	1.4	2.0	2.3	2.5	2.9
SKK_39_007_JS	4.6	0.6	1.3	2.0	2.8	4.6	6.4	7.3	8.1	9.1
SKK_39_008b_JS	7.5	1.7	2.8	3.8	4.9	7.4	10.0	11.2	12.3	13.7
SKK_39_010_JS	10.8	4.8	6.1	7.2	8.3	10.7	13.2	14.3	15.3	16.7
SKK_39_013_JS	4.9	1.7	2.3	2.9	3.5	4.8	6.2	6.8	7.4	8.1
SKK_39_014_JS	2.2	0.5	0.9	1.1	1.4	2.1	2.8	3.1	3.4	3.8
SKK_40_010_JS	1.1	0.1	0.3	0.4	0.6	1.1	1.5	1.7	1.9	2.2
SKK_40_011_JS	8.3	1.8	3.0	4.1	5.4	8.4	11.4	12.8	14.1	15.8
SKK_40_011_JS_2	1.8	0.3	0.6	0.8	1.1	1.7	2.4	2.7	2.9	3.3
SKK_40_012_JS	2.7	0.1	0.5	1.0	1.6	3.1	4.9	5.7	6.5	7.5
SKK_40_013_JS	7.0	2.1	3.1	4.0	4.9	7.0	9.0	10.0	10.9	12.0
SKK_40_014_JS	4.6	0.8	1.5	2.1	2.9	4.6	6.4	7.2	8.0	9.0
SKK_40_014_JS_2	2.3	0.2	0.5	0.9	1.3	2.2	3.3	3.8	4.2	4.8
SKK_40_015_JS	23.7	4.1	7.5	10.9	15.1	25.0	35.6	40.7	45.3	51.2
SKK_40_015_JS_2	3.9	0.3	0.9	1.5	2.2	4.2	6.3	7.3	8.3	9.5
SKK_40_016_JS	13.1	2.9	4.9	6.6	8.7	13.4	18.3	20.7	22.8	25.5
SKK_40_017_JS	8.9	2.1	3.4	4.6	5.9	8.9	12.0	13.5	14.8	16.5
SKK_40_021_JS	15.7	6.6	8.5	10.1	11.9	15.6	19.4	21.1	22.7	24.8
SKK_40_023_JS	1.6	0.2	0.4	0.6	0.9	1.6	2.3	2.6	2.9	3.3
SKK_40_031_JS	12.1	5.9	7.2	8.3	9.4	11.9	14.4	15.6	16.6	17.9
SKK_41_001_JS	20.7	5.0	8.1	10.8	14.0	21.0	28.3	31.8	34.9	38.9
SKK_41_002_JS	13.2	2.9	4.8	6.6	8.7	13.4	18.3	20.6	22.7	25.4
SKK_41_003_JS	9.9	2.8	4.2	5.4	6.8	9.9	13.0	14.5	15.8	17.5
SKK_41_003_JS_2	8.4	2.8	4.0	4.9	6.0	8.3	10.7	11.8	12.8	14.1
SKK_41_004_JS	22.6	6.9	10.1	12.8	16.0	22.7	29.5	32.7	35.7	39.3

SKK_41_005_JS	11.5	1.1	2.8	4.6	7.2	13.7	21.1	24.8	28.1	32.4
SKK_41_006_JS	14.8	2.7	4.8	6.9	9.5	15.5	22.0	25.1	27.9	31.4
SKK_41_007_JS	31.7	7.5	12.1	16.3	21.2	32.3	43.7	49.2	54.1	60.3
SKK_41_009_JS	3.6	0.7	1.2	1.7	2.3	3.6	5.0	5.6	6.2	7.0
SKK_41_010_JS	6.8	1.8	2.8	3.7	4.7	6.8	9.0	10.0	11.0	12.1
SKK_41_011_JS	7.4	2.7	3.7	4.5	5.4	7.4	9.3	10.3	11.1	12.2
SKK_41_022_JS	10.3	2.5	4.0	5.3	6.9	10.3	13.8	15.5	17.0	18.9
SKK_42_001_JS	12.5	2.2	4.0	5.8	8.0	13.2	18.7	21.4	23.8	26.9
SKK_42_002_JS	16.0	5.5	7.7	9.5	11.6	16.0	20.4	22.5	24.3	26.7
SKK_42_003_JS	18.3	6.7	9.2	11.2	13.4	18.2	23.1	25.4	27.4	30.1
SKK_42_003_JS_2	2.9	0.4	0.8	1.2	1.8	3.1	4.5	5.1	5.8	6.5
SKK_42_004_JS	6.4	2.1	3.0	3.7	4.5	6.3	8.1	9.0	9.7	10.7
SKK_42_005_JS	4.9	1.7	2.4	2.9	3.5	4.8	6.1	6.7	7.3	8.0
SKK_42_006_JS	5.9	0.7	1.6	2.4	3.5	6.1	8.8	10.1	11.3	12.8
SKK_42_006_JS_2	28.4	10.4	14.2	17.4	20.8	28.3	35.8	39.3	42.5	46.5
SKK_42_009_JS	23.4	12.5	14.9	16.8	18.9	23.4	27.8	30.0	31.9	34.3
SKK_42_010_JS	28.3	13.0	16.3	19.0	21.9	28.2	34.5	37.5	40.2	43.6
SKK_42_012_JS	15.2	3.7	5.9	7.9	10.2	15.4	20.7	23.2	25.5	28.4
SKK_42_015_JS	34.2	10.6	15.5	19.5	24.2	34.3	44.5	49.4	53.8	59.3
SKK_42_018_JS	2.6	0.8	1.2	1.4	1.8	2.5	3.2	3.6	3.9	4.3
SKK_43_001_JS	13.5	2.4	4.4	6.3	8.6	14.2	20.2	23.1	25.7	29.0
SKK_43_002_JS	10.6	4.1	5.5	6.6	7.9	10.5	13.2	14.5	15.7	17.1
SKK_43_003_JS	14.4	5.6	7.4	9.0	10.7	14.3	17.9	19.6	21.1	23.1
SKK_43_003_JS_2	5.3	0.5	1.3	2.1	3.2	5.8	8.7	10.1	11.4	13.0
SKK_43_004_JS	20.3	4.8	7.8	10.5	13.6	20.4	27.5	30.8	33.9	37.7
SKK_43_004_JS_2	25.3	6.2	9.9	13.2	17.0	25.5	34.2	38.4	42.1	46.9
SKK_43_005_JS	6.1	0.6	1.5	2.4	3.6	6.2	9.1	10.5	11.7	13.3
SKK_43_005_JS_2	36.4	11.3	16.5	20.8	25.7	36.3	46.9	52.0	56.6	62.3
SKK_43_006_JS	27.4	9.6	13.3	16.4	19.9	27.4	34.9	38.4	41.6	45.7
SKK_43_008_JS	33.8	9.2	14.1	18.4	23.3	34.2	45.2	50.4	55.2	61.2
SKK_43_012_JS	34.4	10.9	15.8	19.8	24.5	34.5	44.7	49.5	53.8	59.3
SKK_43_015_JS	11.5	2.1	3.8	5.4	7.4	12.0	16.9	19.3	21.4	24.1
SKK_43_022_JS	22.8	6.5	9.8	12.6	15.9	22.9	30.1	33.6	36.6	40.5
SKK_43_d_NK	33.2	10.0	14.7	18.7	23.3	33.2	43.3	48.1	52.3	57.8
SKK_44_001_JS	16.2	5.7	7.9	9.7	11.8	16.2	20.7	22.8	24.7	27.1
SKK_44_002_JS	15.3	4.8	6.9	8.8	10.8	15.3	19.8	22.0	23.9	26.4
SKK_44_003_JS	18.6	5.8	8.5	10.7	13.2	18.5	23.9	26.4	28.7	31.6
SKK_44_003_JS_2	9.9	1.2	2.6	4.1	6.1	10.9	16.2	18.8	21.1	24.1
SKK_44_004_JS	78.9	42.9	50.8	57.0	63.9	78.6	93.2	100.2	106.4	114.3
SKK_44_005_JS	12.4	1.8	3.6	5.3	7.6	12.9	18.4	21.2	23.6	26.7
SKK_44_009_JS	27.9	11.5	15.1	17.9	21.1	27.9	34.6	37.8	40.7	44.4

SKK_44_011_JS	13.9	4.2	6.2	7.9	9.8	13.9	18.1	20.0	21.8	24.1
SKK_44_012_JS	9.4	2.4	3.8	5.0	6.4	9.4	12.6	14.1	15.4	17.1
SKK_44_014_JS	28.2	15.5	18.3	20.5	23.0	28.2	33.4	35.9	38.1	40.9
SKK_44_a_JS	7.8	3.2	4.2	5.0	5.9	7.8	9.7	10.6	11.4	12.4
SKK_44_a_JS_2	1.5	0.1	0.4	0.6	0.9	1.7	2.5	2.9	3.2	3.7
SKK_45_001_JS	33.6	11.4	16.1	20.0	24.3	33.7	43.1	47.6	51.6	56.7
SKK_45_002_JS	61.9	21.4	30.0	37.0	44.9	61.9	79.0	87.1	94.4	103.7
SKK_45_003_JS	19.4	6.5	9.2	11.5	14.0	19.4	24.9	27.5	29.8	32.7
SKK_45_004_JS	15.5	4.5	6.7	8.6	10.7	15.4	20.1	22.4	24.4	26.9
SKK_45_005_JS	30.3	5.8	10.2	14.4	19.6	31.6	44.2	50.2	55.7	62.7
SKK_45_005_JS_2	5.1	0.6	1.3	2.1	3.0	5.4	7.9	9.2	10.3	11.7
SKK_45_006_JS	65.7	20.0	29.4	37.3	46.4	65.9	85.7	95.1	103.6	114.3
SKK_45_008_JS	29.6	13.8	17.3	20.0	23.1	29.5	36.0	39.0	41.8	45.3
SKK_45_009_JS	22.7	5.8	9.1	12.0	15.5	23.0	30.7	34.4	37.7	41.9
SKK_45_014_JS	22.2	6.5	9.7	12.4	15.6	22.3	29.2	32.5	35.4	39.2
SKK_45_015_JS	2.6	0.7	1.1	1.4	1.8	2.5	3.3	3.7	4.0	4.4
SKK_45_016_JS	29.8	10.7	14.7	18.1	21.8	29.9	37.9	41.8	45.2	49.6
SKK_45_019_JS	16.7	6.3	8.5	10.3	12.3	16.7	21.0	23.1	25.0	27.3
SKK_46_001_JS	74.1	15.0	25.7	35.9	48.4	77.1	107.1	121.6	134.7	151.3
SKK_46_001b_JS	66.5	21.2	30.6	38.5	47.5	66.9	86.4	95.7	104.1	114.7
SKK_46_002_JS	54.3	23.3	30.0	35.4	41.5	54.3	67.1	73.2	78.6	85.5
SKK_46_003_JS	17.0	4.5	7.0	9.2	11.7	17.1	22.7	25.3	27.7	30.8
SKK_46_004_JS	48.0	12.5	19.5	25.6	32.8	48.5	64.6	72.3	79.2	88.0
SKK_46_005_JS	32.1	11.9	16.3	19.8	23.7	32.1	40.5	44.6	48.2	52.7
SKK_46_006_JS	20.1	6.4	9.2	11.6	14.3	20.1	26.0	28.8	31.3	34.5

Other Samples Grain Size in mm

Sample Name	**Mean**	**d05**	**d10**	**d16**	**d25**	**d50**	**d75**	**d84**	**d90**	**d95**
2011-SHK-JS-014	28.6	0.7	1.4	2.0	2.9	5.0	7.3	8.4	9.4	10.7
2011-SHK-NK-069	16.5	0.4	0.8	1.3	1.8	3.3	4.9	5.7	6.4	7.3
2011-SHK-NK-068	8.2	1.9	3.1	4.2	5.5	8.3	11.3	12.7	14.0	15.6
2011-SHK-NK-061	9.2	1.9	3.3	4.5	6.1	9.6	13.2	15.0	16.6	18.7
2011-SHK-NK-071	19.3	5.9	8.7	11.0	13.7	19.4	25.2	28.0	30.5	33.7
2011-SHK-NK-073	9.3	2.6	4.0	5.1	6.4	9.4	12.3	13.7	15.0	16.6
2011-SHK-JS-063	1.5	0.5	0.7	0.9	1.1	1.5	2.0	2.2	2.4	2.6
2011-SHK-NK-059	0.6	0.2	0.3	0.3	0.4	0.6	0.7	0.8	0.9	0.9
2011-SHK-JS-21	0.3	0.1	0.1	0.2	0.2	0.3	0.5	0.5	0.6	0.7
2011-SHK-JS-21	0.4	0.1	0.1	0.2	0.2	0.4	0.5	0.6	0.6	0.7
2011-UNK-JS-017A	1.8	0.4	0.7	0.9	1.2	1.9	2.6	2.9	3.2	3.6
2011-SHK-NK-059	0.5	0.1	0.2	0.3	0.3	0.5	0.7	0.8	0.8	0.9
2011-SHK-JS-013	0.9	0.3	0.4	0.5	0.6	0.9	1.1	1.3	1.4	1.5

2011-UNK-JS-017B	0.6	0.1	0.2	0.3	0.4	0.6	0.7	0.8	0.9	1.0
2011-UNK-JS-077	1.0	0.2	0.4	0.5	0.7	1.1	1.5	1.6	1.8	2.0
2011-SHK-NK-048	0.4	0.1	0.2	0.2	0.3	0.4	0.5	0.5	0.5	0.6
2011-SHK-NK-110	3.1	1.6	2.0	2.2	2.5	3.1	3.7	3.9	4.2	4.5
2011-SHK-NK-070	2.2	0.9	1.2	1.4	1.7	2.2	2.7	2.9	3.1	3.4
2011-UNK-JS-162	1.9	0.7	1.0	1.2	1.4	1.9	2.3	2.5	2.7	3.0
2011 SHK-JS-015	0.8	0.2	0.4	0.4	0.6	0.8	1.0	1.1	1.2	1.3
2011-SHK-JS-063	1.0	0.3	0.5	0.6	0.7	1.0	1.3	1.4	1.5	1.7
2011-SHK-JS-008	0.7	0.2	0.3	0.4	0.5	0.7	0.9	1.0	1.1	1.2
2011-SHK-NK-101	1.2	0.4	0.6	0.7	0.9	1.2	1.6	1.7	1.9	2.1
2011-SHK-JS-018	0.2	0.0	0.1	0.1	0.1	0.2	0.3	0.3	0.4	0.4
2011-SHK-NK-085	0.3	0.1	0.1	0.2	0.2	0.3	0.5	0.5	0.6	0.6
2011-UNK-JS-135	1.2	0.3	0.4	0.6	0.8	1.2	1.6	1.8	2.0	2.3
2011-SHK-JS-024	0.4	0.1	0.1	0.2	0.2	0.4	0.5	0.6	0.6	0.7
2011-SHK-NK-062	2.2	0.7	1.0	1.3	1.6	2.2	2.8	3.1	3.4	3.7
2011-SHK-JS-010	1.9	0.4	0.7	1.0	1.3	1.9	2.6	2.9	3.2	3.6
2011-UNK-NK-003B	3.5	1.0	1.5	1.9	2.4	3.5	4.6	5.2	5.6	6.2
2011-UNK-JS-075	1.3	0.3	0.5	0.7	0.8	1.3	1.7	1.9	2.1	2.3
2011-UNK-JS-165	3.5	1.7	2.1	2.4	2.8	3.5	4.3	4.7	5.0	5.4
2011-UNK-JS-163	3.1	1.3	1.7	2.0	2.3	3.1	3.8	4.1	4.5	4.9
2011-UNK-JS-134	4.5	1.6	2.2	2.7	3.3	4.5	5.7	6.3	6.8	7.5
2011-UNK-JS-060	2.8	0.7	1.1	1.5	1.9	2.9	3.9	4.4	4.8	5.4
2011-UNK-JS-061	4.0	1.5	2.1	2.5	3.0	4.1	5.2	5.7	6.2	6.8
2011-UNK-JS-111	4.6	1.4	2.0	2.6	3.2	4.6	6.0	6.7	7.3	8.0
2011-SHK-JS-011	4.0	1.9	2.3	2.7	3.1	3.9	4.8	5.2	5.6	6.0
2011-UNK-NK-085	1.8	0.4	0.6	0.9	1.2	1.8	2.5	2.9	3.2	3.6
2011-SHK-JS-012	3.7	1.8	2.2	2.6	2.9	3.7	4.5	4.9	5.2	5.6
2011-SHK-NK-060	6.8	3.4	4.1	4.7	5.4	6.8	8.2	8.9	9.5	10.2
2011-SHK-NK-102	1.7	0.4	0.6	0.8	1.1	1.7	2.4	2.7	3.0	3.3
2011-SHK-MD-002	2.1	0.8	1.0	1.3	1.5	2.1	2.8	3.0	3.3	3.6

Appendix C: Storm Surge and Wave Runup Results

MIROC5 RCP 4.5 Projected Bering Sea Storms

Year	Start Date	Duration - Combined Storms (days)	Surge Ht (m)	Runup New Site (m)	Runup Old Site (m)
2026	7/6/26	7	2.4	1.2	1.4
2026	7/24/26	12	2.7	1.0	1.1
2026	8/15/26	5	2.3	0.7	0.8
2026	9/1/26	9	2.7	1.6	1.6
2026	10/9/26	6	2.4	1.7	1.8
2027	8/10/27	16	2.3	1.2	1.4
2027	8/30/27	4	2.3	0.7	0.9
2027	9/15/27	8	2.4	1.5	1.6
2027	10/18/27	7	2.3	1.9	1.9
2028	7/9/28	5	2.0	0.7	0.9
2028	7/22/28	6	2.6	1.2	1.3
2028	8/7/28	2	2.1	0.9	1.0
2028	8/14/28	15	2.1	2.0	2.0
2028	9/13/28	5	2.5	1.3	1.4
2028	9/23/28	5	2.2	1.1	1.2
2028	10/9/28	6	2.1	1.0	1.1
2029	7/2/29	3	2.0	0.6	0.8
2029	8/26/29	8	2.8	2.3	2.4
2029	9/11/29	12	2.3	1.8	1.9
2029	10/1/29	3	2.3	1.3	1.5
2030	7/6/30	6	2.0	0.6	0.8
2030	7/28/30	9	2.4	1.8	2.0
2030	10/9/30	21	3.1	2.8	2.6
2031	7/7/31	4	2.1	0.6	0.7
2031	9/1/31	6	3.4	1.7	1.8
2031	9/23/31	11	2.8	3.4	3.2
2032	7/28/32	3	2.0	0.7	0.9
2032	8/24/32	7	2.2	1.7	1.8
2032	9/5/32	5	2.2	0.9	1.1
2032	9/25/32	5	2.6	1.0	1.1
2032	10/18/32	7	2.7	1.6	1.7
2033	7/30/33	4	2.5	1.4	1.5
2033	8/20/33	7	2.1	1.0	1.1
2033	9/9/33	15	2.7	1.6	1.9
2033	10/5/33	5	2.2	1.8	2.0
2034	7/10/34	4	2.0	0.7	0.9
2034	7/25/34	4	2.5	0.6	0.8

2034	8/2/34	4	2.5	0.6	0.8
2034	8/12/34	3	2.6	0.8	0.9
2034	8/28/34	3	2.1	1.2	1.3
2034	9/10/34	4	2.1	0.9	1.0
2034	9/27/34	7	3.0	1.8	1.9
2035	7/1/35	9	2.0	0.7	0.8
2035	7/28/35	6	2.8	1.2	1.2
2035	9/20/35	4	2.2	1.0	1.2
2036	9/13/36	4	2.3	1.9	2.0
2036	10/14/36	6	2.4	2.4	2.9
2037	8/14/37	6	2.7	1.1	1.2
2037	9/1/37	3	3.1	0.8	0.9
2037	9/28/37	6	2.4	1.6	1.6
2037	10/12/37	16	2.6	2.2	2.5
2038	7/19/38	14	2.7	0.9	1.0
2038	8/23/38	5	2.0	0.9	1.0
2038	9/27/38	6	3.2	1.6	1.9
2039	8/22/39	5	2.0	0.6	0.7
2039	9/16/39	9	2.6	1.4	1.6
2039	10/9/39	7	2.4	4.1	4.2
2040	7/1/40	3	3.2	0.9	1.1
2040	8/19/40	5	2.3	0.9	1.0
2040	9/10/40	11	2.9	1.0	1.4
2040	10/14/40	8	2.7	1.7	1.9
2041	7/13/41	10	2.1	0.6	0.6
2041	9/22/41	3	2.2	1.4	1.6
2041	10/19/41	11	5.5	3.4	2.7
2042	8/16/42	6	2.4	1.3	1.4
2042	9/20/42	9	2.5	1.6	1.8
2042	10/11/42	16	4.9	3.1	2.9
2043	10/20/43	4	4.1	1.9	2.2
2044	7/24/44	3	2.5	0.7	0.8
2044	8/3/44	3	2.2	1.0	1.2
2044	9/5/44	8	2.5	1.7	1.8
2044	10/16/44	10	2.7	2.3	2.5
2045	7/15/45	24	4.9	1.0	1.2
2045	8/15/45	5	2.5	0.8	0.9
2045	8/28/45	5	2.6	1.6	1.8
2045	9/19/45	6	2.3	1.1	1.2
2081	7/11/81	4	2.2	1.5	1.6
2081	8/17/81	4	2.4	1.7	1.8

2081	9/5/81	15	2.2	1.0	1.2
2081	9/29/81	4	2.5	1.9	1.9
2081	10/8/81	10	2.5	2.2	2.4
2082	7/12/82	12	2.0	1.5	1.6
2082	7/29/82	5	2.1	1.0	1.1
2082	8/29/82	12	2.7	2.0	2.0
2082	10/15/82	5	2.4	1.1	1.3
2082	10/27/82	4	2.2	1.5	1.6
2083	7/27/83	4	2.1	0.6	0.8
2083	9/14/83	4	2.7	1.5	1.6
2083	9/30/83	11	3.3	1.8	2.0
2084	7/13/84	16	2.2	0.9	1.0
2084	8/8/84	10	5.0	1.4	1.5
2084	8/30/84	4	2.2	0.8	1.0
2084	9/20/84	7	2.3	0.9	1.1
2084	10/29/84	2	2.4	1.9	2.1
2085	8/3/85	6	1.9	0.7	0.9
2085	8/27/85	6	2.2	0.7	0.8
2085	9/9/85	7	2.2	0.9	1.0
2085	10/15/85	14	2.6	2.0	2.1
2086	7/13/86	6	2.6	0.2	1.2
2086	8/19/86	7	2.2	0.8	1.2
2086	9/4/86	11	2.0	1.0	1.1
2086	9/23/86	5	2.7	1.7	2.1
2086	10/11/86	5	3.3	1.9	2.0
2086	10/20/86	9	3.3	1.5	1.6
2087	9/15/87	6	2.3	1.5	1.7
2087	9/28/87	4	2.7	1.0	1.2
2088	7/12/88	4	2.2	0.7	0.9
2088	8/7/88	9	2.1	2.0	2.1
2088	8/31/88	12	2.3	2.5	2.7
2088	10/7/88	5	2.5	1.3	1.4
2089	9/25/89	9	2.7	0.7	0.8
2090	7/15/90	2	2.0	1.5	1.5
2090	8/3/90	3	2.5	1.1	1.3
2090	8/21/90	6	2.8	1.4	1.5
2090	9/9/90	5	2.0	0.6	0.7
2091	7/25/91	7	2.1	0.9	1.0
2091	9/3/91	5	2.1	0.7	0.8
2092	7/29/92	3	2.1	1.0	1.1
2092	9/15/92	5	2.1	0.6	0.7

2093	7/25/93	10	2.3	0.7	0.9
2093	9/1/93	5	2.6	1.7	1.8
2093	10/1/93	5	3.1	1.2	1.3
2093	10/22/93	5	2.2	0.9	1.1
2094	7/23/94	4	2.5	0.7	0.8
2094	8/13/94	4	2.0	1.9	1.9
2094	8/21/94	6	2.0	3.1	3.4
2094	10/28/94	3	2.4	0.7	0.8
2095	7/7/95	4	2.0	1.4	1.6
2095	7/20/95	6	2.1	0.8	0.9
2095	8/22/95	5	2.6	0.6	0.7
2096	7/3/96	4	2.0	0.8	0.9
2096	7/14/96	3	2.5	0.5	0.6
2096	8/7/96	6	2.2	2.9	2.8
2096	9/6/96	5	3.2	0.9	1.0
2096	9/27/96	8	2.1	1.7	1.9
2096	10/20/96	11	2.6	1.0	1.1
2097	7/19/97	5	2.6	0.6	0.8
2097	7/31/97	3	2.0	1.2	1.3
2097	9/3/97	13	2.3	1.0	1.1
2098	8/20/98	4	2.0	1.5	1.6
2098	10/4/98	7	2.0	3.5	3.7
2098	10/25/98	5	3.7	1.2	1.2
2099	7/3/99	4	2.2	0.6	0.7
2099	7/23/99	5	2.3	1.5	1.5
2099	8/30/99	4	2.1	0.8	0.9
2099	10/13/99	4	2.2	0.6	0.8
2100	8/2/00	4	2.7	1.1	1.2
2100	8/29/00	5	2.2	1.1	1.2
2100	10/7/00	5	2.3	2.3	2.6
2100	10/21/00	5	2.2	0.9	2.3

MIROC5 RCP 8.5 Projected Bering Sea Storms

Year	Start Date	Duration - Combined Storms (days)	Surge Ht (m)	Runup New Site (m)	Runup Old Site (m)
2026	9/25/26	5	2.0	1.5	1.6
2027	9/17/27	5	1.7	1.9	1.9
2027	10/10/27	5	2.1	1.4	1.5
2027	10/23/27	6	3.7	1.2	1.6
2028	8/24/28	5	2.8	0.8	0.8
2028	9/18/28	7	2.3	1.0	1.1
2028	9/29/28	5	3.2	1.5	1.7

2029	8/30/29	4	2.3	1.0	1.2
2029	10/10/29	3	1.8	2.3	2.4
2029	10/23/29	5	3.2	2.4	2.5
2030	9/24/30	5	2.4	1.2	1.3
2031	7/14/31	4	1.8	0.9	1.0
2031	9/22/31	5	2.4	1.3	1.4
2032	7/30/32	5	1.9	2.2	2.3
2032	8/14/32	6	2.6	0.8	0.9
2032	10/8/32	3	1.8	1.2	1.2
2032	10/25/32	6	1.8	1.0	1.2
2033	7/29/33	5	2.2	0.8	0.9
2033	10/14/33	6	2.4	3.3	3.3
2034	8/16/34	4	1.9	0.7	0.8
2034	8/27/34	3	2.9	1.0	1.1
2034	9/7/34	2	2.4	1.1	1.4
2035	7/13/35	3	3.0	1.0	1.0
2035	10/7/35	4	1.9	1.5	1.7
2036	8/30/36	14	1.8	0.8	0.9
2037	10/25/37	5	3.2	2.3	2.4
2038	7/27/38	4	2.1	0.6	0.6
2038	8/21/38	10	2.4	1.0	1.1
2038	10/1/38	3	4.8	1.4	1.5
2038	10/23/38	4	2.4	3.1	3.3
2039	8/19/39	2	1.8	0.3	0.4
2039	9/30/39	9	2.2	1.5	1.5
2040	8/30/40	6	1.8	0.7	0.8
2041	8/30/41	15	1.9	1.3	1.5
2042	10/4/42	4	2.5	1.7	2.1
2042	10/13/42	4	2.0	4.2	4.0
2043	9/23/43	5	1.8	1.0	1.1
2043	10/21/43	10	3.1	3.4	3.3
2044	9/9/44	2	1.8	1.2	1.3
2045	8/24/45	3	1.8	0.6	0.7
2045	9/9/45	4	2.2	1.0	1.2
2045	9/20/45	10	1.9	1.6	1.7
2081	7/1/81	5	2.0	0.7	0.9
2081	7/26/81	5	1.8	1.5	1.6
2082	9/22/82	5	2.4	1.5	1.5
2082	10/22/82	9	1.8	1.8	1.9
2083	7/16/83	3	3.2	1.0	1.2
2083	8/10/83	3	2.3	0.7	0.9

2083	8/17/83	4	2.5	1.6	1.6
2083	9/14/83	5	3.2	1.2	1.4
2083	9/29/83	5	2.5	1.3	1.5
2084	9/17/84	13	2.3	1.0	1.2
2084	10/16/84	3	1.8	1.4	1.6
2085	8/26/85	4	2.1	2.1	2.2
2085	10/7/85	4	1.8	1.3	1.6
2085	10/16/85	5	2.1	1.5	1.7
2085	10/30/85	1	1.8	2.3	2.3
2086	7/30/86	10	2.4	0.8	1.0
2087	8/5/87	5	1.9	0.7	0.8
2088	8/3/88	3	2.7	0.7	1.0
2088	10/13/88	18	2.1	2.3	2.6
2089	7/6/89	3	1.7	1.3	1.4
2090	7/15/90	2	2.2	1.0	1.2
2090	8/24/90	3	1.9	0.7	0.8
2091	7/21/91	5	2.8	0.9	1.0
2091	10/23/91	8	1.9	1.5	1.6
2092	8/7/92	5	2.8	0.8	1.0
2092	10/5/92	4	2.0	1.6	1.8
2093	10/2/93	5	2.4	1.8	1.8
2094	7/10/94	4	1.9	0.6	0.7
2094	9/4/94	3	2.9	0.9	1.0
2094	10/5/94	7	2.1	1.3	1.4
2095	10/3/95	18	2.1	1.7	1.9
2096	7/13/96	4	2.1	0.7	0.8
2096	10/23/96	8	2.0	4.2	4.2
2097	8/25/97	5	1.9	0.6	0.7
2097	10/13/97	10	2.0	4.3	4.3
2098	7/14/98	5	1.8	0.7	0.8
2098	7/24/98	7	3.0	0.8	0.9
2098	8/7/98	3	2.2	0.4	0.6
2098	8/19/98	4	1.7	1.0	1.2
2099	7/22/99	4	1.7	0.7	0.7
2099	8/10/99	2	2.1	0.5	0.6
2099	8/19/99	3	2.6	1.4	1.4
2100	9/6/00	3	2.0	0.5	0.6
2100	10/25/00	5	2.0	3.7	3.6

References Cited

Blier, W.; Keefe, S.; Shaffer, W.A., and Kim, S.C., 1997. Storm surges in the region of western Alaska. *Monthly Weather Review*, 125, 3094–3108.

Buscombe, D.; Rubin, D.M., and Warrick, J.A., 2010. A universal approximation of grain size from images of noncohesive sediment. *Journal of Geophysical Research,* 115, F02015.

Chapman, R.S; Kim, S., and Mark, D.J., 2011. Storm-induced water level prediction study for Shaktoolik, Alaska. Vicksburg, Mississippi: U.S. Army Corps of Engineers, Coastal and Hydraulics Laboratory, 18p.

Cross, A.E, 2010. Synoptic drivers of storm surge in Kotzebue Sound. Fairbanks, Alaska: University of Alaska, Fairbanks, Master's thesis, 84p.

Erikson, L.H., 2012. United States Geological Survey (USGS), *personal communication.*

Federal Emergency Management Agency (FEMA) Staff, 2007. Guidelines and Specifications for Flood Hazard Mapping Partners. Washington, DC: Federal Emergency Management Agency, D.2.8 Wave Runup and Overtopping, 31p.

Glahn, B., Taylor; A., Kurkowski, N., and Shaffer, W.A., 2009. The role of the SLOSH model in National Weather Service storm surge forecasting. *National Weather Digest*, in press.

Hughes, M.G., 1995. Friction factors in wave uprush. *Journal of Coastal Research,* 11(4), 1089-1098.

Johnson, W.R. and Kowalik, Z., 1986. Modeling of storm surges in the Bering Sea and Norton Sound. *Journal of Geophysical Research,* 91, 5119-5128.

Kamphuis, J.W., 2000. *Storm surge, Introduction to coastal engineering and management*. River Edge, New Jersey: World Scientific Publishing Co. Pte. Ltd., 437pp.

Kinsman, N.E.M., and DeRaps, M.R., 2012 [in publication]. Coastal hazard field activities in response to the November 2011 Bering Sea storm, Norton Sound, Alaska. Fairbanks, Alaska: Alaska Division of Geological & Geophysical Surveys Report of Investigation.

Larson, M., and Kraus, N. C., 1989. SBEACH: Numerical Model for Simulating Storm-Induced Beach Change: Report 1, Empirical Foundation and Model Development. Vicksburg, Mississippi: Coastal Engineering Research Center, U.S. Army Corps of Engineers, Waterways Experiment Station, *Technical Report CERC-89-9,* 256p.

Lingaas, J., 2011. Shaktoolik surge forecast for November 2011 storm, *National Weather Service*.

Makkonen, L., 2006. Plotting positions in extreme value analysis: *Journal of Applied Meteorology and Climatology*, 45, 334-340.

Mason, O.K.; Neal, W.J., and Pilkey, O.H., 1997. *Living with the Coast of Alaska*. Duke University Press, 355p.

Mesinger, F.; DiMego, G.; Kalnay, E.; Mitchell, K.; Shafran, P.C.; Ebisuzaki, W.; Jovic, D.; Woollen, J.; Rogers, E.; Berbery, E.H.; Ek, M.B.; Fan, Y.; Grumbine, R.; Higgins, W.; Li, H.; Lin, Y.; Manikin, G.; Parrish, D., and Shi, W., 2006. North American Regional Reanalysis. *Bulletin of the American Meteorological Society*, 87(3), 343-360.

Native Village of Shaktoolik IRA Council. URL: http://www.kawerak.org/tribalHomePages/shaktoolik/index.html; accessed April 5, 2012.

National Climate Data Center (NCDC). URL: http://www.ncdc.noaa.gov/oa/ncdc.html; accessed November 30, 2011.

National Oceanic and Atmospheric Administration (NOAA) Tides and Currents. URL: http://tidesandcurrents.noaa.gov/; accessed November 30, 2011.

Rodionov, S.; Bond, N., and Overland, J., 2007. The Aleutian Low, storm tracks, and winter climate variability in the Bering Sea: Deep Sea Research Part II. *Topical Studies in Oceanography,* 54(23-26), 2560–2577.

Sallenger Jr., A.H., 1983. Measurements of debris-line elevations and beach profiles following a major storm: northern Bering Sea coast of Alaska. *U.S. Geological Survey Open-File Report 83(394),* 11p.

Solomon, S.; Qin, D.; Manning, M.; Chen, Z.; Marquis, M.; Averyt, K.B.; Tignor, M., and Miller, H.L., 2007. *Contribution of Working Group I to the Fourth Assessment Report of the Intergovernmental Panel on Climate Change, 2007*. New York: Cambridge University Press, New York, NY, 996p.

Sorensen, R.M., 1997. *Basic Coastal Engineering.* New York: Chapman and Hall, 301p.

Stabeno, P.J.; Schumacher, J.D., and Ohtani, K., 1999. The physical oceanography of the Bering Sea. In: Loughlin, T.R. and Ohtani, K., Dynamics of the Bering Sea. Fairbanks, Alaska: University of Alaska Sea Grant, pp. 1-28.

Stockdon, H.F.; Holman, R.A.; Howd, P.A., and Sallenger Jr., A.H., 2006. Empirical parameterization of setup, swash, and runup. *Coastal Engineering,* 53, 573-588.

United States Army Corps of Engineers (USACE), 2011. Shaktoolik Coastal Flooding Analysis. Anchorage, Alaska: U.S. Army Corps of Engineers, Alaska District, 36p.

The University Corporation for Atmospheric Scientists, The COMET Program. URL: http://comet.ucar.edu/; accessed February 10, 2012.

Tolman, H.L., 2009. User manual and system documentation of WAVEWATCH III version 3.14.. *NOAA / NWS / NCEP / MMAB Technical Note 276*, 194p.

Warrick, J.A.; Rubin, D.M.; Ruggiero, P.; Harney, J.N.; Draut, A.E., and Buscombe, D., 2009. Cobble cam: grain-size measurements of sand to boulder from digital photographs and autocorrelation analyses. *Earth Surface Processes and Landforms*, 34, 1811–1821.

Wise, J.L.; Comiskey, A.L., and Becker Jr., R., 1981. Storm surge climatology and forecasting in Alaska. Anchorage, Alaska: Arctic Environmental Information and Data Center, University of Alaska, Anchorage, 26p.